kOMUNIKÁCIE
COMMUNICATIONS

OPERATION AND ECONOMICS

MECHANICAL ENGINEERING

ELECTRICAL ENGINEERING

CIVIL ENGINEERING

SAFETY AND SECURITY ENGINEERING

Ondrej Stopka - Ladislav Bartuska - Jacek Caban - Larisa M. Kapustina*

PROPOSAL OF THE FUNCTIONAL SYSTEM FOR THE AIRLINE COMPANIES FINANCIAL SITUATION ASSESSMENT

This paper presents the draft methodology to be applied for evaluating the financial health of airlines. In the introductory part, specific attributes, regarding the individual types of airlines, are described. Subsequent parts of the manuscript outline advantages and disadvantages to measure airlines performance when implementing financial indicators, as well as a general procedure to evaluate the financial situation of a company operating in the aviation industry. The most important part of the paper includes the proposal of the specific functional system to evaluate the economic performance of airlines. Financial evaluation itself (evaluation of financial indicators of the enterprise's economic performance) is performed through a particular case study when comparing several existing airlines.

Keywords: *financial assessment, airlines, financial analysis, financial situation, economic performance*

1. Introduction

Airline companies face many different challenges, some of which may affect their performance and others that might result in their closure [1]. Worldwide public and private agencies take action to improve air transportation operations. Those changes seek to address challenges posed by increasing air traffic, increasing diversity of air traffic, aging infrastructure and ongoing efforts to make air transportation safer and more efficient [2]. In recent years, the European aviation sector has gone through a drastic change on both the supply and the demand side [3]. In contrast to many other industries, the driving forces governing those changes do not depend mainly on technological factors, but on developments in the legal, institutional and cultural domains of the aviation market [3]. Numerous studies have shown that air transportation makes a significant contribution to a country's economic and social development and represents an important engine of economic growth for nations [4]. Airlines core activities include:

- Air passenger transport,
  - regular,
  - charter,
- Air transport of freight, mail, consignments.

Regular air passenger transport –t refers to scheduled transportation of passengers. Free seats are publicly offered on websites or in air carriers´ branches. Operators of such flights operate a network of lines depending on the market size and the operator´s financial strength.

Charter air passenger transport – refers to unscheduled, irregular air transport services of passengers. Air carriers operate air transport at request. Mostly these are "holiday" flights or flights offered by travel agencies acting as customers. Flight price is then established based on the agreement between the air carrier and the travel agency (customer).

Air transportation of freight, mail, consignment – air carriers specializing in freight transport mostly operate long-distance flights. They are typically subsidiaries of passenger carriers. Consignment transportation is ensured by mail carriers, who operate connecting flights collecting or dispatching consignments from / to hubs (major nodes – airports) and then transporting them to final destinations.

A business is said to have significant market power when it can profitably raise and maintain process above the level that would prevail in a competitive market [5]. The assessment of market power is therefore an assessment of consumers to changes in price or quality [5]. For the cost-efficient operation of airlines and efficient functioning of airlines and efficient operation of all the main and additional services, continuous performance measurement is necessary.

Measuring airline performance using financial indicators helps the company to act in accordance with its financial capabilities and tackle the problems identified by means of such metrics. It can be the first indicators of defects and deficiencies in operation or other corporate functions.

2. Advantages and disadvantages of measuring airline performance using financial indicators

Systems of measuring company's performance, based on exact financial indicators, retain the features of basic financial analysis indicators including the deficiencies [6]. Their major drawbacks are their orientation to the past and past phenomena, their simplicity and the related inability of a complete description of a company in its complexity and their necessary interpretation, which is always dependent on the evaluator and is therefore subjective [7].

* [1]Ondrej Stopka, [1]Ladislav Bartuska, [2]Jacek Caban, [3]Larisa M. Kapustina
[1]Department of Transport and Logistics, Faculty of Technology, Institute of Technology and Business in Ceske Budejovice, Czech Republic
[2]Faculty of Production Engineering, University of Life Science in Lublin, Poland
[3]Ural State University of Economics, Yekaterinburg, Russia
E-mail: stopka@mail.vstecb.cz

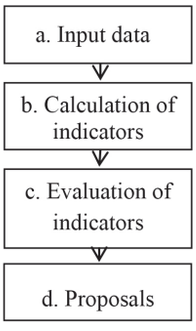

Figure 1 *Process of airline financial evaluation*

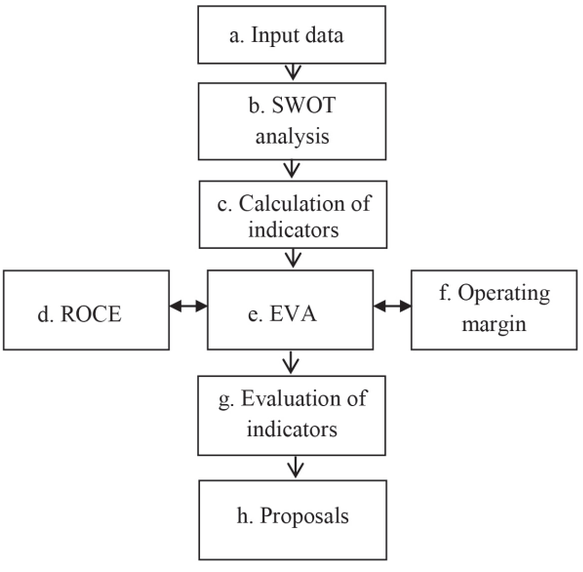

Figure 2 *Proposed airlines financial evaluation procedure*

On the other hand, it should be noted that using the financial indicators brings several advantages. The most important ones include easy data collection and their processing [8], as well as the possibility to compare the indicators of one or more companies over time, which reflects the fact that the structure of such indicators is based on accounting standards.

3. Data and methods

The fundamental method of assessing the airline economic performance is to carry out financial analysis (see Figure 1) [9]. It also shows the performance of the company in the past as well as the strengths and weaknesses of the company´s economic performance.

Moreover, it evaluates the expected development in the future and analyzes the consequences of individual optimizing measures, choosing the most suitable one. Airline performance is closely related to the financial soundness of the company [10].

The basic input data necessary for evaluating the airline economic performance include [10-11]:

- Number of employees
- Number of passengers transported
- Assets
- Current assets
- Fixed assets
- Stock (less relevant in the case of airlines)
- Liabilities
- Current liabilities
- Borrowed capital
- Long-term liabilities
- Equity
- Sales
- Profit
- Personnel costs.

Calculating indicators of financial analysis includes [12-13]:

- Liquidity indicators
- Activity indicators
- Productivity indicators
- Profitability indicators.

4. Results and discussion

The main task of an airlines economic evaluation system is to gain the maximum relevant information from the statements and other available information resources, to analyse and assess the financial soundness of the companies and to prepare the groundwork for necessary management decisions within the recommended optimization measures. In the process of financial analysis, the above-mentioned procedure (see Figure 1) must be followed. A modified procedure (see Figure 2) of airlines financial evaluation, as well as the proposed indicators, will be described in the following parts of the paper.

4.1 The SWOT analysis of airline financial health

The SWOT analysis [14-15] suggests external and internal elements, opportunities and threats that might influence the functional airline financial evaluation system (see an example of SWOT analysis below).

Strengths:

- High competitiveness of the company
- Using experience with the existing evaluation systems
- Complex services offer
- Cost minimization
- High profitability;

Weaknesses:

- Untested system
- Ambiguous system identification
- Problematic promotion
- No history
- Service prices higher than those offered by competitors;

Opportunities:

- Wide targeting
- New markets

- Business clientele
- Promotion through less used communication channels
- Individual approach to customers;

Threats:

- Rejection from customers
- Competition
- Similar companies entering the market
- Low return on investment
- Zero reaction to promotion.

4.2 Calculation of airlines financial analysis indicators

For more detailed financial performance evaluation of airlines, other financial analysis indicators should be completed [13]. Changes proposal, in the context of financial analysis, consists primarily in of calculating the indicators of [16]:

- liquidity
- activity
- productivity
- profitability – return on capital employed (ROCE)
- economic value added (EVA),
- operating margin.

a) Liquidity indicator (Quick Asset Ratio)

Quick Asset ratio (see Equation (1)) is calculated as a proportion of current liabilities in current assets, while the stock is not included in the calculation (for aviation industry companies, stock is of minimum importance). It is an indicator essential for maintaining the operation of the company and indicator which is often not readily converted into cash. In the case of companies offering services, quick asset ratio is almost equal to current asset ratio. The recommended current asset ratio value is in the range between 1 and 1.5 [8].

$$Quick\ Asset\ Ratio = \frac{Current\ assets - stock}{current\ liabilities}\,[-]. \tag{1}$$

b) Activity indicator (Return on total assets)

Return on total assets, or the number of assets turns (see Equation (2)) is the most complex indicator in this group. The indicator, also referred to as productivity of the capital invested, measures the efficient use of all the assets of a company. It indicates the appreciation of fixed and current assets in airline activities regardless of financial resources to cover such assets [13].

$$Return\ on\ total\ assets = \frac{total\ sales}{total\ assets}\,[-]. \tag{2}$$

c) Productivity indicator

Labour productivity (also referred to as effective using of resources) expresses the relation between the economic benefits (economic outputs) and the resources invested (inputs) (see Equation (3)) [7].

$$Labor\ productivity = \frac{total\ annual\ sales}{H}\,[€/h], \tag{3}$$

where: H – number of hours worked by all the employees per year [h/year].

d) Profitability indicator – Return on Capital Employed (ROCE)

This financial analysis indicator (see Equation (4)) [16]. Return on capital employed indicates how much the company obtained from 1 € invested by shareholders.

Capital employed is the total amount of capital that a company has utilized in order to generate profits. It is the sum of shareholders' equity and debt liabilities. In addition, it can be simplified as total assets minus current liabilities [13].

$$ROCE = \frac{EBIT}{Capital\ emloyed}\,[-], \tag{4}$$

where: EBIT - Earnings before Interest and Taxes [€].

e) Economic value added (EVA)

The EVA is a measure of company's performance created in order to motivate managers to focus on the company's value growth. The economic value-added model is based on the economic profit, which cannot be confused with accounting profit. Economic profit refers to the yields surplus after paying for the services of production factors, including both equity and borrowed capital [12].

The EVA thus measures the value created by a company by means of its business activities in comparison to another (the second best) investment opportunity with the same business risk. If the EVA values are positive (see Equation (5)) [13, 17], that indicates that the company creates the value for its owners; if the EVA values are negative, the value for the owners is being destroyed.

$$EVA_{rel.} = \frac{EVA}{personal\ costs + WACC * NOA} = \\ = \frac{EBIT * (1-t) - C * WACC}{personal\ costs + \left(R_d * (1-t) * D/C + R_e * E/C\right) * NOA}, \tag{5}$$

where:

$EVA_{rel.}$ – EVA indicator (relative value) [-];
WACC – Weighted Average Cost of Capital [€];
NOA – Net Operating Assets [€];
t – corporate tax rate [-];
R_d – cost of debt [€];
D – Debts (market value of the firm's debt) [€];
R_e – cost of equity [€];
E – Equity (market value of the firm's equity) [€];
C – invested capital – capital tied up in assets intended for operation activities (equity and debts) [€].

f) Operating margin

Operating margin describes the ratio measuring the pricing strategy and operational efficiency of the company in question (see Equation (6)) [13]. Operating margin describes the sales share in the company after all the variable costs of services provided (e.g. wages, fuel, energy, repairs and maintenance of airplanes, outsourcing, etc.) are covered. A good operating margin is essential for the company to cover variable costs, such as interest on loans [8].

$$Operating\ mar\ gin = \frac{operating\ profit}{Total\ sales}\,[-], \tag{6}$$

Table 1 *Criteria values for individual solution options (in 2017)*

Criterion (C_i)/airline company (A_i)		A_1	A_2	A_3	A_4
C_1	Quick Asset Ratio [-]	1.16	0.72	0.53	0.86
C_2	Return on total assets [-]	1.92	0.40	2.37	0.90
C_3	Labour productivity per hour [€/h]	181.25	0.07	0.69	12.11
C_4	Return on capital employed [-]	0.59	0.14	0.21	0.43
C_5	$EVA_{rel.}$ [-]	1.03	-6.53	-2.27	3.74
C_6	Operating margin [-]	5.82	4.87	3.69	6.04

Table 2 *Determining the weighing of criteria (criteria paired comparison)*

	C_1	C_2	C_3	C_4	C_5	C_6	Coefficient + 1	Sum	Weight
C_1	-	1	0	0	0	0	1	2	0.10
C_2	0	-	0	0	0	0	1	1	0.05
C_3	1	1	-	0	0	1	1	4	0.20
C_4	1	1	1	-	0	1	1	5	0.25
C_5	1	1	1	1	-	1	1	6	0.30
C_6	0	1	0	0	0	-	1	2	0.10
Σ	-	-	-	-	-	-	-	20	1

Table 3 *Paired comparison of individual alternatives for all criteria*

	A_1	A_2	A_3	A_4
C_1	0.40	0.20	0.10	0.30
C_2	0.30	0.10	0.40	0.20
C_3	0.40	0.10	0.20	0.30
C_4	0.40	0.10	0.20	0.30
C_5	0.30	0.10	0.20	0.40
C_6	0.30	0.20	0.10	0.40

Table 4 *Decision matrix and determining alternatives for airlines*

	Weighing of criteria	Alpha – A_1	Beta – A_2	Gamma – A_3	Delta – A_4	Σ
C_1	0.10	0.40	0.20	0.10	0.30	-
C_2	0.05	0.30	0.10	0.40	0.20	-
C_3	0.20	0.40	0.10	0.20	0.30	-
C_4	0.25	0.40	0.10	0.20	0.30	-
C_5	0.30	0.30	0.10	0.20	0.40	-
C_6	0.10	0.30	0.20	0.10	0.40	-
Weighted sum	-	0.30	0.20	0.10	0.40	1
Order of alternatives	-	2	3	4	1	-

4.3 Evaluation of airlines financial performance indicators – a case study

As a model example of financial situation final evaluation, the following maximization criteria (see Table 1), based on the recommended financial analysis ratios in the context of creating the particular functional system of airlines economic evaluation, are used:

- Quick Asset Ratio – C_1 [-],
- Return on Total Assets – C_2 [-],
- Labour productivity per hour – C_3 [€/h],
- Return on Capital Employed (ROCE) – C_4 [-],
- Relative Economic Value Added ($EVA_{rel.}$) – C_5 [-],
- Operating margin – C_6 [-].

For the purpose of evaluating the individual alternatives of financial performance solutions, four fictitious airlines and their values for the given criteria (Table 1) were chosen:

- Airline Alpha – A_1,
- Airline Beta – A_2,
- Airline Gamma – A_3,
- Airline Delta – A_4.

Values for the criteria were quantified based on the input data in the context of financial analysis for each airline.

Subsequently, weighing of the individual criteria were determined (C_1 – C_6) based on the paired comparison method, (see Table 2). This method consists in comparing each criteria pair. To ensure that the criteria with the resulting value of 0 are not excluded from evaluation, coefficient 1 was added to all the values [18-19].

By analogy (based on the paired comparison method), comparison of individual alternatives (airlines) is carried out subsequently for all determined criteria (C_1 – C_6). This way the individual alternatives weighing for all the criteria will be obtained.

The results of paired comparison for all the criteria are shown in the Table 3.

For quantification of results in order to determine the order of alternatives for airlines (in descending order) and identification of a company with objectively best economic (financial) health, the multi-criteria analysis method is applied. More particularly, the FDMM – Forces Decision Matrix Method (see Table 4) is used.

According to results of the multi-criteria analysis for FDMM (Forces Decision Matrix Method) and based on the set criteria (selected financial analysis indicators), the airline with the best financial health seems to be Airline Delta.

5. Conclusions

Within this research, a methodology (functional system) for evaluating financial performance (evaluating the financial situation) of airlines was created. This methodology includes analysis of the external, internal and competitive environment, financial analysis and creating models (functional system) for quantification of financial analysis results.

Parts of the methodology concerning analysis of external, internal and competitive environments (SWOT analysis as a part of the proposed functional evaluation system) follow development of the air transport in the world. Analyses are focused mainly on the future development of the air transport.

Parts of the methodology, regarding the financial analyses of individual companies (calculation and subsequent evaluation of airlines financial analysis indicators), provide information on performance of the evaluated airlines (financial health). To compare the results of airlines financial analysis, a system for financial analysis results quantification was created.

Using this system, it is possible to identify the differences in successful performance of the individual companies.

The advantage of the created airline economic performance evaluation system is mainly the possibility to compare the performance of freely chosen airlines based on the freely chosen financial analysis indicators and multi-criteria analysis method for final evaluation.

Acknowledgement

This contribution was created within realization of the research project LTC17040 named "*The operation of regional airports in the Czech Republic and Slovakia and their impact on the economic development of the region / Regionalni letiste v Ceske a Slovenske republice a vliv jejich provozu na ekonomicky rozvoj regionu*" of the INTER-EXCELLENCE program, the INTER-COST subprogram.

References

[1] ISMAIL, N. A., JENATABADI, H. S. The influence of firm age on the relationships of airline performance, economic situation and internal operation. *Transportation Research Part A: Policy and Practice* [online]. 2014, **67**, p. 212-224. ISSN 0965-8564/eISSN 1879-2375. Available from: https://doi.org/10.1016/j.tra.2014.06.010

[2] KUHN, K. D. Using structural topic modeling to identify latent topics and trends in aviation incident reports. *Transportation Research Part C: Emerging Technologies* [online]. 2018, **87**, p. 105-122. ISSN 0968-090X/eISSN 1879-2359. Available from: https://doi.org/10.1016/j.trc.2017.12.018

[3] ALDERIGHI, M., et al. Competition in the European aviation market: the entry of low-cost airlines. *Journal of Transport Geography* [online]. 2012, **24**, p. 223-233. ISSN 0966-6923/eISSN 1873-1236. Available from: https://doi.org/10.1016/j.jtrangeo.2012.02.008

[4] GINIEIS, M., SANCHEZ-REBULL, M. V., CAMPA-PLANAS, F. The academic journal literature on air transport: Analysis using systematic literature review methodology. *Journal of Air Transport Management* [online]. 2012, **19**, p. 31-35. ISSN 0969-6997/eISSN 1873-2089. Available from: https://doi.org/10.1016/j.jairtraman.2011.12.005

[5] THELLE, M. H., SONNE, M.C. Airport competition in Europe. *Journal of Air Transport Management* [online]. 2018, **67**, p. 232-240. ISSN 0969-6997/eISSN 1873-2089. Available from: https://doi.org/10.1016/j.jairtraman.2017.03.005

[6] SEDLACEK, J. *Accounting data in the hands of a manager: Financial analysis in the corporate management* (in Czech). 2. ed. Prague: Computer Press, 2001. ISBN 80-722-6562-8.

[7] BINOVA, H., BREZINA, E. Proposal for a financial model operation of regional trains in the Pilsen region. *LOGI – Scientific Journal on Transport and Logistics*. 2015, **6**(1), p. 13-25. ISSN 1804-3216.

[8] PAVELKOVA, D., KNAPKOVA, A. *Business performance from a financial manager point of view* (in Czech). 2. ed. Prague: Linde, 2009. ISBN 978-80-86131-85-6.

[9] BLOCK, S. B., HIRT, G. A. *Foundations of financial management*. Homewood: Irwin, 1992. ISBN 0-256-08355.

[10] MORRELL, P. S. *Airline finance*. 3. ed., Aldershot, Hampshire: Ashgate Publishing Company, 2007. ISBN 978-0-7546-7000-1.

[11] KROLLOVA, S. Technological aspects of aircraft ground de-icing *and anti-icing system at Bratislava airport. LOGI* – Scientific Journal on Transport and Logistics. 2015, **6**(2), p. 13-27. ISSN 1804-3216.

[12] HOLLOWAY, S. *Straight and level: Practical airline economics*. Bodmin, Cornwall: Ashgate Publishing Company, 2003. ISBN 0-7546-1930-3.

[13] MARIK, M., MARIKOVA, P.: *Modern methods for corporate performance evaluation and valuation: Economic value added, market value added, CF ROI* (in Czech). Overwrite and expanded ed. Prague: Ekopress, 2005. ISBN 80-861-1961-0.

[14] ZITRICKY, V., GASPARIK, J., PECENY, L. The methodology of rating quality standards in the regional passenger transport. *Transport Problems* [online]. 2015, **10**, p. 59-72. ISSN 1896-0596/eISSN 2300-861X. Available from: https://doi.org/10.21307/tp-2015-062

[15] SEVKLI, M., et al. Development of a fuzzy ANP based SWOT analysis for the airline industry in Turkey. *Expert Systems with Applications* [online]. 2012, **39**(1), p. 14-24. ISSN 0957-4174/ISSN-L 0957-4174. Available from: https://doi.org/10.1016/j.eswa.2011.06.047

[16] SIM, K. L., SONG, C. J., KILLOUGH, L. N. service quality: service recovery, and financial performance: An analysis of the US airline industry. *Advances in Management Accounting* [online]. 2010, **18**, p. 27-53. ISBN 978-1-84950-754-7/eISBN 978-1-84950-755-4. Available from: https://doi.org/10.1108/S1474-7871(2010)0000018005

[17] SOFRANKOVA, B., et al. Identification of key performance indicators with the application of mathematical and statistical methods. *Journal of Financial Studies and Research* [online]. 2017, **2017**, Article ID 403204, p. 1-11. ISSN 2166-000X. Available from: https://doi.org/10.5171/2017.403204

[18] SKRUCANY, T., et al. Comparison of chosen environmental aspects in individual road transport and railway passenger transport. *Procedia Engineering* [online]. 2017, **192**, p. 806-811. ISSN 1877-7058. Available from: https://doi.org/10.1016/j.proeng.2017.06.139

[19] OLIVKOVA, I.: methodology for assessment of electronic payment systems in transport using AHP method. In 17th International Conference on Reliability and Statistics in Transportation and Communication (RelStat 2017) : proceedings. Vol. 36. Lecture Notes in Networks and Systems book series. Springer, Cham, 2018. ISBN 978-3-319-74453-7/eISBN 978-3-319-74454-4, p. 290-299. Available from: https://doi.org/10.1007/978-3-319-74454-4_28

Katerina Pojkarova - Dalibor Gottwald*

DO AIR PASSENGERS DECIDE RATIONALLY? CASE STUDY OF TRAVELLERS ON ROUTE PRAGUE-LONDON

Decision-making is an integral part of every human's life, both personal and professional, and today's highly globalized world brings many different factors that affect the decision-making process. General economic theory of utility is grounded in the assumption that people make decisions rationally. Recently, however, its limits have been challenged by both scientific and professional public - the theory of rational choice acknowledges only a limited number of factors that influence the decision-making. The aim of the present article is to discover whether the current debate can be applicable to decision-making processes of flight passengers in a case study of travelers on route from Prague to London. The article presents results of a primary research carried out by authors in 2018. The survey set to explore validity of choice theory in the sector of logistics, in particular in decision-making processes of passengers who buy flight ticket on route Prague - London. At the base of result it can be confirmed that the classical theory of rational choice in economical perspective has been proven false. When people's behavior, as a result of their decision making, serves as a basis for future predictions of development in a given area, it is essential to take into account other, usually hidden factors, which also affect the decision-making process.

Keywords: *rational choice theory, passengers, air transport, decision making, irrational decisions*

1. Introduction and background

Rational choice theory, a theory explaining human behavior in decision-making processes related to economic issues, has until only recently been a central paradigm in economics. The theory views an individual as *homo economicus* who makes choices in a rational manner, seeking to minimize loss and maximize gain, while being systematically economical and taking into account various aspects at the same time [1]. This approach has been used in economics and the last decades saw its outreach into other areas, most notably sociology and political sciences [2, 3]. Implementation of the theory into other areas has resulted in a debate over its validity and the increasingly globalized environment gave way to criticism of its purely economic interpretations. The main vein of criticism is its limitations in terms of number of factors that the theory acknowledges. Many specialists believe that humans are influenced by a wide range of hidden irrational factors that stem from early life stages, including emotions, societal norms and prejudices, and together with a wide array of marketing activities influence the decision-making processes [4, 5]. Severe income polarity is one of the proofs of human irrationality. If people behaved rationally, the following statement would be true: The more an employee earns, the more motivated he or she is to deliver a better work performance. Validity of this statement has been verified in a number of experiments. One of them investigated the effect of small, medium and high bonuses on intellectual performance of employees. Results have shown that groups that have been promised the highest bonus performed the worst [6]. This result can be explained using Kahneman and Tversky prospect theory, especially in terms of a loss aversion. The fear of losing a high yearly bonus, which the employees count on throughout the year, is more stressful than motivating for their intellectual performance [7]. Such experiments show that it is essential to know relationships between remuneration, motivation, stress and performance. Generally, it can be said that humans are not rational, especially when in stressful situations or under pressure. In this way, a certain deficiency of the classical theory of rational choice can be seen [6, 8, 9]. There are several articles published on this topic, where irrational behavior is tested in different areas such as eating habits, tourism, politics or psychology [10-13]. The aim of this article is to verify if people are rational in their decision-making. The article presents results of a primary research carried out by authors in 2018. The survey is set to explore validity of choice theory in the sector of logistics, in particular in decision-making processes of passengers who buy flight ticket on route Prague - London.

2. Methodology

Data used in this article were gathered in an online questionnaire survey, whose respondents were air passengers.

2.1 Subject of survey

The questionnaire was administered through Facebook pages of a flight tickets seller Happyfly.cz and through selected Facebook pages that deal with travelling or provide tips on cheap flight tickets, namely: *Cestovani a turistika (Travel and tourism); Cestovani - zabava, inspirace i pouceni (Travel - entertainment, inspiration and teaching); Cestovani po svete s detmi (Traveling around the world with children); Vylety a cestovani (Trips and travelling); Milujeme letadla - letani (cestovani) (We love planes*

* **Katerina Pojkarova, Dalibor Gottwald**
Faculty of Transport Engineering, University of Pardubice, Czech Republic
Email: dalibor.gottwald@upce.cz

- flying (travelling)); Nejvyhodnejsi cestovani (The most benefit travelling); Akcni letenky a cestovani po svete (Action trips and travel around the world); Individualni cestovani (Individual travel); Londyn (London); Milujeme cestovani (We love travelling); Levnocestovani.cz (Cheaptravelling.cz); Cestovadlo (Cestovadlo). The questionnaire was open from June 25, 2018 through August 4, 2018. Altogether, 109 responses were yielded and data were then analyzed.

2.2 Survey design

The questionnaire was designed in such a way that it made possible to verify or falsify the theory of rational choice. It comprised three parts where respondents were gradually provided with information on flights, duration of travel and its cost, and a general identification part. The first part presented respondents with the following **Model situation 1**: *"You are planning a long-weekend trip to London - a regular sightseeing trip with a visit to Westminster Abbey, Tower Bridge, Buckingham Palace etc. You want to leave from Prague and the following ten flights are available. Put them into order based on your preferences (choose at least five flights)."* Respondents could choose from ten flights. In this model situation, they were given information about the *air company*, *departure and arrival times*, *destination airport*, *flight ticket price* and *flight duration*. After selecting at least five flights, they were asked to answer the following question: "*Which criterion was the most important when choosing the order of flights?*". They could choose from *air company, departure and arrival times, location of the destination airport, flight ticket price, flight duration* and *other*. In the case that they selected *other*, respondents were asked to specify their answer.

In the second part of the questionnaire, respondents were presented with **Model situation 2**, which in addition to information provided in Model situation 1 also included information on *duration of journey from London airports to London city center* and *overall time spent travelling* (the most convenient option in terms of overall time spent travelling, i.e. the sum of flight duration and duration of journey from the airport to the center, was highlighted). After selecting the preferred five flights, they were again asked to select the most important criterion for their choice. This time, the selection of criteria also included *duration of journey from the airport to the city center* and *overall time spent travelling*.

The third part of the questionnaire used **Model situation 3**, which, in addition to the information provided in the two preceding model situations, included information on *price of public transport tickets (from London airports to London city center)* and *total cost of transport,* i.e. the sum of the flight ticket price and the price of public transport tickets (the cheapest option was highlighted). Again, respondents were asked to select at least five flights and then select the most important criterion for their choice. This time, the selection of criteria also included options *price of public transport tickets (from London airports to London city center)* and *total cost of transport.*

The last part of the questionnaire comprised general identification questions. Respondents were asked to answer these questions: "*What is your experience with air travel?"* (**area 1**), "*What is your experience with air travel to London?"* (**area 2**), "*What is your experience with arranging trips such as a long weekend abroad, regular trip to cities abroad etc. with the use of air travel?"* [1] (**area 3**) and provide information on their sex (**area 4**) and highest achieved education (**area 5**).

Data gathered in the survey were used to verify the validity of rational choice theory in buying flight tickets. The question related to experience is highly important - it is assumed that experienced respondents will take into account all additional costs, such as price of public transport tickets, or the time spent travelling to the city center from farther airports. Respondents were grouped by areas in the identification analysis and Pearson's chi-squared test was used to verify their consistency in selection of preferred flights in Model situations 1 through 3.

$$x^2 = \sum_{i=1}^{n} \frac{(O_i - E_i)^2}{E_i} = N \sum_{i=1}^{n} \frac{(O_i/N - p_i)^2}{p_i}, \qquad (1)$$

x^2 Pearson's cumulative test statistic, which asymptotically approaches a x^2 distribution,
O_i the number of observations of type i,
N total number of observations,
E_i the expected (theoretical) count of type i, asserted by the null hypothesis that the fraction of type i in the population is p_i,
n the number of cells in the table.

3. Results

Results of the survey show that when only basic information was provided (*air company, departure and arrival times, destination airport, flight ticket price* and *flight duration*, i.e. Model situation 1), most respondents (32 %) selected as their first preferred the Ryanair flight at 6:40 AM, which was the first flight of the day and one of the three most expensive. Only a few respondents preferred late evening or night flights. *Departure and arrival times* was among the most common criteria for their choice - 53.2 % of respondents selected it as the most important one, while only 16.5 % decided by the price.

Figure 1 shows that when given additional information (*duration of journey from London airports to London city center* and *overall time spent travelling*, i.e. Model situation 2), respondents did not change their answers significantly. Again, the most preferred flight was the Ryanair flight at 6:40 AM (34 %). No respondents chose late evening or night flights as the most preferred ones.

Departure and arrival times was again the most important criterion (38.5 %), followed by *flight ticket price* (18.35 %). However, 11.93 % of respondents stated that the main criterion was *duration of journey from London airports to London city center*. This is quite surprising since the preceding section has shown that *flight duration*, also a time criterion, was not deemed important by respondents.

Model situation 3 (see Figure 2) with additional information on *price of public transport tickets (from London airports to London city center)* and *total cost of transport* brought significant changes. This time, 41 % of respondents chose the British Airways flight at

1 "Arranging" is here used to mean buying tickets, finding out about local public transport costs in target destination etc.

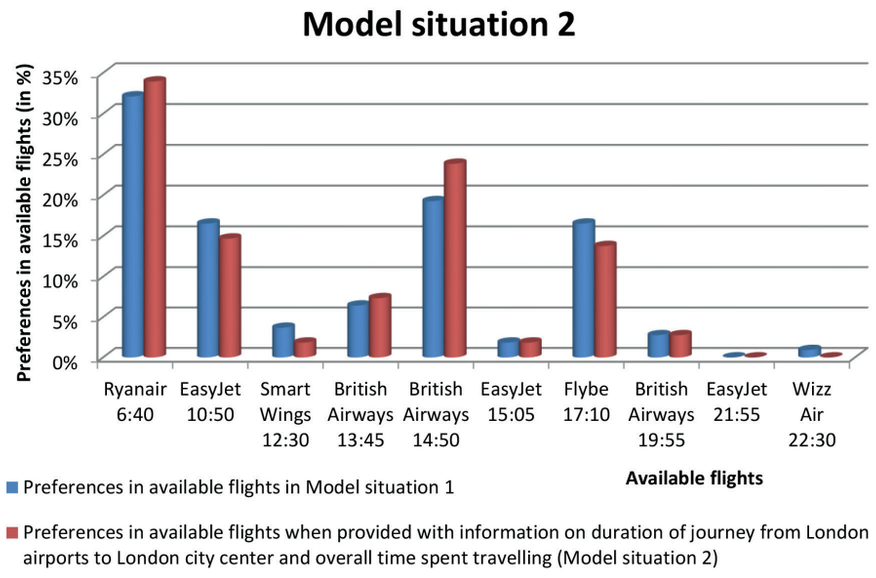

Figure 1 *Model situation 2*

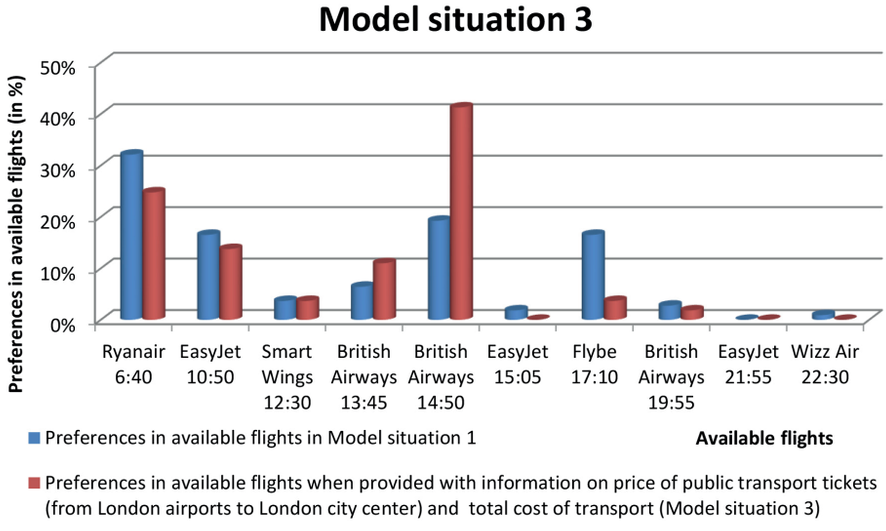

Figure 2 *Model situation 3*

2:50 PM as the best one[2], while the Ryanair flight at 6:40 AM was chosen by 25 % only.

In Model situation 3, the main criterion was *total cost of transport* for 42.2 % while *departure and arrival times* was selected by only 26.6 %, a half less than in the preceding Model situation. One third of respondents stated the same main criterion in all the three model situations - it was *departure and arrival times* for 75 % of them, while the rest opted for *air company* or *flight ticket price*.

In Model situation 1, 25 % of respondents selected *departure and arrival times* as the most important criterion. This gradually changed with adding further information until *total cost of transport* became the most important criterion. It follows that respondents changed their decisions when presented with additional information, which is not very surprising. What is surprising is the fact that the preferred order of flights in Model situations does not comply with the theory of rational choice - respondents did not always choose the option that would minimize their loss and maximize their gain. Respondents were inconsistent in their choice of preferred flights, as well as in criteria that guided their choice.

Comparing experienced and less experienced respondents also brings interesting data. Experienced travelers are those who answered the question "*What is your experience with arranging trips such as a long weekend abroad, regular trip to cities abroad etc. with the use of air travel?*"[3] that they have arranged such a trip at least four or more times. Non-experienced are those who answered they have no such experience. Figures 3 and 4 show differences in changes of preferred flights in experienced and non-experienced respondents in Model situation 3.

Figures 3 and 4 show that non-experienced respondents show greater differences in decisions, but visible changes were made also by more experienced travelers.

2 The overall cost of transport from Prague to London city center is the lowest with the British Airways flight at 2:50 PM.

3 "Arranging" is here used to mean buying tickets, finding out about local public transport costs in target destination etc.

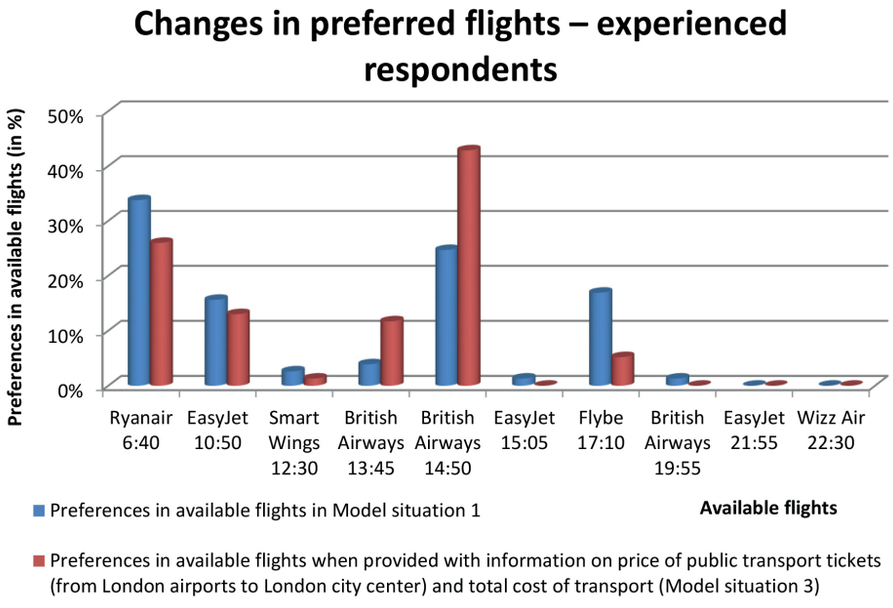

Figure 3 *Changes in preferred flights - experienced respondents*

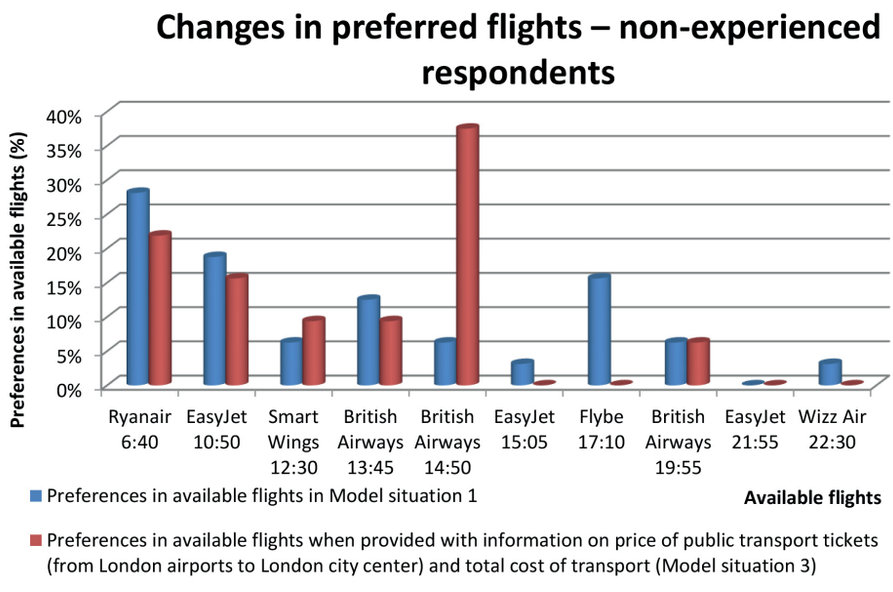

Figure 4 *Changes in preferred flights - non-experienced respondents*

The Pearson's chi-squared test was used to discover whether groups of respondents categorized by areas in identification questions were consistent in their choices of preferred flights in Model situations 1 through 3. Table 1 shows results of the Pearson's chi-squared test.

With statistical error of 5 %, it can be concluded that no group of respondents was consistent in their choices of preferred flights in Model situations 1 through 3. It becomes evident that not even experienced travelers decided rationally. To prove the rational choice theory right, respondents would have to select the same criterion in all model situations, always bearing in mind their economical perspective and always selecting the lowest price over other factors.

4. Discussion and conclusions

The present article examined rationality when buying flight tickets, in particular in travelers on route Prague - London. This is a very current topic since many authors have pointed out the limits of the rational choice theory in its classical economical perspective. People are daily confronted with an immense number of factors that may influence their decisions and it becomes virtually impossible to realize their influence on one's decisions. The probability that the final decision will always be in accordance with the assumption that all the decisions are made to minimize one's loss and maximize his or her gain, is very small.

The preceding section has shown results of authors' survey whose results clearly confirm that passengers do not behave rationally in presented Model situations. Consistency, or

Table 1 *Results of the Pearson's chi-squared test*

Area of identification analysis	x^2	p-value	Statistically significant at an alpha level of 0.05
Experience with air travel (area 1)	0.183	0.669	NO
Experience with travelling to London (area 2)	0.491	0.484	NO
Experience with arranging trips abroad (area 3)	0.410	0.522	NO
Sex (area 4)	1.402	0.236	NO
Achieved education (area 5)	0.417	0.522	NO

rationality, in decision making was not found even in passengers who are, according to their own words, experienced in buying tickets. The difference in consistency has not been confirmed from any investigated perspective: gender, education attained, experience with air travel, experience with travelling to London (see Table 1).

If the rational choice theory was to be confirmed, respondents would have to select one and the same criterion in all the model situations. However, respondents were influenced by the gradually provided information on duration of journey from the airport to the city center, overall time spent travelling, cost of public transport tickets or total cost of transport.

Validity of rational choice theory would be confirmed even if respondents chose different criteria in every model situation because for example Model situation 1 did not include information on overall cost. In such a case they would have to select a criterion that would minimize their loss and maximize their gain to prove the theory right. However, not even that happened in the survey - respondents were inconsistent in their choice of criteria and most of them also in the choice of one criterion in each model situation. Detailed analysis of their answers showed that although respondents stated their decision depended mainly on price, they did not opt for flights with the lowest price in their preferred flights.

To conclude, it can be confirmed that the classical theory of rational choice in economical perspective has been proven false. When people's behavior, as a result of their decision making, serves as a basis for future predictions of development in a given area, it is essential to take into account other, usually hidden factors, which also affect the decision-making process.

References

[1] KAHNEMAN, D. *Thinking, fast and slow*. New York, NY, US: Farrar, Straus and Giroux, 2011. ISBN 978-0-3742-7563-1.

[2] SWEDBORG, R. *Economic and sociology*. Princeton: Princeton University Press, 1990. ISBN 9780691003764.

[3] GREEN, D. P., SHAPIRO, I. *Pathologies of rational choice theory: A critique of applications in political science*. New Haven: Yale University Press, 1996. ISBN 0-300-06636-8.

[4] ARIELY, D. *Predictably irrational: The hidden forces that shape our decisions*. New York: Harper Collins, 2009. ISBN 978-0-06-135323-9.

[5] KISER, E., HECHTER, M. The debate on historical sociology: Rational choice theory and its critics. *American Journal of Sociology* [online]. 1998, **104**(3), 785-816. ISSN 0002-9602/eISSN 1537-5390. Available from: https://doi.org/10.1086/210086

[6] ARIELY, D. *The upside of irrationality: The unexpected benefits of defying logic*. New York: Perennial, 2011. ISBN 978-0-06-199504-0.

[7] KAHNEMAN, D., TVERSKY, A. Prospect Theory: An analysis of decision under risk. *Econometrica* [online]. 1979, **47**(2), p. 263-292. ISSN 00129682/eISSN 14680262. Available from: https://doi.org/10.2307/1914185

[8] INFANTE, G., LECOUTEUX, G., SUGDEN, R. Preference purification and the inner rational agent: a critique of the conventional wisdom of behavioral welfare economics. *Journal of economic methodology* [online]. 2016, **23**(1), p. 1-25. ISSN 1350-178X/eISSN 1469-9427. Available from: https://doi.org/10.1080/1350178X.2015.1070527

[9] VANBERG, V. J. Rationality and rules: Behavioral foundations and policy implications. *History of Economic Ideas* [online]. 2016, **24**(3), p. 95-113. ISSN 11228792/eISSN 17242169. Available from: https://doi.org/10.19272/201606103005

[10] WANG, J., SHEN, M., GAO, Z. Research on the irrational behavior of consumers' safe consumption and its influencing factors. *International Journal of Environmental Research and Public Health* [online]. 2018, **15**(12), 2764. ISSN 1661-7827/eISSN 1660-4601. Available from: https://doi.org/10.3390/ijerph15122764

[11] PARK, S., NICOLAU, J. L. If you, tourist, behave irrationally, I'll find you! *Tourism Management* [online]. 2018, **69**, p. 424-439. ISSN 0261-5177/eISSN 1879-3193. Available from: https://doi.org/10.1016/j.tourman.2018.06.017

[12] AALDERING, L. Research on the irrational behavior of consumers' safe consumption and its influencing factors. *Electoral studies* [online]. 2018, **54**, p. 269-288. ISSN 0261-3794/ISSN-L 0261-3794. Available from: https://doi.org/10.1016/j.electstud.2018.04.010

[13] STAMOVLASIS, D., VAIOPOULOU, J. The role of dysfunctional myths in a decision-making process under bounded rationality: A complex dynamical systems perspective. *Nonlinear Dynamics, Psychology, and Life Sciences* [online]. 2017, **21**(3), p. 267-288. ISSN 1090-0578/ISSN-L 1090-0578.

Peter Mucka - George Juraj Stein - Peter Tobolka*

PASSSENGER RIDE COMFORT AND INTERNATIONAL ROUGHNESS INDEX SPECIFICATIONS IN THE SLOVAK REPUBLIC

New original results are presented on relation between passenger's whole-body vibration (WBV) and longitudinal road unevenness characterised by the International Roughness Index (IRI) in 100-m segments. Measurements were provided in nine different cars of six vehicle categories operated on about 1860 km of road network. Vibration total value based on the root mean square (RMS) of the frequency-weighted acceleration was used to quantify the ride comfort at seat surface and seat base (i.e. vehicle floor) in three orthogonal axes. The relations between passenger's acceleration response, comfort reaction levels according to the ISO 2631-1: 1997 and the IRI road unevenness classes, used by the Slovak Road Administration, were estimated. Results indicated higher WBV by ~ 20 % on the motorways than on the 1st and 2nd class roads in the same IRI road class. Using the same IRI road classes for motorways and the 1st and 2nd class roads seems not to be appropriate from the point of view of the whole-body vibrations.

Keywords: *whole-body vibration, passenger car, road profile, international roughness index (IRI), ride comfort, highways and roads*

1. Introduction

Longitudinal road unevenness is an important parameter of Pavement Management System [1] and in Slovak Republic is characterised by the IRI index. The IRI is the most commonly used worldwide index used for evaluating and managing road systems [2-3].

This study is aimed to identify the relation between the measured WBV of a passenger in a motor vehicle and IRI based on field measurements. Such results have not been previously summarized and discussed. Field measurements that reported this relation were rare in the past and most measurements were provided only in recent years [4-15]. Comprehensive overview of published relations between the WBV and IRI was provided in [16]. Several authors reported the frequency-weighted acceleration on the seat surface on test sections with a known IRI. They used a passenger car with a dummy [7], luxury SUV [9], luxury sedan [15], multifunction vehicle [4, 11], van [13], van and ambulance [5], bus [8] and truck with a trailer [5-6]. Vehicle speed ranged from 30 to 120 km/h. Most of published results were provided in the vertical direction only or in the three orthogonal axes at the seat surface.

Limitation of published results [4-15] is in limited length and number of processed sections; using only one vehicle speed; using only one test vehicle that does not represent a vehicle fleet; only one (vertical) direction for the WBV evaluation; absence of passenger cars among tested vehicles; long time between the IRI measurement and WBV measurement.

For the road network administration and maintenance, ride safety and vehicle R&D purposes, is important to have an idea about induced WBV and comfort level for a particular IRI value, road category and vehicle speed.

The objectives of the work were as follows:

- Provide in-situ measurements of the WBV on the passenger's seat surface and seat base for different vehicle types, road categories and speeds;
- Synchronize measured longitudinal road unevenness data with the WBV measurements;
- Estimate the relation between the IRI, WBV and vehicle speed;
- Compare the IRI road classes used in the Slovak republic and induced WBV in a vehicle;
- Estimate the influence of road category, road unevenness class and vehicle speed on results.

Presented results are novel in the following:

- IRI road classes were not compared to induced vibrations in a vehicle;
- Processing much wider length of road network and range of vehicle speeds;
- Considering nine different passenger cars of six vehicle categories;
- WBV results are evaluated as a function of the IRI road classes, road category and vehicle speed;
- Vehicle speed is considered as a parameter of a regression function;
- Considering six acceleration signals at the seat surface and seat base in three orthogonal axes;
- Short time elapsed between the road roughness and WBV measurements.

* **Peter Mucka, George Juraj Stein, Peter Tobolka**
Institute of Materials and Machine Mechanics, Slovak Academy of Sciences, Bratislava, Slovakia
E-mail: ummsmuc@savba.sk

Table 1 *Expected comfort reactions to vibration environments according to the ISO 2631-1: 1997 [28]*

Vibration total value a_v (m/s^2)	Comfort level
< 0.315	not uncomfortable
0.315-0.63	a little uncomfortable
0.5-1.0	fairly uncomfortable
0.8-1.6	uncomfortable
1.25-2.5	very uncomfortable
> 2	extremely uncomfortable

Table 2 *IRI (mm/m) road unevenness classification in a 20-m segment in Slovakia [20]*

Road class	Motorways and expressways	1st and 2nd class roads	3rd class roads and local highways
1 (very good)	< 1.90	< 1.90	< 3.30
2 (good)	1.91-3.30	1.91-3.30	3.31-5.00
3 (fair)	3.31-5.00	3.31-5.00	5.01-8.00
4 (poor)	5.01-8.00	5.01-10.00	8.01-14.00
5 (very poor)	> 8.00	> 10.00	> 14.00

2. International roughness index

The IRI is essentially a computer-based virtual response-type system based on the response of a mathematical quarter-car vehicle model to a road profile. The IRI is based on simulation of the roughness response of a car travelling at 80 km/h - it is the Reference Average Rectified Slope, which expresses a ratio of the accumulated suspension vertical motion of a vehicle, divided by the distance travelled during the test.

The IRI is a numeric that summarizes roughness qualities impacting vehicle response. The IRI is a dimensionless measure with units (mm/m), (m/km) or (in/mi). The algorithm was proposed by Sayers [17] and is also implemented in prEN 13036-5: 2017 [18] or ASTM E1926-08: 2015 [19]. The IRI is an indicator of longitudinal unevenness often used in Pavement Management Systems around the world [2-3] and in the Slovak Republic [20-26].

The IRI specifications around the world used one, two or more longitudinal profiles at specified distance from the right edge or the centre line of road lane [2]. In Slovakia, thirteen road profiles are processed to calculate the representative IRI value for the segment of road lane [2, 20, 27].

3. Whole-body vibration

ISO 2631-1 [28-29] defines methods for measurement of periodic, random and transient whole-body vibrations. For the comfort of seated persons this clause applies to a frequency range 0.5 to 80 Hz, which occurs in all six axes on the seat pan. Filter W_k specified in ISO 2631-1 is used for frequency weighting in the *z*-direction and all three orthogonal axes on the seat base. Filter W_d is used for the *x*- and *y*- directions at the seat surface.

The WBV was quantified with the vibration total value a_v calculated from six measured signals on the seat surface and seat base in three orthogonal directions: *x*- (longitudinal, i.e. fore-and-aft), *y*- (lateral), and *z*- (vertical). The vibration total value or vector sum a_v of frequency-weighted RMS accelerations is calculated [28] by:

$$a_v = \sqrt{k_{Bx}^2 a_{wBx}^2 + k_{By}^2 a_{wBy}^2 + k_{Bz}^2 a_{wBz}^2 + k_{Sx}^2 a_{wSx}^2 + k_{Sy}^2 a_{wSy}^2 + k_{Sz}^2 a_{wSz}^2} \quad (1)$$

where a_{wSx}, a_{wSy}, a_{wSz} (m/s^2) - the weighted RMS accelerations with respect to the orthogonal axes (*x*-, *y*-, and *z*-) at the seat surface, respectively, a_{wBx}, a_{wBy}, a_{wBz} (m/s^2) - the weighted RMS accelerations at the seat base, k_{Sx}, k_{Sy}, k_{Sz}, k_{Bx}, k_{By}, k_{Bz} - multiplying factors, where $k_{Sx} = k_{Sy} = k_{Sz} = 1$, $k_{Bx} = k_{By} = 0.25$, and $k_{Bz} = 0.4$ for comfort evaluation.

Table 1 presents the scale of the vibration total value a_v acting on a seated human body according to the ISO 2631-1 [28]. The comfort levels in Table 1 correspond to "likely reactions" of passengers in a public transport.

The WBV measurements were provided in a moving vehicle with a compact vibration measurement system [30-31] equipped by the two MEMS three-axial accelerometers CXL04LP3 [32] at passenger's seat surface and seat base (i.e., floor), a GPS sensor - GPS Garmin 18x - 5 Hz [33-34], data acquisition unit DT 9816 [35], acquisition software and a laptop. Figure 1 shows a scheme of an in-situ WBV measurement and evaluation in a test vehicle.

4. Road profile data

Longitudinal road profiles were measured in Slovakia in 2017 by Profilograph GE measuring device. Profile measurements were provided by Road databank of Slovak Road Administration. Profilograph GE records of sixteen parallel profiles (Figure 1). Laser sensor No. 16 typically records the vertical displacement of longitudinal profile at the right edge line of the road lane. Laser sensors No. 2-14 are used that record vertical displacement of the thirteen longitudinal profiles in the transverse distance from 0.3 to 2.4 m from the right edge of the road lane [2, 20, 27]. Sample interval, which is a longitudinal distance between data capture points, was 52.91 mm.

Technical specifications of inertial profilograph are presented in [20]. The Profilograph GE consists of: host vehicle - VW multivan, measuring beam equipped by 16 height sensors (single-spot laser sensors LMI SELCOM 5000), odometer, GPS sensors, operating unit, computer, and software Profilograph for Windows®. The Profilograph GE meets the requirements of an ASTM E950 Class 1 [36] profiling device.

Longitudinal road unevenness evaluation in Slovakia (Table 2) is based on thirteen parallel profiles [20] measured by the Profilograph GE. Maximum IRI of those profiles is used as a representative value in a segment of specified length (20 m or 100 m).

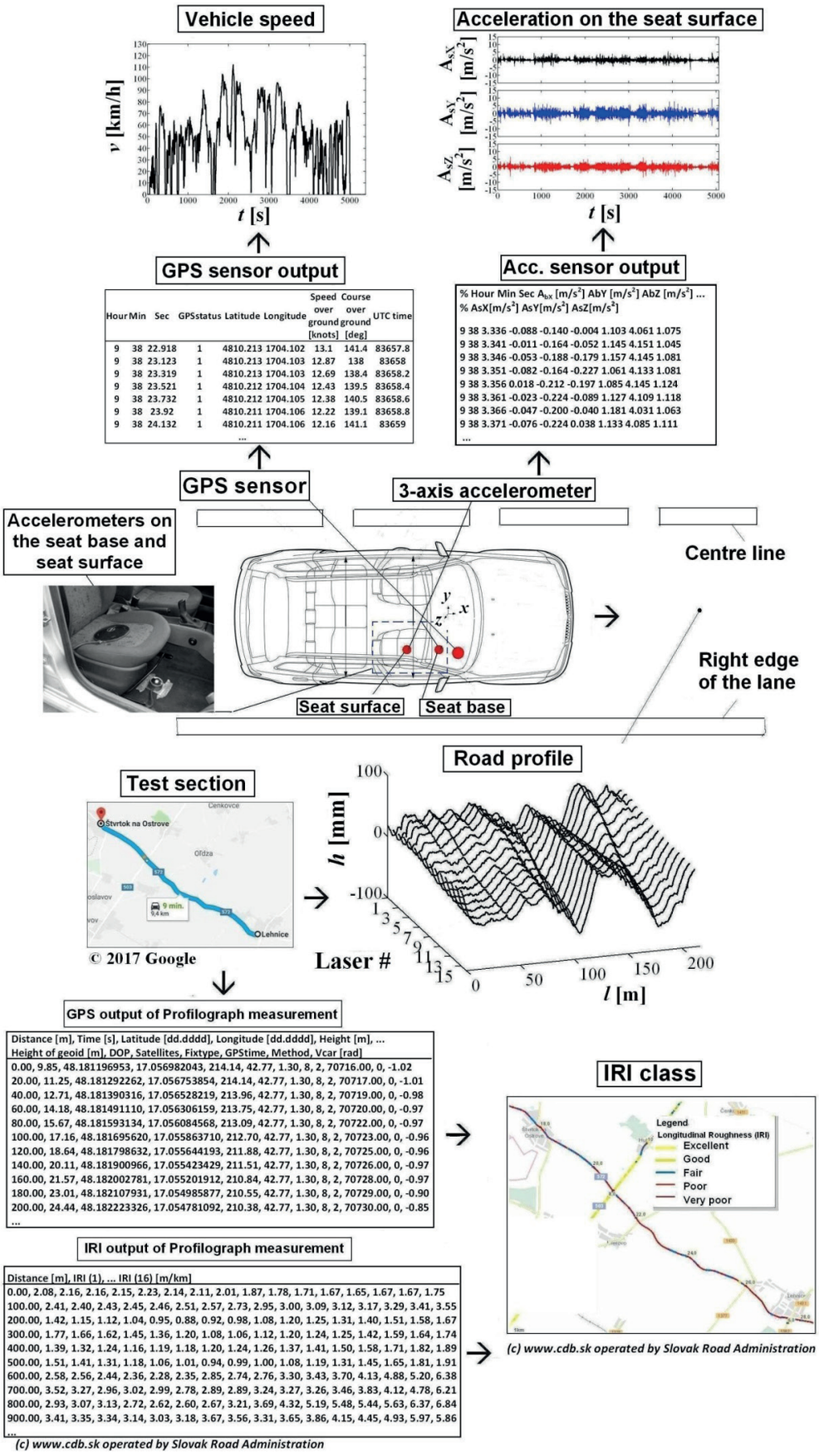

Figure 1 *Scheme of the whole-body vibration measurement in a test vehicle*

Table 3 *Fitting parameters of function IRI = f(a_v,v) [Equation (2)] as a function of road category*

Road category	*N*	Length (km)	b_1	b_2	b_3	RMSE	*R*	R^2
Motorways	3808	380.8	1.859	-0.011	1.251	0.554	0.374	0.140
1st class roads	4684	468.4	5.145	-0.05	3.058	1.1039	0.653	0.427
2nd class roads	5462	546.2	4.472	-0.049	4.651	1.4526	0.518	0.268
1st and 2nd class roads	10146	1014.6	5.696	-0.059	3.866	1.4027	0.645	0.416

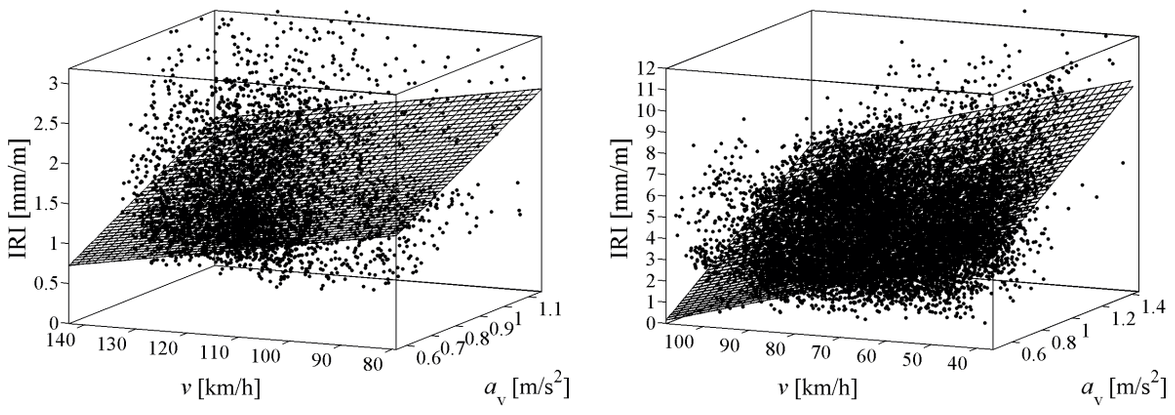

Figure 2 *Relation IRI = f(a_v,v) for all the test vehicles as a function of road category: a) motorways, (b) the 1st and 2nd class roads*

5. Test vehicles survey

Nine test vehicles that are representatives of the best-selling cars in Slovakia in recent years and typical representatives of current vehicle fleet were used: Skoda Fabia II, Skoda Octavia, Skoda Rapid, Skoda Citigo, Skoda Yeti, Skoda Superb, Hyundai i40 combi, Volkswagen Golf Plus, and Ford Transit.

Six different vehicle categories were considered: small and large family car, limousine, city car, sport utility vehicle (SUV) and a cargo van. Vehicles were produced between years 2005 and 2017 and actual vehicle millage was from 1 600 km to 120 000 km. An average time elapsed between the profile measurement and WBV measurement was about 4 months. All measurements were conducted on the same passenger with the weight of 85 kg. Two different test drivers of weight 75 kg and 90 kg conducted the tests.

6. Whole-body vibration and IRI road classes

The IRI data were evaluated by Profilograph GE [20] in sixteen parallel longitudinal profiles and sampled at report interval of 100 m and stored with corresponding geographic coordinates - latitude and longitude data (Figure 1).

The GPS coordinates of the WBV response in a vehicle were synchronized with the GPS data of profile measurements. Processed data should fulfil following conditions for partial processed interval of 100 m:

- Coefficient of variation of a vehicle speed is lower than 10 %;
- Difference in identified start points and final points of a 100-m segment between the WBV and profile measurements is lower than 5 % of the segment length (i.e., 5 m).

The total length of measured sections was about 1860 km and after elimination of section that does not fulfil the abovementioned conditions ~ 1400 km was used for analysis.

Based on processing of measured data, a three-parameter relation between the IRI, a_v and *v* was identified as the most appropriate, which is expressed as follows:

$$\text{IRI} = b_1 a_v + b_2 v + b_3, \tag{2}$$

where b_1, b_2, b_3 are constants of a fitting function. Table 3 shows identified fitting function parameters (Equation 2) for the processed road categories. The lower correlation was expected between IRI and a_v in Table 3. Representative value of the IRI in each 100-m segment is based on the maximum IRI value of thirteen measured profiles. This profile may be different from current wheel paths of a test vehicle. Measurements were provided in nine different test vehicles of different vehicle categories and different vibrations response characteristics. Figure 2 shows measured data of relation of IRI and a_v and *v*, fitted by the regression function (Equation 2) for all the tested vehicles and the two road categories: motorways (Figure 2(a)) and the and 2nd class roads (Figure 2(b)). Parameters of fitting function used in Figure 2 are presented in Table 3. Equation 2 may serve for a basic estimation of IRI values as a function of a passenger's vibrations and speed.

Table 4 shows statistics (mean, standard deviation, percentiles P10, P25, P50, P75, and P90) of total acceleration a_v as a function of IRI road classes for all the nine tested vehicles and all tested sections. Processed test sections on motorways covered only first three IRI road classes used in the Slovak Republic.

Median a_v value (P50) exceeds the lower bound of expected "uncomfortable" human reaction (a_v = 0.8 m/s^2, Table 1) for all three IRI road classes (#1 - #3) and motorways and three IRI road

Table 4 *Vibration total value statistics as a function of IRI road classes and road category*

N	Length (km)	IRI road class	*v* (km/h)		IRI (mm/m)				Vibration total value a_v (m/s²)						
			mean	std	min	max	mean	std	mean	std	P10	P25	P50	P75	P90
Motorways															
2940	294	1	118.3	14.4	0	1.9	1.2	0.32	0.804	0.120	0.648	0.725	0.803	0.880	0.954
837	83.7	2	118.5	14.5	1.9	3.3	2.3	0.34	0.883	0.147	0.683	0.787	0.883	0.985	1.069
31	3.1	3	111.5	14	3.3	5	3.7	0.38	0.940	0.255	0.596	0.739	0.972	1.111	1.262
3808	380.8	All	118.3	14.4	0.65	4.31	1.5	0.6	0.823	0.132	0.653	0.734	0.817	0.905	0.990
1st and 2nd class roads															
601	60.1	1	81.1	14.7	0	1.9	1.5	0.28	0.692	0.122	0.546	0.608	0.691	0.761	0.853
2604	260.4	2	76.7	16.9	1.9	3.3	2.6	0.4	0.746	0.14	0.57	0.649	0.738	0.835	0.931
3468	346.8	3	71.8	18.1	3.3	5	4.2	0.49	0.84	0.19	0.606	0.698	0.828	0.958	1.077
3375	337.5	4	68.2	19.1	5	10	6.2	1.02	0.928	0.238	0.644	0.749	0.91	1.074	1.237
98	9.8	5	48.7	10.1	10	-	11	0.95	0.962	0.262	0.602	0.727	1.005	1.165	1.274
10150	1015	All	72.2	18.5	0.71	16.47	4.4	1.84	0.838	0.21	0.596	0.688	0.809	0.959	1.109

Table 5 *Percentage of travelled sections in comfort level according to the ISO 2631-1 as a function of IRI road classes for motorways*

IRI road class	IRI (mm/m)		a_v (m/s²)					
			< 0.315	0.315-0.63	0.5-1	0.8-1.6	1.25-2.5	> 2
	min	max	not uncomfortable	a little uncomfortable	fairly uncomfortable	uncomfortable	very uncomfortable	extremely uncomfortable
Motorways								
1	0	1.9	0	7	95.1	50.9	0.2	0
2	1.9	3.3	0	5.5	76.7	71.6	0.5	0
3	3.3	5	0	12.9	58.1	67.7	9.7	0
All	0	-	0	6.7	90.8	55.6	0.3	0
1st and 2nd class roads								
1	0	1.9	0	31.4	94	16.1	0	0
2	1.9	3.3	0	20.5	92.8	33.4	0.1	0
3	3.3	5	0	13.5	79.1	55.4	2.1	0
4	5	10	0	8.4	64	66.4	9.3	0.1
5	10	-	0	16.3	46.9	68.4	13.3	0
All	0	-	0	14.7	78.1	51.2	4	0

classes (#3 - #5) for the 1st and 2nd class roads (Table 4). For IRI road class #3 and motorways and IRI road class #5 and the 1st and 2nd class roads a lower bound of "very uncomfortable" level (a_v = 1.25 m/s²) was exceeded by the 90th percentile (P90) of a_v (Table 4).

The median values of a_v are shown in Figure 3. Comparison shows higher vibration total value a_v by 17-22 % for motorways in the same IRI road class. Median values of a_v correspond for a "very good" IRI road class #1 of motorways approximately to "fair" IRI road class #3 of the 1st and 2nd class roads. The reason may be in much higher typical speeds on motorways and in behaviour of nonlinear characteristics of vehicle suspension elements.

Table 5 and Figure 4 present the percentage of travelled sections in particular comfort levels according to the ISO 2631-1 as a function of the IRI road class and road category. Number of sections, total length of sections and the IRI statistics is the same as in Table 4. Sum of percentage in all six comfort level groups

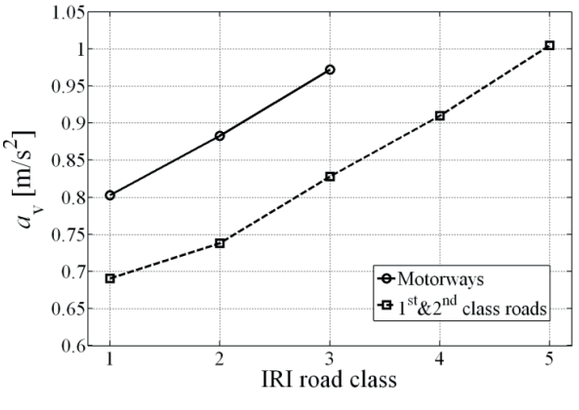

Figure 3 *Median of the passenger vibration total value a_v as a function of IRI road class and road category*

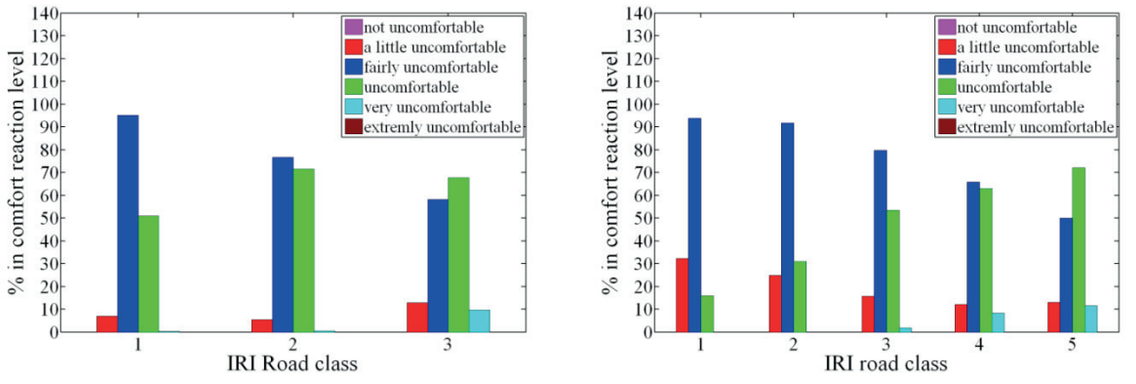

Figure 4 *Percentage of sections in comfort reaction levels according to the ISO 2631-1 as a function of IRI road classes and road category: (a) motorways, (b) the 1st and 2nd class roads*

is over 100 % due to overlapped ranges of particular comfort reaction levels groups (Table 1).

On motorways, 55.6 % of processed segments induced passenger's vibrations higher than the lower bound of expected "uncomfortable" human reaction (0.8 m/s^2) and 0.34 % segments exceeded the lower bound of "very uncomfortable" level. On the 1st and 2nd class roads it was 51.4 % ("uncomfortable") and 4 % ("very uncomfortable").

Results in Table 5 may be commented as follows:

- Negligible portion of sections falls in the best and worst comfort likely reaction levels "not uncomfortable" and "extremely uncomfortable".
- Comfort levels "fairly uncomfortable" and "uncomfortable" prevailed.
- Higher percentage (by 12-38 %) of road segments in the same IRI road class corresponds to "fairly uncomfortable" and "uncomfortable" levels for motorways than for the 1st and 2nd class roads. The comparison is influenced with an unequal number of segments N in groups and higher mean speed by 30 to 40 km/h on motorways on the section of the same road class.
- Road class #1 for motorways and road class #3 for the 1st and 2nd class roads indicate similar percentage of acceleration response in "uncomfortable" category (50.9 % vs. 55.4 %).
- Road class #3 ("fair") for motorways and road class #5 ("very poor") for the 1st and 2nd class roads indicate similar percentage of acceleration response in "uncomfortable" category (67.7 % vs. 68.4 %).

Results in Tables 4 and 5 suggested that IRI threshold values of particular IRI road classes (Table 1) should be a function of the road speed limit or typical travelled speed of a road category. IRI is proportional to the RMS value of suspension relative velocity [37]. The same level of vibrations response can be achieved for two distinct vehicle speeds with consideration of the same RMS value of suspension relative velocity, $\sigma_{vrel}(v_1) = \sigma_{vrel}(v_2)$. Then, the relation for the IRI threshold values should be a function of velocity as follows [38]

$$IRI(v_2) = \left(\frac{v_1}{v_2}\right)^{0.5} IRI(v_1). \qquad (3)$$

Such a choice of the IRI thresholds should meet the same excited suspension relative velocity response for the two different velocities. It should be stated that relation (3) is valid for Gaussian road profiles and vehicle model with linear suspension characteristics. For example, for two speed limits, v_1 = 90 km/h (1st and 2nd class roads) and v_2 = 130 km/h (motorways) it should be hold, IRI(130 km/h) = 0.83 × IRI(90 km/h). Thresholds for the critical road state (IRI road class #5) partially fulfil this assumption. Using Equation (3) to compare IRI thresholds, the correction factor in relation IRI(130) = f(IRI(90)) would be lower at about 0.35-0.5. Used IRI road classifications around the world used sometimes higher IRI thresholds for partial IRI road classes for roads of lower limit speeds [2].

7. Conclusions

A comprehensive overview was provided of the relations between the passenger WBV in a motor vehicle and IRI based on extensive field measurements of a total length of about 1800 km. A summary on this matter has not been previously published in such a wide range.

The novelty of presented results is in estimation of vehicle speed, road category and IRI road class influence on the passenger ride comfort.

The main results of this study were as follows:

1. Parameters of relation between the IRI, passenger vibration total value and vehicle speed were identified as a function of road category. Fitting of measured data suggests that a three-parameter relation is a suitable approximation of this relation.
2. Results specified which combinations of the IRI road class, used in the Slovak Republic, road category and vehicle speed, correspond to particular comfort levels according to the ISO 2631-1.
3. Indication of comfort levels "not uncomfortable" and "extremely uncomfortable" was very rare. Comfort level "fairly uncomfortable" and "uncomfortable" prevailed among comfort categories. About fifty percent of all the processed sections exceeded a lower bound of expected "uncomfortable" reaction (a_v = 0.8 m/s^2). About 4 % of processed sections of

the 1st and 2nd road class exceeded a "very uncomfortable" level.

4. Substantially different passenger's WBV was identified for the same IRI road classes between motorways and the 1st and 2nd class roads. For the same IRI road class, the total passenger vibration was about 20 % higher on motorways. Passenger's WBV for the *i*-th road class of the 1st and 2nd class roads corresponds approximately to the (*i*+2)-th road class of motorways.
5. Experimentally obtained data suggested that the IRI thresholds for partial road classes for motorways should be lower than for the 1st and 2nd class roads to meet approximately the same ride comfort.

Acknowledgements

This work was supported by the Scientific Grant Agency VEGA of the Ministry of Education, Science, Research and Sport of the Slovak Republic and the Slovak Academy of Sciences [Grant No. 2/0089/16]. Authors would like to thank Dinu Covaciu (Transilvania University of Braşov) and Ing. Stanislav Skyva (Road databank of Slovak Road Administration) for consultations and test drivers Mr. Valentovic and Mr. Rozinaj.

References

[1] *TP 024/2006. Pavement management system* (in Slovak). Ministry of Transport, Construction and Regional Development of the Slovak Republic, Bratislava [online], 2006, p. 30. Available from: https://www.ssc.sk/files/documents/technicke-predpisy/tp/tp_024.pdf

[2] MUCKA, P.: International roughness index specifications around the world. *Road Materials and Pavement Design* [online]. 2017, **18**(4), p. 929-965. ISSN 2164-7402. Available from: https://doi.org/10.1080/14680629.2016.1197144

[3] MERRITT, D. K., CHANG, G. K., RUTLEDGE, J. L. *Best practices for achieving and measuring pavement smoothness. A synthesis of state-of-practice*. Report No. FHWA/LA.14/550. Austin, TX: TheTranstec Group, Inc., 2015, p. 58.

[4] WANG, F., EASA, S.: Analytical evaluation of ride comfort on asphalt concrete pavements. *Journal of Testing Evaluation* [online]. 2016, **44**(4), p. 1671-1682. ISSN 0090-3973/e-ISSN 1945-7553. Available from: https://doi.org/10.1520/JTE20140339

[5] AHLIN, K., GRANLUND, J., LUNDSTROM, R. *Whole-body vibration when riding on rough roads - A shocking study*. Rep. 2000:31E. Borlange: Swedish Road Administration, 2002, p. 81. ISSN 1401-9612.

[6] HASSAN, R. A., McMANUS, K. Assessment of interaction between road roughness and heavy vehicles. *Transportation Research Record* [online]. 2003, **1819**, p. 236-243. ISSN 03611981/eISSN 21694052. Available from: https://doi.org/10.3141/1819b-30

[7] IHS, A., GRUDEMO, S., WIKLUND, M. *The influence of road surface condition on driving comfort* (in Swedish). VTI Report No. 957. Linkoping: Swedish National Road and Transport Research Institute, 2004, p. 131.

[8] FICHERA, G., SCIONTI, M., GARESCI, F. Experimental correlation between the road roughness and the comfort perceived in bus cabins. *SAE Technical Paper* [online]. 2007, 2007-01-0352. Available from: https://doi.org/10.4271/2007-01-0352

[9] PERERA, R. W., KOHN, S. D., BYRUM, C. R. *Smoothness criteria for concrete pavements*. Rep. DTFH61-03-C-00105. Washington, DC: Federal Highway Administration, 2009.

[10] WANG, S., ZHANG, J., YANG, Z. Experiment on asphalt pavement roughness evaluation based on passengers' physiological and psychological reaction. In 10th International Conference of Chinese Transportation Professionals (ICCTP) 2010: Integrated Transportation Systems: Green, Intelligent, Reliable : proceedings. H. Wei, Y. Wang, J. Rong, J. Weng, eds. American Society of Civil Engineers, Reston, VA, 2010. ISBN 978-0-7844-1127-8, p. 3852-3863.

[11] ZHANG, J., DU, Y., SU, R. Investigating the relationship between pavement roughness and heart-rate variability by road driving test. In 3rd International Conference on Road Safety and Simulation, Transport Research Board : proceedings [online]. Washington, DC, 2011. Available from: http://onlinepubs.trb.org/onlinepubs/conferences/2011/RSS/2/Zhang,J.pdf

[12] GRANLUND, J. Ride vibration and road condition. In ROADEX IV Final Seminar [online]. The ROADEX Implementing Accessibility Project, The Northern Periphery Programme. Rovaniemi, Finland, 2012 [accessed 2015-05-14]. Available from: http://www.roadex.org/wp-content/uploads/2014/01/11.-Ride-vibration-and-road-condition-J-Granlund.pdf>(May. 14, 2015).

[13] LEE, D.-H., et al. Study about the evaluation of driving stability using 3-axis accelerometer test. *Journal of the Korean Society of Road Engineers.* 2012, **14**(3), p. 141-149.

[14] HU, J., et al. *Research on comfort and safety threshold of the pavement roughness*. Report No. 17-02974. Transportation Research Board 96th Annual Meeting. Washington DC, United States: Transportation Research Board, 2017, p. 14.

[15] ZURAULIS, V., PECELIUNAS, R., JAKUTIS, G. Semi-active suspension influence on comfort sensation of a vehicle occupant. *Agricultural Engineering* [online]. 2014, **46**(1), p. 116-124. ISSN 1392-1134/eISSN 2345-0371. Available from: https://doi.org/10.15544/ageng.2014.011

[16] MUCKA, P. Road roughness limit values based on measured vehicle vibration. *Journal of Infrastructure Systems* [online]. 2017, **23**(2), p. 1-13. ISSN 1076-0342/eISSN 1943-555X. Available from: https://doi.org/10.1061/(ASCE)IS.1943-555X.0000325

[17] SAYERS, M. W. On the calculation of international roughness index from longitudinal road profile. *Transportation Research Record* [online]. 1995, **1501**, 1995, p. 1-12. ISSN 0361-1981/ eISSN 2169-4052. Available from: http://onlinepubs.trb.org/Onlinepubs/trr/1995/1501/1501-001.pdf

[18] *prEN 13036-5. Road and airfield surface characteristics - Test methods. Part 5: Determination of longitudinal unevenness indices*. Brussels: European Committee for Standardization (CEN), 2017.

[19] *E1926-08. Standard practice for computing International Roughness Index of roads from longitudinal profile measurements*. West Conshohocken, PA: ASTM, 2015.

[20] *TP 056/2012. Measurement and evaluation of road roughness using Profilograph GE* (in Slovak). Ministry of Transport, Construction and Regional Development of the Slovak Republic, Bratislava, SR [online], 2012, p. 20. Available from: https://www.ssc.sk/files/documents/technicke-predpisy/tp/tp_056.pdf

[21] *TP 057/2018. Methodology for using HDM-4 in the conditions of Slovak republic* (in Slovak), Ministry of Transport, Construction and Regional Development of the Slovak Republic, Bratislava, SR [online], 2018, p. 79. Available from: https://www.ssc.sk/files/documents/technicke-predpisy/tp/tp_057.pdf

[22] KOVAC, M., et al. *Diagnostic of Parameters of Roads Operational Capability (in Slovak)*. Zilina: EDIS, University of Zilina, 2012. ISBN 978-80-554-0568-1.

[23] CELKO, J., et al. Pavement diagnosis as integrant of the pavement system. *Communications - Scientific Letters of the University of Zilina* [online]. 2008, **10**(2), p. 44-49. ISSN 1335-4205/eISSN 2585-7878. Available from: http://komunikacie.uniza.sk/index.php/communications/article/view/1044

[24] CELKO, J., KOVAC, M., DECKY, M. Analysis of selected pavement serviceability parameters. *Communications - Scientific Letters of the University of Zilina* [online]. 2011, **13**(3), p. 56-62. ISSN 1335-4205/eISSN 2585-7878. Available from: http://komunikacie.uniza.sk/index.php/communications/article/view/864

[25] MIKOLAJ, J., REMEK, L., PEPUCHA, L. Overview of the road network management system. *Communications - Scientific Letters of the University of Zilina* [online]. 2014, **16**(4), p. 53-57. ISSN 1335-4205/eISSN 2585-7878. Available from: http://komunikacie.uniza.sk/index.php/communications/article/view/576

[26] DECKY, M., KOVAC, M. *The longitudinal road evenness of the road network* (in Slovak). Zilina: EDIS, University of Zilina, 2014. ISBN 978-80-554-0925-2.

[27] MUCKA, P.: Porovnanie klasifikacie pozdĺznej nerovnosti podla IRI v Slovenskej a Ceskej republike (Comparison of the classification of longitudinal road unevenness according to IRI in the Slovak Republic and the Czech Republic). *Silnicni Obzor.* 2018, in print. ISSN 0322-7154.

[28] *ISO 2631-1. Mechanical vibration and shock - Evaluation of human response to whole-body vibration. Part I: General requirements*. Geneva, Switzerland: International Standardization Organization, 1997.

[29] GRIFFIN, M. J. Discomfort from feeling vehicle vibration. *Vehicle Systems Dynamics* [online]. 2007, 45(7-8), p. 679-698. ISSN 0042-3114/eISSN 1744-5159. Available from: https://doi.org/10.1080/00423110701422426

[30] STEIN, G. J., CHMURNY, R., ROSIK, V. Compact vibration measuring system for in-vehicle applications. *Measurement Science Review* [online]. 2011, **11**(5), p. 154-159. ISSN 1335-8871. Available from: https://doi.org/10.2478/v10048-011-0030-1

[31] STEIN, G. J., CHMURNY, R., ROSIK, V. Measurement and analysis of low frequency vibration. *Measurement Science Review* [online]. 2007, **7**(4), p. 47-50. ISSN 1335-8871. Available from: http://www.measurement.sk/2007/S3/Stein.pdf

[32] Crossbow CLX Series Datasheet. *Crossbow Technology* [online]. San Jose, CA [accessed 2018-05-01]. Available from: https://www.willow.co.uk/LP1.pdf

[33] GPS 18x Technical Specifications. *Garmin International, Inc*. [online]. Olathe, KS, Oct 2011 [accessed 2018-04-30]. Available from: https://static.garmincdn.com/pumac/GPS_18x_Tech_Specs.pdf

[34] COVACIU, D, PREDA, I, CIOLAN, G. GPS based data acquisition system for mobile applications. *Acta Technica Jaurinensis* [online]. 2011, **4**(4), p. 453-464. eISSN 2064-5228. Available from: https://acta.sze.hu/index.php/acta/article/view/265

[35] DT9816 Series User's Manual. *Data Translation, Inc.* [online]. Locke Drive Marlboro, MA, 2015, p. 108 [accessed 2018-04-30]. Available from: https://datatranslation.box.com/shared/static/9c7ad0d4l4e6a3f67795.pdf

[36] *ASTM E950/E950M-09. Standard test method for measuring the longitudinal profile of traveled surfaces with an accelerometer established inertial profiling reference.* West Conshohocken, PA: ASTM International, 2009.

[37] SUN, L., ZHANG, Z., RUTH, J. Modeling indirect statistics of surface roughness. *Journal of Transportation Engineering* [online]. 2001, **127**(2), p. 105-111. ISSN 0733947X. Available from: http://citeseerx.ist.psu.edu/viewdoc/download?doi=10.1.1.716.4546&rep=rep1&type=pdf

[38] MUCKA, P. Influence of profile specification on International Roughness Index. *Journal of Infrastructure Systems.* 2018, accepted for publication. ISSN 1076-0342/eISSN 1943-555X.

https://doi.org/10.26552/com.C.2019.1.22-27

Miroslav Neslusan - Jan Moravec*

INFLUENCE OF COMPONENTS BENDING ON THE CONSECUTIVE PLASMA NITRIDATION AND BARKHAUSEN NOISE EMISSION

This paper deals with the non destructive evaluation of components after the plasma nitridation via the Barkhausen noise techniques. Effect of different surface states before the plasma nitriding is studied via the non destructive Barkhausen noise technique, as well as the conventional destructive techniques. Bending of flat samples to different bending angles was performed and magnetic, as well as conventional destructive testing, was carried out on the outer, inner and flat surfaces. The results of experiments show that the Barkhausen noise emission is a function of the heat treatment, whereas intensity of bending and the corresponding deformation are only minor. The different states of the surface before the plasma nitriding result into the similar thickness of the compound layer. Furthermore, the underlying diffusion of near the surface layer state is different.

Keywords: *bending, plasma nitridation, Barkhausen noise*

1. Introduction

Nitriding is the outstanding concept in which the hard surface is mixed with the tough core. Nitriding thermo chemical process is usually conducted to improve fatigue life, wear or corrosion resistance of the components' surface [1-4]. High hardness of nitrided layers originates from hard nitride micro precipitates due to low solubility of nitrogen in α-iron. Nitrogen is produced by decomposition of ammonia NH_3 atmosphere and diffusion layer (as the main nitriding region) is coated by the adjoining compound layer. The diffusion layer usually contains small volume of nitrogen dissolved in α-iron together with the face-centered cubic γ'-nitride Fe_4N and hexahedral ε-nitride $Fe_{2-3}N$ (sometimes orthorhombic ζ-nitride Fe_2N) [2]. On the other hand, the compound layer is entirely composed of ε and γ' nitrides its thickness is much less compared to diffusion one. Nitriding is widely used in the automotive industry, in the forging industry for the enhancement of forge dies and in the die-casting industry. As opposed to the carburizing, nitriding requires the lowest temperatures (up to 550 °C) of all the thermo chemical diffusion techniques [2]. This means that steel does not undergo any phase transformations. Moreover, the high hardness of nitrided layers is initiated directly during the diffusion process, whereas case - carburized components require subsequent heat treatment. On the other hand, nitriding cannot be completed in the cycle time of the carburizing process. The nitriding process can be carried out in a variety of manners. Except gaseous, salt bath or fluidized bed, the plasma nitriding is widely used in many real industrial applications, as well. The physical principle of this procedure is based on the glow discharge plasma assisted decomposition of N_2. The surface is heated by bombardment with highly energetic positive ions in the plasma.

As opposed to the conventional gas nitriding, plasma nitriding produced compound layer free of porous, better dimensional accuracy of components, higher ductility of nitrided layers, better mechanical properties, surface free annealing and remarkable reduction in the nitriding time. Numerous investigations focused on plasma nitriding procedure have been conducted using various nitriding regimes as well as materials. Marot at al. [5] found that improved nitrogen transport can be obtained after nitridation in NH_3 plasma without cathodic bias on the samples. Such cold conditions allow the iron matrix to be nitrided in a depth range of 100-400 μm at a temperature as low as 350 °C.

The main disadvantage of the plasma nitriding can be viewed in more complex process control due to many parameters affecting metallurgy of nitrided components, such as nitriding time, temperature of the workpiece and chamber, process gas, work and support fixturing area, power voltage, current density, vacuum level, pulses duration, etc. For this reason, the plasma nitriding process needs quite a sophisticated process control, as well as the post processing validation in which the plasma nitridation parameters are correlated with the surface state of components, expressed in such terms as thickness of diffusion and compound layers, their chemistry, hardness profile, surface defects, etc. For instance, Flori at al. [6] analyzed an industrial plasma-nitrided sample which was detected having two types of defects: an external defective layer covering almost all the surface of the nitrided case and a structure with segregations bands. The authors analyzed the samples after plasma nitriding by means of the X-ray photoelectron spectroscopy, electron probe microanalysis, light microscopy and microhardness measurements, for a better understanding of phenomena taking place at the industrial plasma nitriding of steels as well as more accurate valuation of the technological parameters of this thermo chemical treatment. The post processing validation is usually executed via the long

* **Miroslav Neslusan, Jan Moravec**
Faculty of Mechanical Engineering, University of Zilina, Slovakia
E-mail: mirolav.neslusan@fstroj.uniza.sk

Figure 1 *Samples after bending*

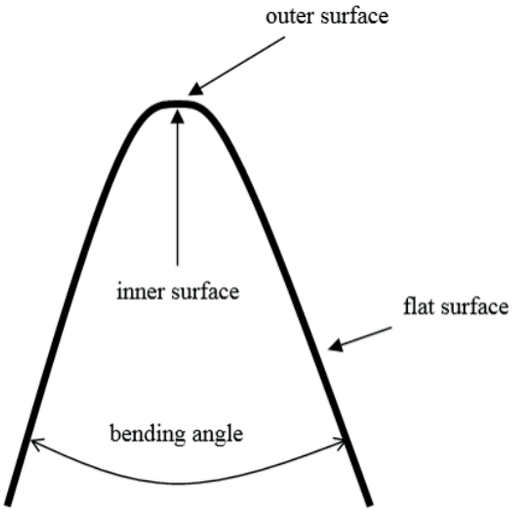

Figure 2 *Brief sketch of the sample bending and analysed surfaces*

term and high costs destructive tests, such as metallographic observations, micro indentation and application of the SEM, XRD or other techniques. Being so, any reliable non destructive concept, developed for such purpose, would be beneficial.

One of the possible aspects of the plasma nitriding process is preparation of the surface prior to plasma nitriding. Expressed in other words, samples history - especially the surface state - could vary due to micro and macro geometry, as well as the surface hardening, intensity of mechanical and thermal load, corresponding dislocation density, density of crystalline lattice defects or microstructure. Industrial experience indicates that for instance components undergoing intensive plastic deformation (for instance bending) could suffer from unstable compound layer, as well as the lower hardness of diffusion layer, when the consecutive plasma nitriding process is carried out after bending.

It is well known that the Bloch Walls (BWs) in ferromagnetic bodies, during their motion, interfere with all the crystalline defects such as grain boundaries, dislocation cell, precipitates as well as other non ferromagnetic phases [7-12]. The compound layer, entirely composed of nitrides, should be considered as the non ferromagnetic region progressively decreasing the magnetic Barkhausen noise (MBN) received on the free surface along with gradual increase in its thickness. Moreover, the fine nitrides, embedded within the diffusion layer, strongly pin the BWs thus contributing to the lower MBN emission [13-15]. Being so, the BN technique would be promising method for the non destructive post processing monitoring of nitriding (focused on plasma nitriding in this study). The BN originate from irreversible and discontinuous BWs motion and the BN emission is strongly related to microstructure state, as well as to the stress state. The plasma nitriding process remarkably alters the microstructure in the diffusion layer since it establishes very fine nitrides hindering the BWs motion. Thus, the different density of nitrides would affect the MBN emission.

A concept in which components after the plasma nitriding process could be monitored via the BN should be based on contrast between the high MBN emission, associated with reduced nitrides density, and vice versa. This paper discusses the potentials of the MBN technique for monitoring components of variable bending angle and the consecutive plasma nitriding process.

2. Conditions of experiments

The MBN measurement was performed by use of the Rollscan 350 device and software package μScan in the frequency range of 10 to 1000 kHz (magnetizing frequency 125 Hz, magnetizing voltage 5 V, 10 bursts and therefore 5 magnetizing cycles). The magnetic measurements were carried out in the axial direction (direction perpendicular to the direction of bending stress). Estimated sensing depth is about 50 μm.

The Vickers microhardness readings were conducted by the Härteprüfgerät EMCO N3D micro-hardness tester by applying force of 50 g for 10 seconds. Microhardness was determined by averaging 3 repetitive measurements (3 microhardness profiles spaced 0.1 mm). To reveal the microstructure transformation, induced by the nitriding process, 20 mm long pieces were routinely prepared for metallographic observations (hot molded, ground, polished and etched by 3% Nital for 10 seconds). Four series of flat samples (150x30x4 mm) were made of steel 16MnCr5. Each series contains 5 samples bended on variable bending angle in the range 0 ÷ 90° as Figure 1 illustrates. Figure 2 shows the analyzed areas on the samples. The first series was bent; the second one was annealed in the furnace at temperature 650°C for 2 hours. The third series was annealed after bending and plasma nitrided afterwards. The last series was only plasma nitrided after bending. the plasma nitriding process was performed at temperature 485°C for 8 hours.

3. Results of experiments

Figure 3 illustrates metallographic observation of bent surfaces for two different bending angles. It is obvious that the surface matrix is strained in direction of the applied stress. It is well known that the dislocation slip is initiated as soon as the yield stress of the material is exceeded. Increasing intensity of

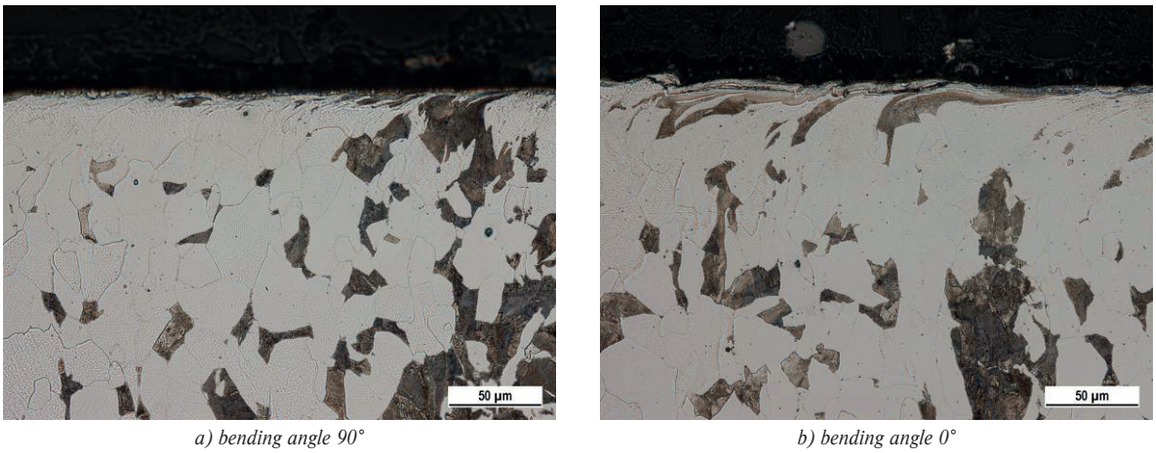

a) bending angle 90° *b) bending angle 0°*

Figure 3 *Metallographic images of surface after bending - the inner surface*

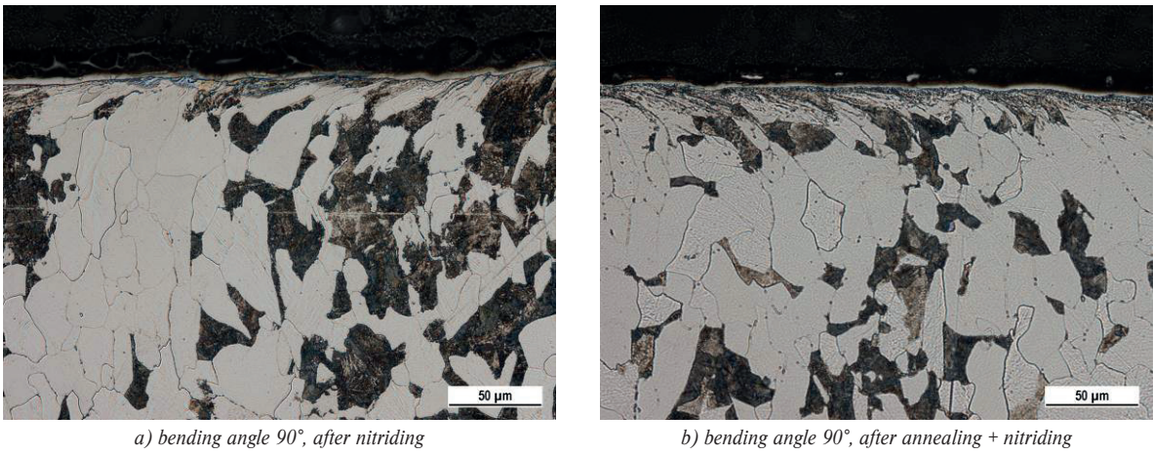

a) bending angle 90°, after nitriding *b) bending angle 90°, after annealing + nitriding*

Figure 4 *Metallographic images of the inner surface*

bending (plastic deformation) increases dislocation density in the deformed surfaces. Therefore the thickness of the layer affected by plastic deformation increases together with plastic strain. Such behavior takes place when bending angle is increasing from 90 ° up to the 0 °. The bending process produces tensile stresses in the outer surface of the samples, whereas the inner one is compressed. For this reason, unstressed samples contain compressive residual stresses in the outer surface and tensile residual stresses in the inner surface.

Increasing bending angle from 90° up to the 0° increases density of the lattice defects (especially dislocation density). Increasing dislocation density and the transformation processes affect the consecutive plasma nitriding process in two contradictory effects. The first one enhances nitrides to be embedded in the matrix since dislocation cells are clustered by vacancies as preferential sites for nitrides. The second effect hinders embedding nitrides in the matrix, as soon as the density of lattice defects exceeds the critical threshold.

Metallographic observation of the outer, as well as inner surfaces, after the plasma nitriding process and combination of annealing + nitriding is depicted in Figures 4 and 5. These images illustrate thin compound layer entirely composed of nitrides, which appears as white. The underlying structure represents the mixture of the steel matrix and very fine nitrides. However, the nitrides are very fine and cannot be seen on metallographic figures (neither on the SEM scans). The detailed analysis indicates that the thickness of compound layers for the inner and outer surface, as well as for variable bending angles, is similar (see also Figures 6 and 7) and varies in the range from 1 up to 3.5 µm.

From the MBN point of view, the compound layer is considered as a non-ferromagnetic layer not contributing to the MBN received by the pick-up coil on the free surface. Moreover, thickness of the compound layer is much less than that of the MBN sensing layer (about 50 µm). The compound layer is therefore considered as the gap between the pick-up coil and the steel matrix. This layer contributes to the MBN signal attenuation, as well as makes the magnetic field in the steel matrix weaker.

Certain differences can be found considering microhardness of the diffusion layer (see Figure 8). On one hand, the microhardness in the deeper region is slightly lower for only nitrided samples. On the other hand, the difference in the microhardness increases in the near the surface layer, thus in the bending affected zone and the MBN sensitive layer.

Figure 9 depicts that the flat surface exhibits nearly the same MBN emission. Such a behavior is associated with the fact that these surfaces remain unaffected by the bending process. Therefore, annealing does not take a significant role in the consecutive plasma nitriding process. On the other hand, Figures

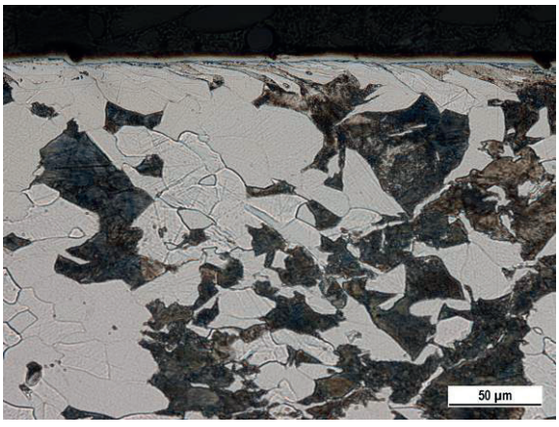

a) bending angle 90°, after nitriding

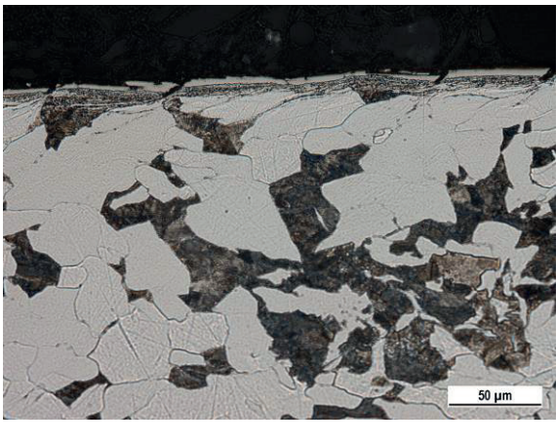

b) bending angle 90°, after annealing + nitriding

Figure 5 *Metallographic images of the outer surface*

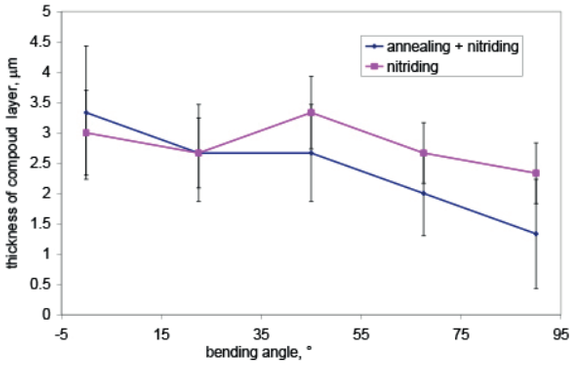

Figure 6 *Thickness of the compound layer versus the bending angle - the inner surface*

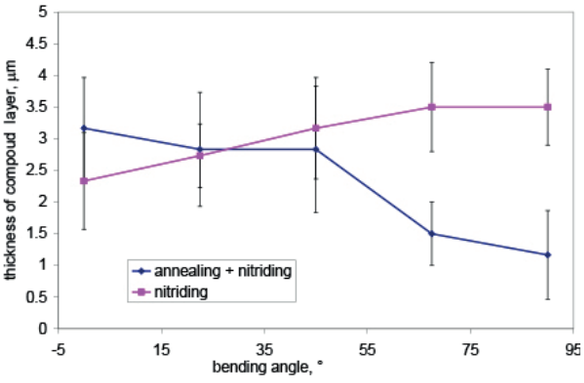

Figure 7 *Thickness of the compound layer versus the bending angle - the outer surface*

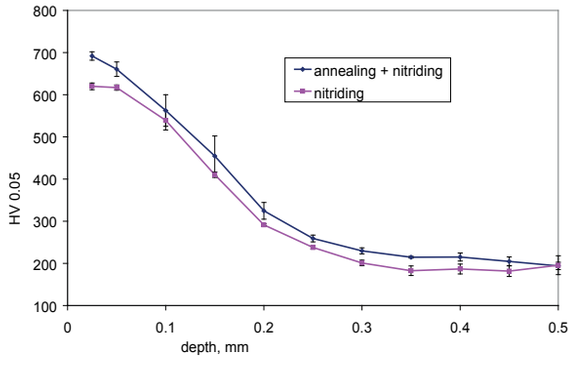

Figure 8 *Microhardness profiles for the inner surface, bending angle 90°*

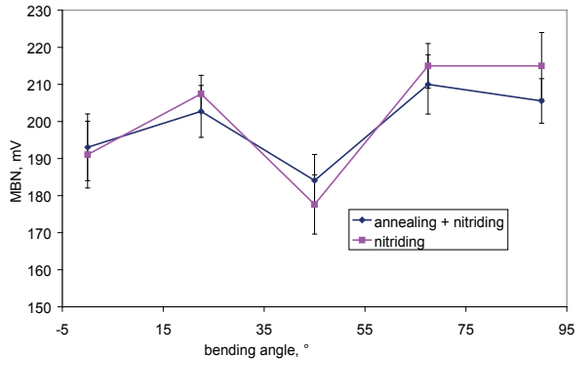

Figure 9 *MBN versus the bending angle - flat surface*

10 and 11 clearly show that the MBN emission for annealed + nitrided surfaces is remarkably lower than for the surface undergoing only the nitriding process after bending.

As it was mentioned above, the compound layer does not contribute to the MBN emission received on the free surface. Being so, the differences between the MBN values, considering the different regimes of the heat treatment, should be associated with the diffusion matrix as the region below the compound layer. Its properties can be easily expressed in term of microhardness, since the hardness of a body after nitriding is driven by the density of the nitrides. Nitrides in the matrix strongly hinder the domain walls motion. For this reason, the lower MBN emissions for annealed + nitrided samples are attributed to the higher density of nitrides, which in turn corresponds to the higher microhardness on the matrix. Such finding can be supported by the number of the MBN pulses as they are illustrated in Figure 12. These pulses more or less correspond with the density of nitrides and therefore number of collisions of domains walls with these nitrides [13]. It can be clearly found that the number of detected MBN pulses for only nitrided samples is lower than that for annealed and nitrided

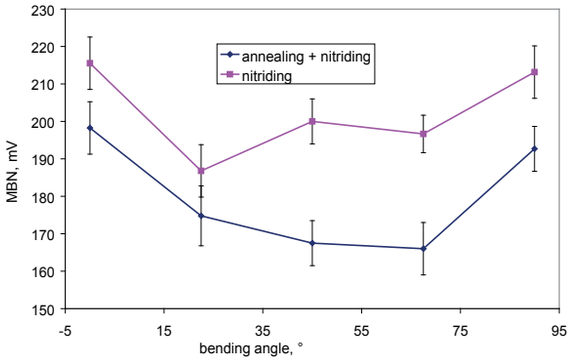

Figure 10 *MBN versus the bending angle - inner surface*

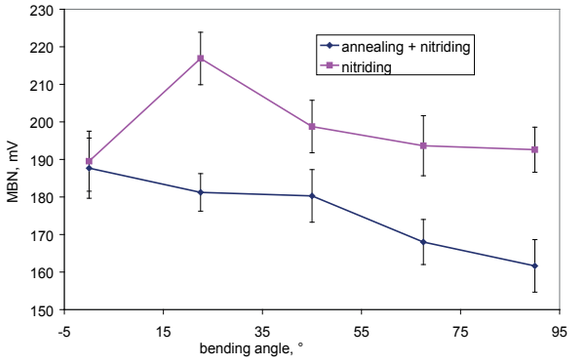

Figure 11 *MBN versus the bending angle - outer surface*

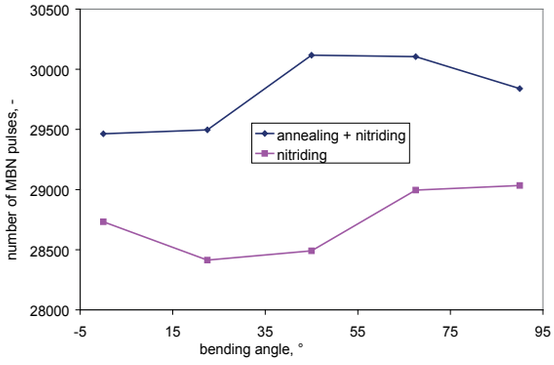

Figure 12 *MBN pulses versus the bending angle - the inner surface*

samples. It seems that annealing before nitriding process can contribute to the higher hardness of the diffusion layer and can be easily and directly measured via the MBN technique.

Figures 10 and 11 also demonstrate that the influence of the bending angle and therefore intensity of the plastic deformation on the nitriding process is complicated. The inner surface does not exhibit monotonous evolution of the MBN against the bending angle. On the other hand, the MBN values tend to increase with increasing intensity of the plastic deformation (when the bending angle decreases from 90° to 0°).

4. Conclusions

It is necessary to notice that other BN parameters (except conventional rms value) could be potentially extracted from the raw BN signal as well and used for the non destructive monitoring of surfaces such as MBN envelopes, position of envelope maximum, number of the BN pulses, etc. This is only the pilot study focused on monitoring surfaces after the plasma nitriding and further analysis will be carried out in the near future. However, this study indicates that the MBN emission is a promising technique for monitoring of components after the nitriding process.

Acknowledgement

This study was supported by the VEGA project n. 1/0121/17 and KEGA project n. 008ZU-4/2018.

References

[1] TOTTEN, G. E. *Steel Heat Treatment*. 2nd ed. Oregon: Taylor&Francis Group, 2006. ISBN 9780849384554.

[2] MIRJANI, M., et al. Investigation of the effects of time and temperature of oxidation on corrosion behavior of plasma nitrided AISI 4140 steel. *Surface & Coatings Technology* [online]. 2012, **206**(21), p. 4389-4393. ISSN 0257-8972/eISSN 1879-3347. Available from: https://doi.org/10.1016/j.surfcoat.2012.04.064

[3] ATAPOUR, M., ASHRAFIZADEH, F. Cyclic oxidation of plasma nitrided valve steels. *Physics Procedia* [online]. 2012, **32**, p. 853-860. ISSN 1875-3892/eISSN 1875-3892. Available from: https://doi.org/10.1016/j.phpro.2012.03.646

[4] NADDAF, M., et al. Nitridation of steel using a microwave ECR plasma. *Vacuum* [online]. 2002, **64**, p. 163-168. ISSN 0042-207X/eISSN 1879-2715. Available from: https://kundoc.com/pdf-nitridation-of-steel-using-a-microwave-ecr-plasma-.html

[5] MAROT, L., et al. Improved nitrogen transport in Fe-C alloys during NH_3 plasma nitridation. *Materials Letters*. 2000, **44**, p. 35-38. ISSN 0167-577X/eISSN 1873-4979.

[6] FLORI, M., et all. (2008). *EPMA and microstructural analysis of a defective industrial plasma-nitrided steel*. Surf. & Coat. Technol. 202, pp. 5887-5894.

[7] MOORTHY, V., et al. Evaluation of heat treatment and deformation induced changes in material properties in gear steels using magnetic Barkhausen noise analysis. Conference ICBM 03 : proceedings. Tampere, Finland, 2001, p. 63-84.

[8] RANJAN, R., et al. Magnetic properties of decarburized steels: An investigation of the effects of grain size and carbon content. *IEEE Transactions on Magnetics* [online]. 1987, **23**(3), p. 1869-1876. ISSN 0018-9464. Available from: https://doi.org/10.1109/TMAG.1987.1065175

[9] CIZEK, J., et all. Modification of steel surfaces induced by turning: non-destructive characterization using Barkhausen noise and positron annihilation. *Journal of Physics D: Applied Physics.* 2014, **47**(44), p. 1-17. ISSN 0022-3727/eISSN 1361-6463.

[10] NESLUSAN, M., et al. Monitoring of grinding burn via Barkhausen noise emission in case-hardened steel in large-bearing production. *Journal of Materials Processing Technology* [online]. 2017, **240**(C), p. 104-117. ISSN 0924-0136/eISSN 1873-4774. Available from: https:// doi.org/ 10.1016/j.jmatprotec.2016.09.015

[11] MICUCH, M., et al. Micro magnetic study of cutting conditions and grinding wheel wear influence on surface integrity. *Manufacturing Technology*. 2014, 14(1), p. 66-71. ISSN 1213-2489.

[12] NESLUSAN, M., et. al. Application of Barkhausen noise for analysis of surface integrity after hard turning. *Manufacturing technology*. 2012, 12(12), p. 60-65. ISSN 1213-2489.

[13] FARDA, R. Vplyv rezimu tepelneho a chemicko-tepelneho spracovania na emisiu Barkhausenovho sumu (Impact of the thermal and chemical-heat treatment regime on the emission of Barkhausen noise). Zilina, KOVT SjF ZU, 2017.

[14] NESLUSAN, M., et. al. (2015). Barkhausen noise Emission in milled Surfaces. *Communications - Scientific Letters of the University of Zilina* [online]. 2015, **17**(3), p. 57-61. ISSN 1335-4205/eISSN 2585-7878. Available from: http://komunikacie.uniza.sk/index.php/communications/article/view/447

[15] DUBEC, J., et al. Influence of tool workpiece interface on surface integrity after turning. *Communications - Scientific Letters of the University of Zilina* [online]. 2014, **16**(3A), p. 200-205. ISSN 1335-4205/eISSN 2585-7878. Available from: http://komunikacie.uniza.sk/index.php/communications/article/view/567

Oleksij Fomin - Juraj Gerlici - Alyona Lovska - Kateryna Kravchenko
Pavlo Prokopenko - Anna Fomina - Vladimir Hauser*

DURABILITY DETERMINATION OF THE BEARING STRUCTURE OF AN OPEN FREIGHT WAGON BODY MADE OF ROUND PIPES DURING ITS TRANSPORTATION ON THE RAILWAY FERRY

In order to reduce the cost of designing and manufacturing of the new-generation open wagons, it is proposed to construct their carrying systems from round pipes. In order to exploit the proposed designs of wagons in international rail-water communication, it is assumed that they will be equipped with assemblies for fastening of chain binders. The maximal values of accelerations, as components of dynamic load acting on open wagons, made from round pipes during their transportation on a railway ferry, are determined. It is established that when moving the body in the vertical direction for a wagon located on the upper deck, the maximum acceleration value is 0.84 g, with angular displacement relative to the transverse axis for the extreme from the anchor point of the wagon body - is 0.1 g, with angular displacement around the longitudinal axis for the extreme from the bulwark of the body of the wagon - is 0.24 g. The conducted researches will enable increased efficiency of operation of open wagons through international transport corridors.

Keywords: *open freight wagon, bearing structure, strength, loading, rail-ferry transportation*

1. Introduction

The increased rates of cargo transportation across the territory of Ukraine, which is a link of the more important transport corridors between Europe and Asia, call for introduction of the new designs of wagons, with improved technical and operational parameters. It is known that one of the most demanded types of cars is an open wagon. In order to increase the efficiency of the open wagon operation and reduce the cost of their production, it is necessary to find new alternative solutions for their design while ensuring the conditions of durability and operational reliability [1-4].

2. Analysis of recent research

The research work of the Omsk State Technical University (Omsk) is devoted to the study of the strength of the open wagons' bodies, made of aluminium alloys, taking into account the physical nonlinearity of the material. In this case, a generalized method of forces [5] is used. However, attention was not paid to determination of stresses in the elements of the body of an open wagon, during its transportation on a railway ferry.

The question of the possibility of the service life extension of an open car in operation is considered [6]. The method of technical diagnostics of open wagons is developed, based on which it is proposed to determine the final service life of open wagons based on calculations of strength, stability and remaining life.

It should be noted that the finite element model of the open wagon, presented in [6] did not take into account the possibility of applying the loads acting on it through means of fastening, relative to the decks of the railway ferries. Recommendations on use of the software for assessing the performance of railway transport facilities are given in [7]. Due to the fact that, when using of modern methods for strength analysis, there is no recommendation on the required degree of discretization of certain objects' zones, development of the new methods for calculation and results analysis is proposed.

Investigations on the optimization of bodies of open wagons are given in [8]. The corrected analysis of the stressed state and the structural and parametric optimization of the side walls and frames of the wagons were made in his work. A modified plate-rod model is proposed for calculation of the stresses in the body.

It is important to note that in the calculation schemes of wagon bodies author did not take into account the efforts that will act on the body during its carriage on railway ferries.

Promising ways to improve the technical and economic indexes of freight wagons and the direction to improve their dynamic properties by introducing elastic damping elements are considered in [9]. The study of the strength of improved structures of the freight wagons bodies, during their transportation on a railway ferry, is not carried out.

Measures to improve the bearing structure of the open car body in order to ensure the reliability of its attachment on the deck of the railway ferry are given in [10]. The results of the strength calculations of the body, taking into account its fixing against the deck on the proposed structural units at the

* [1]Oleksij Fomin, [2]Juraj Gerlici, [3]Alyona Lovska, [5]Kateryna Kravchenko, [4]Pavlo Prokopenko, [5]Anna Fomina, [2]Vladimir Hauser
[1]Department of Cars and Carriage Facilities, State University of Infrastructure and Technology, Ukraine
[2]Department of Transport and Handling Machines, Faculty of Mechanical Engineering, University of Zilina, Slovakia
[3]Department of Cars, Ukrainian State University of Railway Transport, Ukraine
[4]Branch Research and design and technological Institute of Railway Transport "PJSC Ukrzaliznytsya", Ukraine
[5]Department of railway, road transport and handling machines, Volodymyr Dahl East Ukrainian National University, Ukraine
E-mail: fominaleksejviktorovic@gmail.com

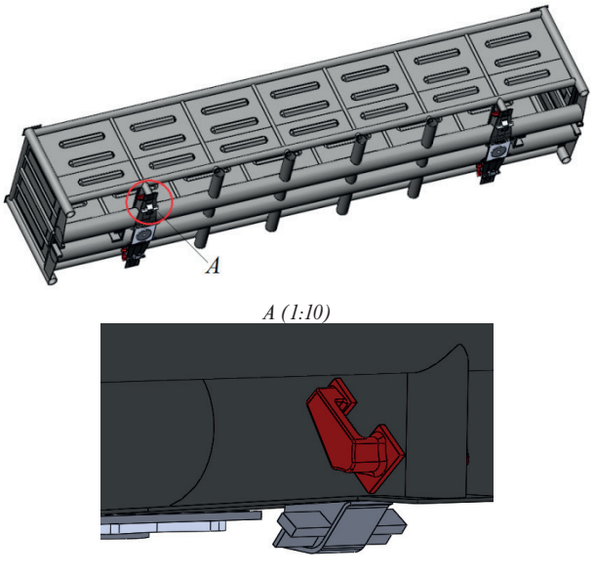

Figure 1 *The open wagon of an improved design with assemblies for railroad decks*

balancing of the railway ferry, have been made. It was concluded that the proposed solutions are feasible. There is no research on optimizing the performance of the carrying structure of the open wagon in operation.

The research of dynamics of a railway wagon with an open loading platform is given in [11]. The calculation is carried out in the software MSC Adams. Investigation of stability against the swinging over the wagon was carried out when it is entered into a curve with a radius of 250 m, taking into account different speeds of motion.

The issue of the rolling stock design, for the transportation of heavy goods is considered in [12]. Research of dynamics and durability was carried out with the help of modern softwares ProMechanica and CosmosWorks. When designing the carrying structure of the conveyor, a study on the possibility of its build from various types of materials was conducted.

The structural features of the wagon for intermodal transportation are discussed in [13]. The wagon has an undersized middle part and the presence of the carriage assembly makes it possible to load/unload the vehicle on/off by its own weight.

The results of studies to determine the nature and extent of impact of different freight bogies on the strength of the carrying systems of wagons are considered in [14]. The question of determining the parameters of the bearing structures of wagons bodies' durability, during their transportation on railway ferries, was not investigated in the considered works.

The features of theoretical and experimental studies on implementation of the bond joint of the back-frame of wagon for pellet transportation are considered in [15]. The obtained results confirm the constructive efficiency of the bond joint of the back-frame of wagons for pellet transportation during the established fifteen-year service life.

The rationale for extending the service life of open wagons that have exhausted their standard service life is carried out in [16]. To determine the dynamic loading of the open car body during a shunting, a mathematical model was made, the results of which were taken into account in the study of the strength of the open car body, taking into account the operational wearing of structural elements.

Features of creation of a promising concept of a coupling gear of open cars are given in [17]. To substantiate the use of the proposed concept, mathematical and computer modeling of the loading of the open car body during a shunting was carried out.

The task of determining the strength factors of the car body elements during its transportation on the railway ferry is not set in these works.

The purpose of the article is explanation of features of the stability factors definition of an open wagon body bearing structure, made from of pipes, during its transportation on a railway ferry.

3. The main content

In order to reduce the material capacity of the bearing structures of the open wagon bodies, providing the conditions of strength and operational reliability, it is suggested and scientifically based use of round pipes as elements of their bearing systems.

For the possibility of transportation of an open wagon on a railway ferry, it is proposed to install components for fastening of chain ties on its centre pin bolster (Figure 1) [10].

In order to determine the dynamic load that acts on the carrying structure of the open wagon body when being transported on a railway ferry, the mathematical model, presented in [18], is used. The model takes into account the movement of the wagon in the main types of fluctuations of the railway ferry - translational movement relative to the vertical axis (1), angular displacement around the transverse axis (2), angular displacement around the longitudinal axis (3):

$$D' \cdot \ddot{q}_1 + \Lambda_z \cdot \dot{q}_1 = \Lambda_z \cdot \dot{F}(t); \tag{1}$$

$$I_\varphi \cdot \ddot{q}_2 + \left(\Lambda_\varphi \cdot \frac{L}{2}\right)\dot{q}_2 = p' \cdot \frac{h}{2} + \Lambda_\varphi \cdot \frac{L}{2} \cdot \dot{F}(t); \tag{2}$$

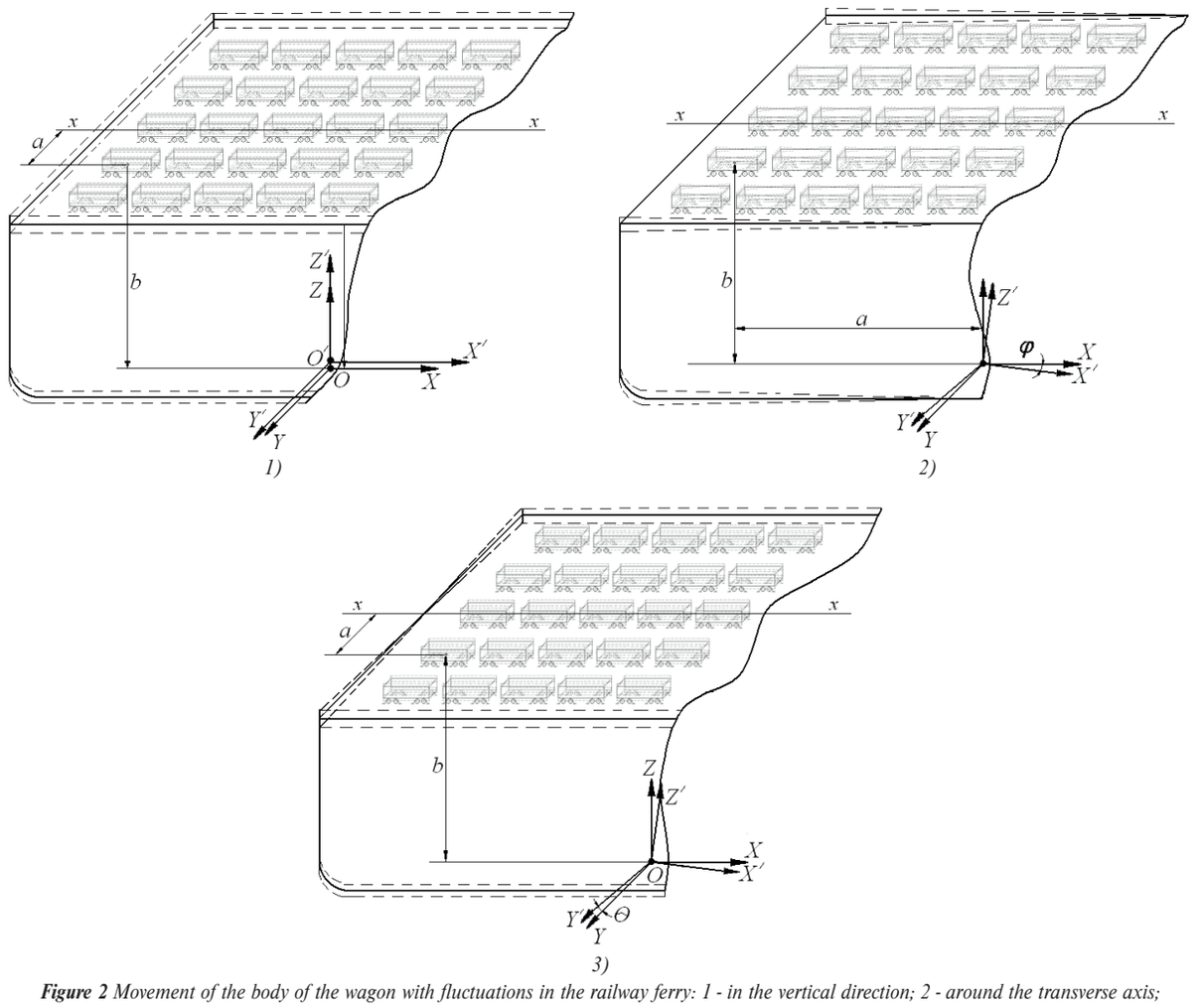

Figure 2 *Movement of the body of the wagon with fluctuations in the railway ferry: 1 - in the vertical direction; 2 - around the transverse axis; 3 - around the longitudinal axis*

$$I_\theta \cdot \ddot{q}_3 + \left(\Lambda_\theta \cdot \frac{B}{2}\right)\dot{q}_3 = p' \cdot \frac{h}{2} + \Lambda_\theta \cdot \frac{B}{2} \cdot \dot{F}(t); \quad (3)$$

where $q_1 = z, q_2 = \varphi, q_3 = \theta$ are generalized coordinates corresponding to:

z - the displacement of the body relative to the vertical axis passing through its center of gravity,

φ - the angular displacement around the transverse axis,

θ - the angular displacement around the longitudinal axis.

The origin of the coordinate system is located at the center of gravity of the railway ferry;

D' - massive water repression,

L, B - respectively, the length and width of the railway ferry,

h - the height of the board of the railway ferry,

Λ_i - coefficient of resistance fluctuations,

p′ - wind load,

I_φ, I_θ - a moment of inertia of the railway ferry with cars placed on decks with pitching and rolling, respectively,

$F(t)$ - the law of a force variation that disturbs the movement of a railway ferry with the bodies of cars located on its decks.

The diagrams of movements of the wagon body fixed to the deck of the railway ferry are shown in Figure 2.

When compiling the mathematical model it is taken into account that the wagon body is rigidly fixed relative to the deck and moves with it. The impact of sea waves on the body of a railway ferry, with wagons placed on its deck, was not taken into account.

The input parameters of the mathematical model are: geometrical characteristics of the railway ferry, hydrometeorological characteristics of the navigation waters, coordinates of the placement of wagon bodies on the decks of the railway ferry.

The research for the transportation of wagons on the ferry “Heroes of Shipka” in the Black Sea area was conducted.

To solve the differential equations of the body of the wagon, a calculation program was compiled in the medium of the Mathcad package [19-20], for which they were reduced to the normal form of the Cauchy and then integrated into the Runge-Kutta method.

The numerical values of the maximum accelerations, acting on the body of wagons located relative to the decks of the railway ferry, were as follows: when moving the body in the vertical direction for the wagon, placed on the upper deck - 0.84 g, with the angular displacement relative to the transverse axis for the extreme from the anchors of the body of the wagon - 0.1 g, with angular displacement around the longitudinal axis for the extreme from the bulwark body of the wagon - 0.24 g.

The conducted numerical values of accelerations, as components of the dynamic load acting on the body of the wagon

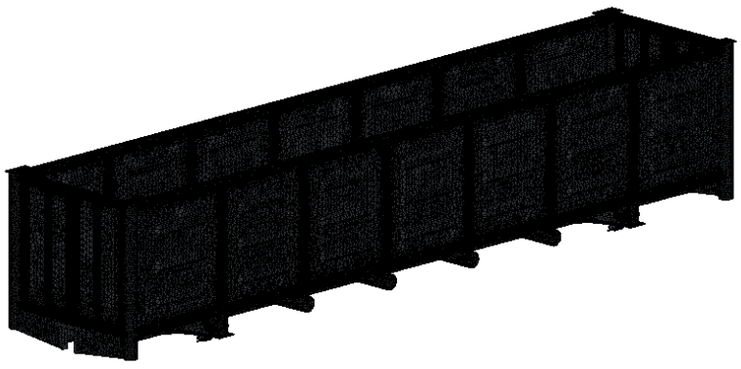

Figure 3 *Finite-element model of the body of the open wagon*

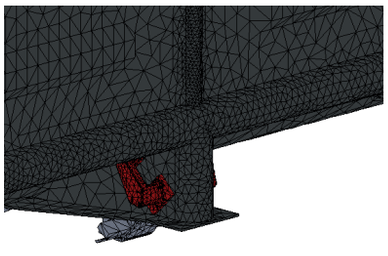

Figure 4 *Fragment of the finite-element model of the open wagon body in the zone of placement of the unit for fastening the chain tie*

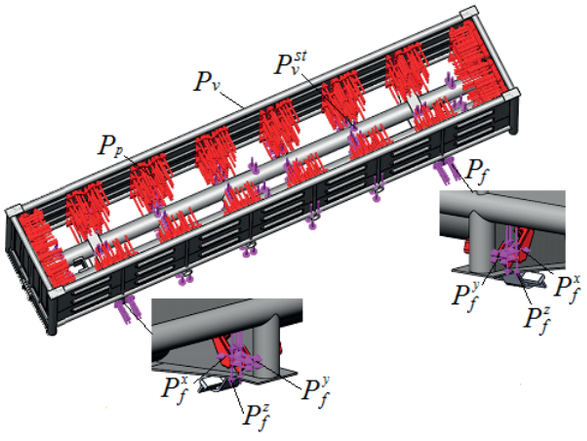

Figure 5 *Model of the body of the open wagon strength*

Table 1 *Strength factors of the bearing structure of the open wagon body during its transportation on the railway ferry*

Strength indicator	Movement type		
	Moving relative to the vertical axis	Angles relative to the transverse axis	Angles relative to the longitudinal axis
Stresses, MPa	208.3	227.5	293.1
Moving in construction knots, mm	9.76	9.97	15.6
Equivalent deformation	$2.25 \cdot 10^{-3}$	$2.2 \cdot 10^{-3}$	$2.5 \cdot 10^{-3}$

when transported on a railway ferry, are taken into account in its strength analysis. The strength test was conducted using the finite element method in the CosmosWorks software.

Finite element model of the body of the open wagon is given in Figures 3, 4. Due to the fact that the hatch covers are not tightly attached to the body frame, but hingedly and perform the function of the elements transmitting the load on the rigidly connected elements of the frame, they were not taken into account in the strength model.

When creating a finite element model, isoparametric tetrahedra were used, the optimal number of which was determined by the graph-analytical method. The number of elements of the grid was 717728, the number of nodes 227767, the maximum dimension of the element 85 mm, the minimum dimension 17 mm, the maximum aspect ratio of the elements was 985.34, the percentage of elements with a ratio of sides less than 3 was - 31.7, with a ratio of sides more than 10 was 11.2.

The model of the open wagon body strength at angular displacements relative to the longitudinal axis (case of the greatest loading of the bearing structure) takes into account the following loads: vertical static load P_v^{st} wind load P_v discharge of bulk cargo F_B (coal) P_f (Figure 5). As a result of the spatial arrangement of the chain tie, the force P_f, which will be transmitted to the bearing structure of the body of the open wagon by means of it, was decomposed into components. The real areas of applying loads to the assemblies of fastening of chain ties were modeled by setting of special elements - mending plates, the configuration of which is identical to the geometry of the contact zone of the hook interaction. It enabled simulating the fastening of the body of the open wagon relative to the deck with a maximum approximation.

The fastening of the model was carried out in the zones of supporting of the body of the open wagon on the bogies, as well as the supporting surfaces of mechanical stop-jacks.

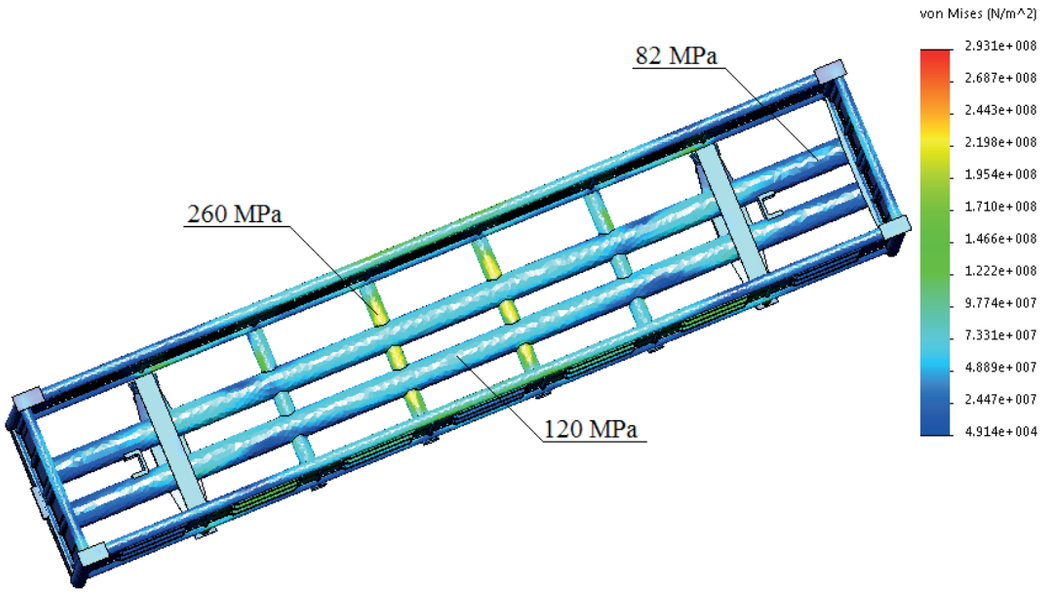

Figure 6 *The stressed state of the bearing structure of the open wagon body at angular displacements relative to the longitudinal axis*

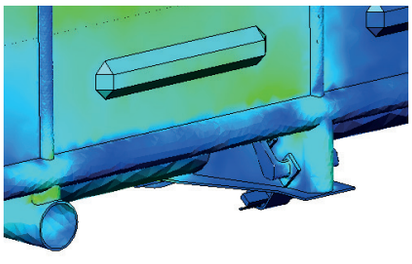

Figure 7 *The stressed state of the bearing structure of the open wagon body in the zone of placement of the unit for fastening the chain binder*

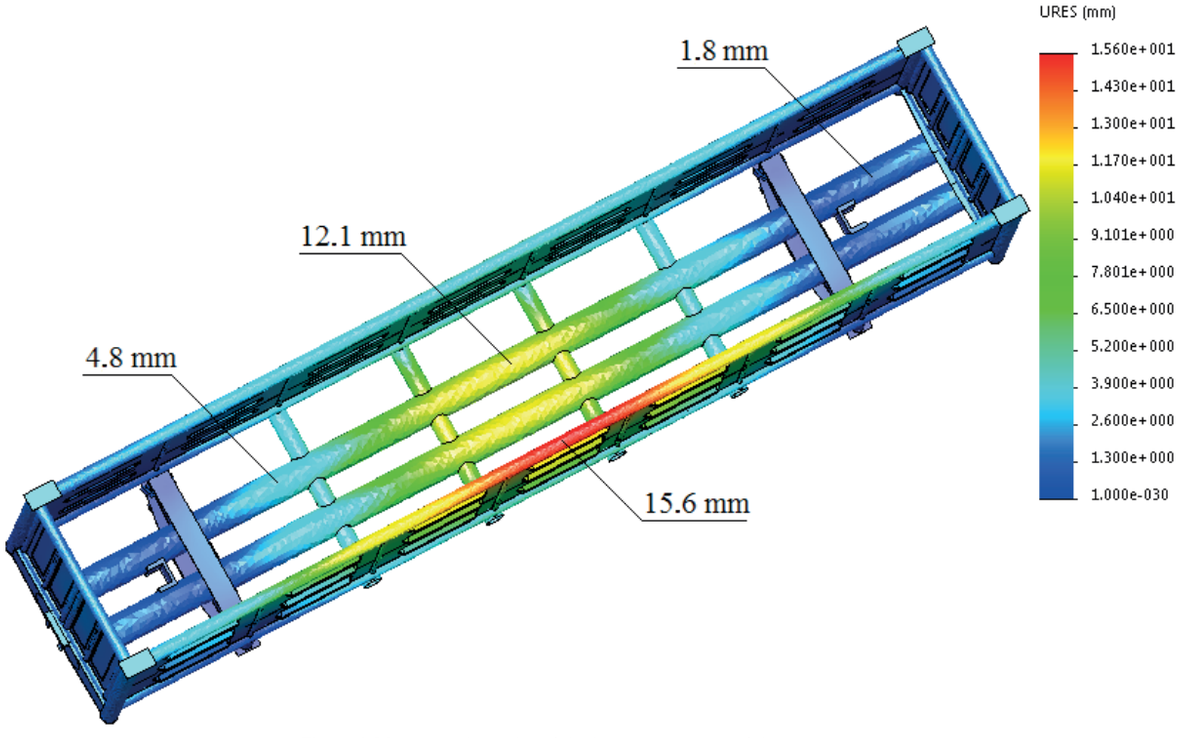

Figure 8 *Moving in the nodes of the bearing structure of the open wagon*

The results of the calculation are shown in Figures 6 - 8. From the conducted studies it can be concluded that the maximum equivalent stresses arise in the middle part of the frame and make up about 260 MPa, that is, they do not exceed the permissible values [21]. Maximum displacements arise in the middle part of the side wall of the body of the open wagon from its slope at the roll and amount to 15.6 mm.

It is important to note that the maximum equivalent stresses of the body of the open wagon, bearing elements of which are made of round pipes, are almost 7% lower than in the typical construction [10].

The results of the strength analysis of other schemes of displacements of the open wagon body are given in Table 1.

4. Conclusions

1. To reduce the cost of design and manufacturing of the new generation of the open wagon bodies, it is proposed to design their carrying systems from round pipes. In order to exploit the proposed designs of wagons in international rail-water communication, it is assumed that stacking of assemblies for fastening of chain binders is provided for them;
2. Maximum values of acceleration as the components of dynamic load, acting on open wagons, made of round pipes, during its transportation on a railway ferry are determined. It is established that when the displacement of the body in the vertical direction for a wagon located on the upper deck, the maximum acceleration value is 0.84 g, when angular displacement relative to the transverse axis for the extreme from the anchor point of the wagon body - is 0.1 g, when angular displacement around the longitudinal axis for the extreme from the bulwark of the body of the wagon - is 0.24 g;
3. The results of the strength analysis of the carrying structure of the open wagon body during its transportation on the railway ferry made it possible to conclude that the maximum equivalent stresses arise at the angular movements of the railway ferry, relative to the longitudinal axis and make up about 260 MPa, that is, they do not exceed the permissible ones;
4. The conducted research will enable an increase of the open wagons operation efficiency through international transport corridors.

References

[1] FABIAN, T. P., et al. Versatile, efficient and long wagon for intermodal transport in Europe. *Communications - Scientific Letters of the University of Zilina* [online]. 2013, **15**(2), p. 118-123. ISSN 1335-4205/eISSN 2585-7878. Available from: http://komunikacie.uniza.sk/index.php/communications/article/view/628

[2] DIZO, J., HARUSINEC, J., BLATNICKY, M. Computation of modal properties of two types of freight wagon bogie frames using the finite element method. *Manufacturing Technology* [online]. 2018, **18**(2), p. 208-214. ISSN 1213-2489. Available from: https://arl.ujep.cz/arl-ujep/en/csg/?repo=ujeprepo&key=62113834886

[3] STASTNIAK, P., MORAVCIK, M. Freight bogie prototype properties analysis by means of simulation computations. *Manufacturing Technology*. 2017, **17**(3), p. 381-388. ISSN 1213-2489.

[4] HAUSER, V., et al. Car body and bogie connection modification for track curves passability improvement. In 22nd Slovak-Polish Scientific Conference on Machine Modelling and Simulations (MMS 2017) : proceedings. Vol. 157. MATEC Web of Conferences [online], 2018. eISSN 2261-236X. Available from: https://doi.org/10.1051/matecconf/201815703009

[5] GELVER, S. A. Investigation of the stressed-deformed state of the body of a freight open wagon of aluminium alloys, taking into account the physical nonlinearity of the material (in Russian). *Ural Transport*. 2008, **4**(19), p. 20-23. ISSN 1815-9400.

[6] AFANASYEV, A. E. Improving the technique for assessing the technical condition and the rationale for extending the service life of open wagons (in Russian). *Ural Transport*. 2008, **1**(16), p. 49-52. ISSN 1815-9400.

[7] MSC Software. *MSC Software Corporation* [online] Available from: http://www.mscsoftware.ru

[8] BEYN, D. G. *Optimization of bodies of freight wagons of open type with a bearing floor* (in Russian). Author's abstract of Ph.D. dissertation in Technical Sciences. Bryansk, Russia, 2011.

[9] FOMIN, O. V. Increase of the freight wagons ideality degree and prognostication of their evolution stages (in Russian). *Scientific Bulletin of National Mining University* [online]. 2015, **4**(3), p. 68-76. ISSN 2071-2227/eISSN 2223-2362. Available from: http://nv.nmu.org.ua/index.php/ru/component/jdownloads/finish/54-03/8333-2015-03-fomin/0

[10] LOVSKA, A. A. Peculiarities of computer modeling of strength of body bearing construction of gondola car during transportation by ferry-bridge. *Metallurgical and Mining Industry* [online]. 2015, **1**, p. 49-54. ISSN 2076-0507/eISSN 2078-8312. Available from: http://www.metaljournal.com.ua/assets/Journal/english-edition/MMI_2015_1/10%20Lovska.pdf

[11] NADER, M., et al. A railway car as an innovative engineering solution for transportation of semitrailers and road kits for intermodal transport. *Logistyka*. 2014, **4**, p. 2272-2279. ISSN 1231-5478.

[12] PRIYA DIVYA, G., SWARNAKUMAR, I. A. Modeling and analysis of twenty tonne heavy duty trolley. *International Journal of Innovative Technology and Research* [online]. 2014, **2**(6), p. 1568-1580. ISSN 2320-5547. Available from: http://www.ijitr.com/index.php/ojs/article/view/421/pdf

[13] KRASON, W., NIEZGODA, T. FE numerical tests of railway wagon for intermodal transport according to PN-EU standards. *Bulletin of the Polish Academy of Sciences Technical Sciences* [online]. 2014, **62**(4), p. 843-851. ISSN 0239-7528. Available from: https://doi.org/10.2478/bpasts-2014-0093

[14] MYAMLIN, S., et al. Determination of the dynamic characteristics of freight wagons with various bogie. *Transport* [online]. 2015, **30**(1), p. 88-92. ISSN 1648-4142/eISSN 1648-3480. Available from: https://doi.org/10.3846/16484142.2015.1020565

[15] FOMIN, O., et al. Experimental confirmation of the theory of implementation of the coupled design of center girder of the hopper wagons for iron ore pellets. *Eastern-European Journal of Enterprise Technologies* [online]. 2017, **5**(1)(89), p. 1-19. ISSN 1729-3774/eISSN 1729-4061. Available from: https://doi.org/10.15587/1729-4061.2017.109588

[16] OKOROKOV, A. M., et al. Research into a possibility to prolong the time of operation of universal semi-wagon bodies that have exhausted their standard resource. *Eastern-European journal of enterprise technologies* [online]. 2018, **3**(7)(93), p. 20-26. ISSN 1729-3774/eISSN 1729-4061. Available from: https://doi.org/10.15587/1729-4061.2018.131309)

[17] FOMIN, O. V., LOVSKA, A. O., PLAKHTII, O. A., NERUBATSKYI, V. P. The influence of implementation of circular pipes in load-bearing structures of bodies of freight cars on their physico-mechanical properties. *Scientific Bulletin of National Mining University* [online]. 2017, **6**, p. 89-96. ISSN 2071-2227/eISSN 2223-2362. Available from: http://nvngu.in.ua/jdownloads/pdf/2017/06/06_2017_Fomin.pdf

[18] LOVSKA, A. O. *Improvement of bearing structures of open wagon bodies for increasing the reliability of their fastening on railroad ferries* (in Ukrainian). Aauthor's abstract of Ph.D. dissertation in Technical Sciences. Kyiv, Ukraine, 2013.

[19] KIRYANOV, D. V. *Mathcad 13* (in Russian). BKhV - St. Petersburg, 2006, p. 608. ISBN 978-5941578498.

[20] ALYAMOVSKY, A. A. *SolidWorks/COSMOSWorks 2006 - 2007. Engineering analysis by the finite element method* (in Russian). DMK, Series "Designing", Moscow, 2007, p. 784.

[21] EN 12663-2. Railway applications - Structural requirements of railway vehicle bodies - Part 2: Freight wagons.

Michal Frivaldsky - Jan Morgos*

DC-DC CONVERTER DESIGN ISSUES FOR HIGH-EFFICIENT DC MICROGRID

In this article, the electrical properties, as well as the economic aspects of the modular and non-modular solution of the DC-DC photovoltaic converter for DC microgrid subsystem, are described. Principally a theoretical overview of the circuit configuration for the selected DC-DC stage of the DC microgrid system is shown. It is dealt with the comparison of the one non-modular high - voltage SiC-based dual - interleaved converter operating at the low switching frequency and with modular low voltage GaN-based DC-DC converters operating at high switching frequencies. The main focus is given to the research of the dependency that arises from the different module count, overall efficiency, costs, and power density (system volume). High efficiency, reduced overall volume, and maximum power density are important factors within modern and progressive solar systems. It is assumed that with the increase of switching frequency within the modular system the volume reduction of the passive components will be highly demanded, thus PCB dimensions and overall volume can be reduced. This dependency is investigated, while the total volume of the non-modular system is a unit of the measure. For these purposes, the design of variant solution was done, and consequently mutually compared in the way of simulations and experimental measurements.

Keywords: *modular system, efficiency, cost, GaN, SiC*

1. Introduction

Humankind has come to a stage where it is evident that the climatic changes of our planet are so extensive that our way of life cannot be sustained for a long time. The measures to reduce the impact on the climate changes also include a change of the process of the use of primary energy source - fossil fuels. Nowadays, many attempts have been done in order to shift from fossil fuels to clean or renewable primary energy sources (photovoltaic systems, wind and water turbines, energy hubs and smart-grids) [1-4].

Strong development of the green and alternative or renewable energy systems (RES) has been intensively investigated for almost a decade. In most of the European countries, it has occurred since 2008, when the European Union's effort to introduce mandatory RES shares in the energy sector for all EU Member States culminated [5].

The electricity system and the overall energy sector are currently under the influence of significant changes. On the one hand, there is increasing pressure on new, mostly small, electricity sources. Whether it is the use of solar energy or biomass (biogas, the conversion of bio-waste to energy, etc.), but also other technologies. At the same time, however, there is a gradual change in consumer models. Global requirements on the energy consumption continuously grow. One of the ways how to provide smooth and reliable energy distribution lies also in the utilization of the very highly efficient systems with considerable power densities [6, 7].

From this point of view, it is therefore important to develop hardware and software solutions that would provide optimal energy management between the supply grid and consumer (household) and also between individual components of the energy system of modern household (primary sources of energy, accumulation of energy, and energy distribution to the consumers). Moreover, if such an intelligent power hub could co-operate with other nodes in its vicinity (narrower or wider), the technical conditions would be created for the massive use of electric cars and renewable sources without negative impact on the power distribution grid [8, 9].

In this paper, a proposal for the intelligent power hub is given, while the more detailed focus is given on the construction block of the power converter system. It deals with DC-DC photovoltaic converter, which can be designed in several ways [10]. In this paper, the modular and non-modular solution of the buck-boost bi-directional converter is considered, while the focus is given on the mutual comparison of the efficiency, cost and power density for the target application.

2. The concept of an energy hub for DC microgrid

Due to increased use of the portion of solar energy and other renewable energy sources, it is necessary to consider with intelligent energy hubs within DC-microgrids of the households. There is also the visible rise of the use of electric vehicles that also influences the concept of smart energy hubs. Such hub has to optimally manage energy flow between individual energy storage systems and energy sources/consumers. Also, there is a need to gain information about energy consumption and state of the charge of energy storage systems. There is the possibility of an Internet connection and possibility to control and monitor system from anywhere with the use of IoT systems.

- A principal block diagram of the concept of perspective energy hub is shown in Figure 1. The system consists of photovoltaic cells,

* **Michal Frivaldsky, Jan Morgos**
Department of Mechatronics and Electronics, University of Zilina, Slovakia
E-mail: michal.frivaldsky@fel.uniza.sk

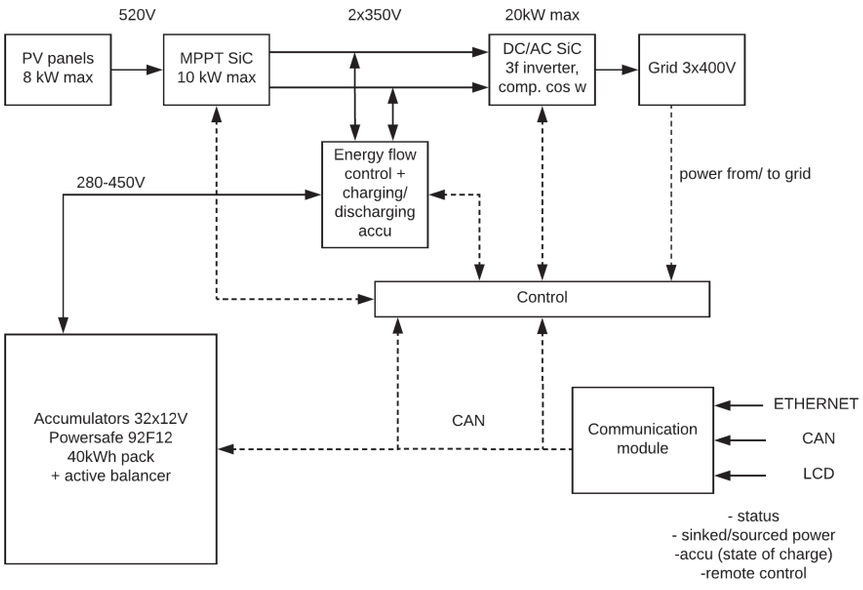

Figure 1 *Block diagram of the proposed energy*

Table 1 *Table of input parameters for the proposed system*

Parameter	Value
Output voltage range from PV panels	500 - 560 V DC
Output power from PV panels	10 kW peak
Output voltage (DC bus voltage)	600 V DC
Output MPPT converter power	10 kW peak

- Maximum power point tracking (MPPT)DC-DC converter,
- energy management block,
- three-phase inverter,
- energy storage block, a
- bidirectional DC-DC converter for charging/discharging of the energy storage system,
- control and communicating block.

In this paper, the attention is given to the MPPT DC-DC converter block, while topological optimization is realized in the way of achieving the highest possible efficiency, lowest possible costs and dimensions for defined input-output conditions. Comparison of the modular and non-modular concept is described.

3. The non-modular and modular concept of DC-DC MPPT converter

In this part topological analysis of MPPT DC-DC converter is given. Since the design of MPPT converter has to be adjusted to the target application (exact number of cells/modules) the input/output parameters are exactly defined, and the proposed solutions are designed considering required voltages and currents (Table 1).

Principal block diagrams for non-modular and modular solutions are shown in Figure 2. Input voltage for the non-modular system is directly connected to the input of the converter at full level (serially connected PV strings). For the modular system, the input voltage is divided between the serial connection of the modular converter blocks. The output voltage for both concepts shall be 600 V, thus for the non-modular solution the output is single, while the modular solution is defined again by the serial connection of the outputs of the individual converters in order to generate an output voltage of 600 V.

Main circuit topology of the non-modular solution is based on the non-isolated DC-DC interleaved synchronous boost converter with SiC-based transistors and diodes. A circuit schematic of this converter is shown in Figure 3. Due to interleaved topology, it is possible to achieve low current and voltage stress for the semiconductor components, and lower voltage and current ripple at the output filtering capacitor. Another benefit is also reduction of the volume of boost inductor and improved thermal performance of the total system.

Individual building blocks of the modular system, shown on Figure 4, are based on the GaN technology of the semiconductor components. Due to dividing the power and voltages to separate individual blocks, it is possible to increase switching frequency several times. One DC-DC converter thus operates with lower voltage and power (thus low voltage - high current, high frequency switching devices can be used). Such approach might reduce dimensions of used components (magnetic components, capacitors, PCB). Thanks to lower dimensions it is possible to design converters with smaller PCB, while the volume of a complex modular system would be smaller compared to the non-modular system.

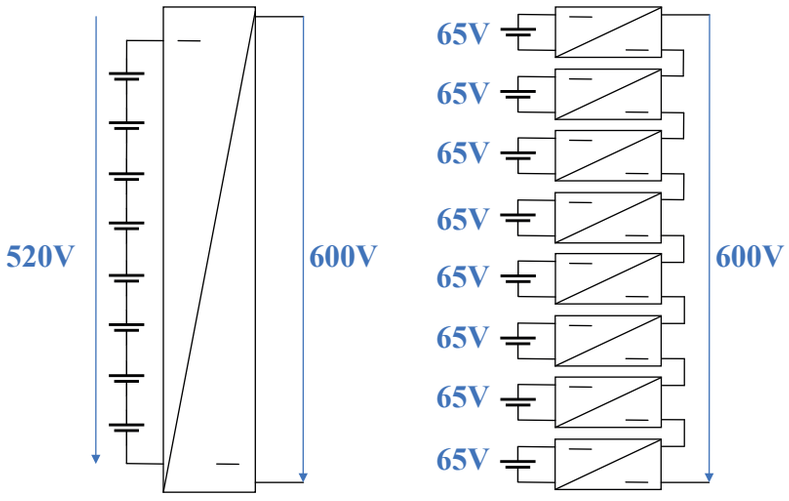

Figure 2 *Block diagram for a non-modular (left) and modular solution (right) of DC-DC MPPT converter*

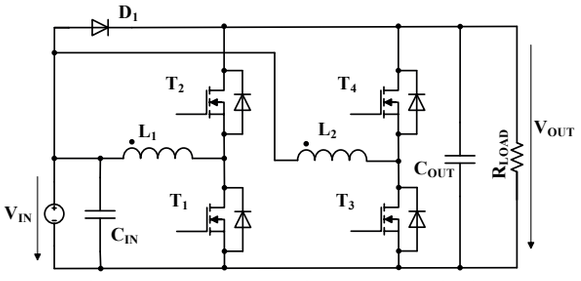

Figure 3 *An electrical schematic of non-modular DC-DC converter utilizing SiC technology of semiconductor devices*

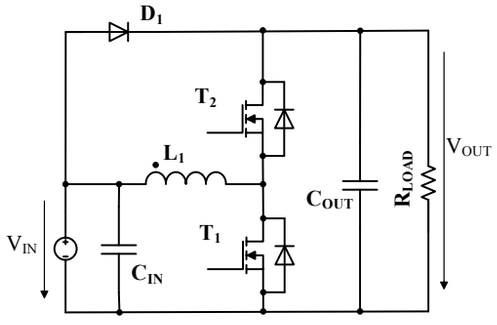

Figure 4 *An electrical schematic of modular DC-DC converter utilizing GaN technology of semiconductor devices*

Next Equations (1) - (3) have been used for the determination of the main circuit components that are affecting the converter volume. The input and output variables have been modified, i.e. input/output voltage and duty cycle, when modular and the non-modular concept was considered. The percentage of the ripple of the output variables was the same even the numbers of the modules vary.

$$L[H] = \frac{V_{in} * (V_{out} - V_{in})}{\Delta i_L * I_{out\_max} * f_{sw} * V_{out}}, \quad (1)$$

where:
U_{in} - input converter voltage [V],
U_{out} - output converter voltage [V],
f_{sw} - switching frequency [Hz],
Δi_L - ripple of inductor current [%],
I_{out_max} - maximum output current [A].

$$D[\%] = 1 - \frac{V_{in\_min}}{V_{out}}, \quad (2)$$

where:
U_{in} - minimum input converter voltage [V],
U_{out} - output converter voltage [V].

$$C_{out}[F] = \frac{I_{out\_max} * D}{f_{sw} * \Delta V_{out}}, \quad (3)$$

where:
I_{out_max} - maximum output current [A],
D - duty cycle [%],
f_{sw} - switching frequency [kHz],
ΔU_{out} - ripple of output voltage [%],
U_{out} - output voltage [V].

Figure 5 and Figure 6 show 3D dependency of the values of boost inductor L and filter capacitor C_{OUT} when the number of modules and switching frequency vary, while input/output parameters are relevant for individual module count. It must be noted, that the interpretation considers with one component, when the computation was realized. Thus for whole module solution, the result must be multiplied by the relevant number of the considered modules. Table 2 shows input/output parameters that have been included within calculation of the L and C_{out}. At this point the need for the semiconductor devices is considered. It is seen, that for the situation when 2 up to 4 stages are considered there is a necessity to use high-voltage GaN transistors (650 V), while the target price and investments for the design of the proposed system will markedly increase. When a higher number of modules (over 4) is considered, the input and output voltage will be divided by the DC-DC stages, thus transistors with lower breakdown voltage U_{DS} can be used (100 V). As a satisfaction, the transistor costs will also be reduced compared to the high-voltage solution.

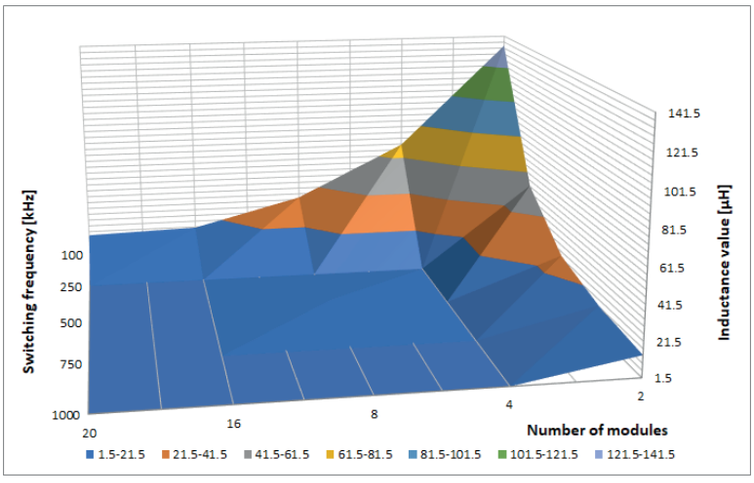

Figure 5 *3D dependency of the inductance L value on number of modules and switching frequency*

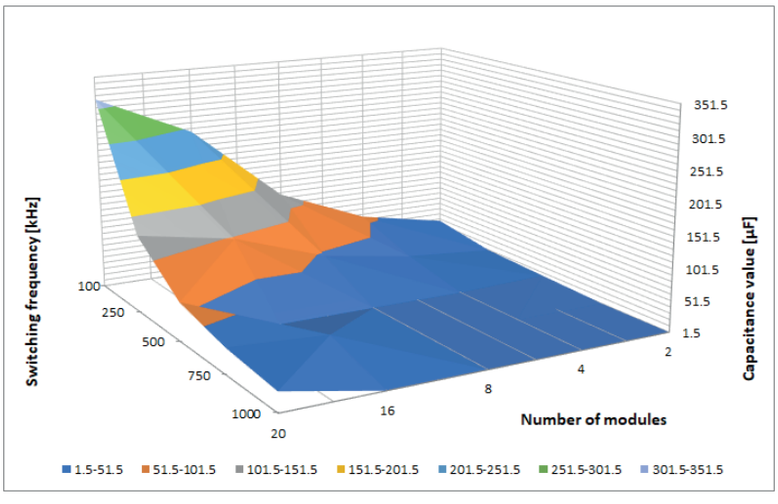

Figure 6 *3D dependency of the capacitance C_{out} value on the number of modules and switching frequency*

Table 2 *Table of input parameters of the proposed system*

Module count	Input voltage	Output voltage	Output power	V_{DS} [V]	I_D [A]	R_{DSon} [mΩ]
1 (nonmodular)	520	600	10000	1200 (SiC)	30	75
2	260	300	5000	650 (GaN)	30	55
4	130	150	2500	650 (GaN)	30	55
8	65	75	1250	100 (GaN)	30	15
16	32.5	37.5	625	100 (GaN)	45	15
20	26	30	500.5	100 (GaN)	45	15

4. Comparison of the properties of the modular and non-modular solution - costs, efficiency, volume, performance

At this place, the economic performance together with efficiency and power density calculation are given. Initially, Table 3 shows an expert estimation of the investments necessary for the design of proposed solutions of the MPPT DC-DC converter. The estimation considers with the whole bill of materials of electronic parts (power semiconductor components, drivers, magnetic components, passive components and PCB), while standard distribution network was considered. It is seen, that the initial costs of the non-modular DC-DC interleaved converter based on the SiC technology is comparable to the initial costs that are relevant for almost up to 16-stage modular DC-DC converter. Figure 7 shows graphical interpretation of the costs related in dependency on the number of modules, while switching frequency is also variable. From Figure 7 can be seen, that with the increase of the switching frequency the costs are decreasing, what is related to the fact, that smaller reactive components can be used within

Table 3 *Table of build costs of the proposed system*

	T	Cin	Cout	L	PCB	oths	total
non modular (50 kHz)	20	12	40	150	490	40	712 €
2 modules (100 kHz)	65	11	14	22	320	20	432 €
4 modules (100 kHz)	130	22	26	56	275	22	509 €
8 modules (100 kHz)	83	28	37	80	210	27	438 €
16 modules (100 kHz)	167	38	180	73	320	40	778 €
20 modules (100 kHz)	209	65	210	100	280	50	864 €

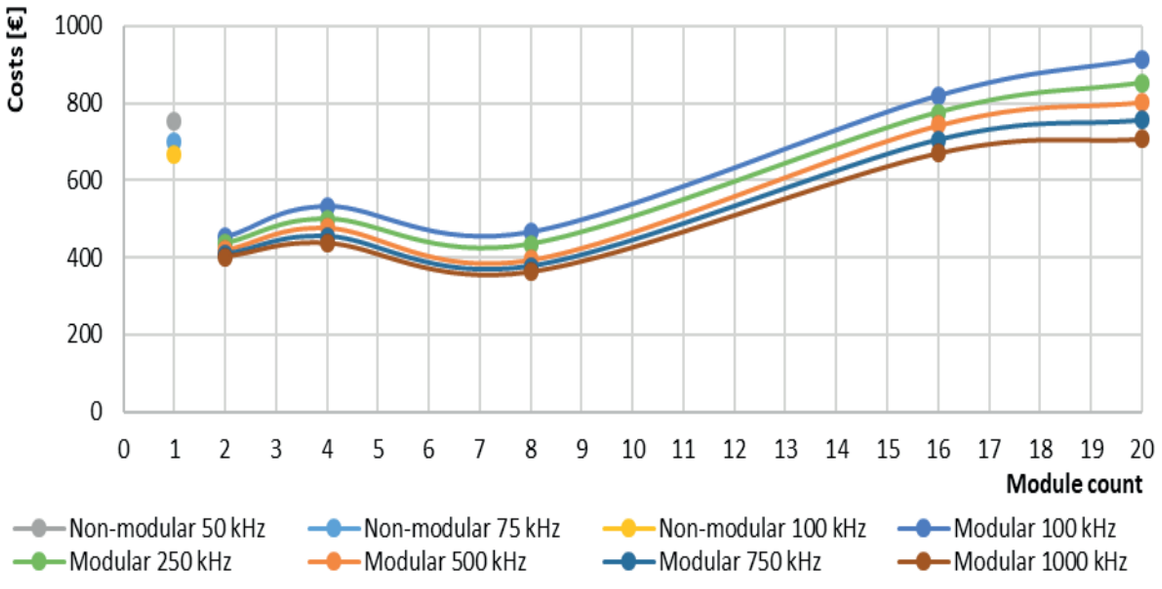

Figure 7 *Comparison of costs of non-modular and modular solution in dependency on switching frequency and number of modules*

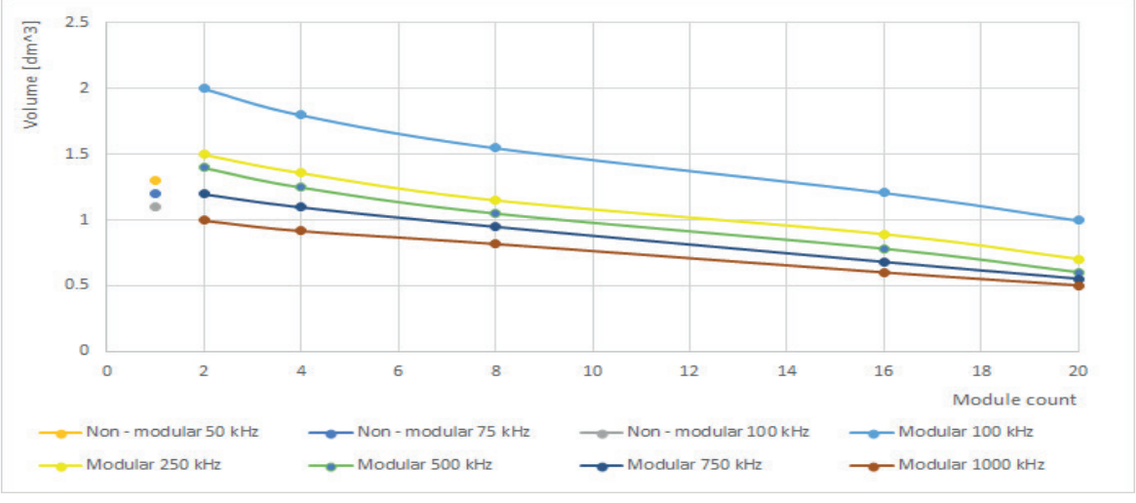

Figure 8 *Comparison of build volumes of modular solutions for different switching frequencies and for different module count*

the converter´s main circuit. Also, the drop of the cost is visible around the 8 count of the modules. It is caused due to fact, that the transistor with lower drain-source voltage can be used within main circuit, thus the price for the semiconductor reduces.

Considering volume (power density), non-modular solution exhibits performance that is dependent on the switching frequency and input/output parameters that are limited due to power delivery and semiconductor performance. For high power levels, it is expected to operate at lower frequencies in order to prevent from unwanted negative impacts (safety reasons, EMC etc.), while robust semiconductors must be used (IGBT, SiC MOSFETS). On the other hand, modular solution enables to split individual

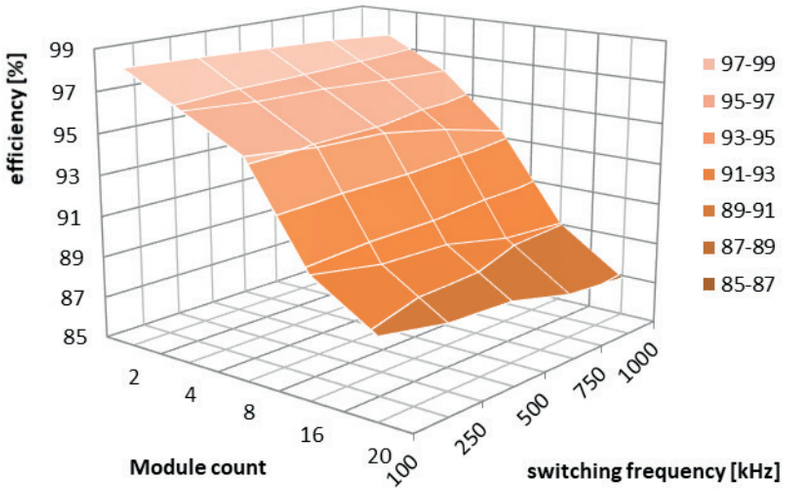

Figure 9 *Comparison of efficiencies of modular solutions for different switching frequencies and for different module count*

Table 4 *Table of input/output voltage and current ripples for non-modular and modular solutions*

Module count	Input voltage ripple	Input current ripple	Output voltage ripple	Output current ripple
1 (SiC)	0.04 %	36.5 %	3.96 %	3.88 %
2 (GaN)	0.02 %	5.31 %	0.33 %	0.35 %
4 (GaN)	0.03 %	5.63 %	0.21 %	0.22 %
8 (GaN)	0.08 %	6.37 %	0.21 %	0.21 %

converters to lower input/output operating levels. Therefore the high-switching frequency operation is easily to utilize. With this increase, the volume of the passive components can be visibly reduced. Moreover, when GaN technology is considered, also the volume of the semiconductors minimizes. GaN-based converter system has a big advantage if very small volume and weight are required. Typical examples are mobile systems, compact converter systems or electromobiles e.g. Figure 8 shows dependency of the volume on the number of modules, while switching frequency is also variable parameter. It is seen that with the increase of switching frequency the total volume of the modular converter system can be reduced below the volume of the non-modular solution, whereby this is valid from 250 kHz of switching frequency and above 5 numbers of the modules.

Graphical comparison of overall efficiency of the modular solution in dependency on module count and switching frequency is shown in Figure 9. Individual results have been received from the PSpice simulations, while high-precision models of semiconductors and passive components have been utilized. Non-modular solution was evaluated for the 75 kHz, whereby the efficiency was 98.5 % and is not plotted. For the calculation of efficiency of modular solution, Equations (4) and (5) were used. It is obvious that with the increasing module count, there is a decrease of overall efficiency of the modular solution. Also the increase of switching frequency causes the decrease of overall efficiency due to increase of switching and conduction losses.

$$\eta = \frac{P_{out}}{P_{in}}, \tag{4}$$

The efficiency of modular system can be calculated as:

$$\eta^* = \frac{n * P^*_{out}}{n * P^*_{in}} = \frac{P^*_{out}}{P^*_{in}}, \tag{5}$$

where:
n - module count,
η – efficiency,
Pin - input power,
Pout - output power.

From Figure 9 is seen that the main disadvantage of the increase of module count is efficiency decrease. Therefore optimizations within main circuit must be done in order to reduce the most of conduction losses (due to higher currents). For this reason there shall be compromise between previously mentioned abilities (power density and costs) and target efficiency. Almost 8 module systems are able to operate at relatively very high efficiency 95 % and high switching frequency (500 kHz). In this way the volume can be decreased compared to non-modular solution (Figure 8) while investments can be reduced by more than 40 % of non-modular costs.

Final comparison of presented design approaches was realized through investigation of the input/output current/voltage ripple. From Table 4 is seen, that visible reduction can be achieved with modular solution thus improving the distortion of input/output waveforms. This is beneficial for sensitive loads.

5. Conclusion

In this article differences between modular and non-modular solutions for photovoltaic MPPT converters have been described. Initially the main circuit of the individual solution have been shown for selected application. Main focus was given on the performance from cost, volume and efficiency point of view. It was shown, that modular solution enables more design flexibility whereby mentioned parameters can be modified to the target application. Investigation was performed in parametric ways, and individual variables were described in dependency on the operating conditions of presented solutions.

As regards the evaluation of the financial charges for individual system constructions, the modulation rate is not directly increasing investments what was related to the different component selection. The modular cost can be lower compared to non-modular up to a certain count of the modules (up to 16). Due to the high spin rate, the system can be constructed from a small amount of modulation, which reduces the total volume of the system. The modular system provides a smaller dimension to the number of modules 10 compared to a non-modular system but increases the number of individual building blocks in the modular system directly to the overall efficiency of the system.

Next steps in our research will be: design, practical realization of the physical samples and testing of the proposed modular system.

Acknowledgements

The authors wish to thank Slovak grant agency APVV for the project no. 0396-15 - Research of perspective high-frequency converter systems with GaN technology. Authors also would like to thank for the support from the national grant agency VEGA for the project no. 1/0547/18 - Research of possibilities for system optimization of WET technology.

References

[1] SEDO, J., KASCAK, S. Design of output LCL filter and control of single-phase inverter for grid-connected system. *Electrical Engineering - Archiv fur Elektrotechnik* [online]. 2017, **99**(4), p. 1217-1232. ISSN 0948-7921/eISSN 1432-0487. Available from: https://doi.org/10.1007/s00202-017-0617-0

[2] AIELLO, G., et al. A high efficiency interleaved PFC front-end converter for EV battery charger. *Communications - Scientific Letters of the University of Zilina* [online]. 2018, **20**(1), p. 86-92. ISSN 1335-4205/eISSN 2585-7878. Available from: http://komunikacie.uniza.sk/index.php/communications/article/view/52

[3] GALAD, MARTIN, et al. Analysis of state of charge estimation methods for smart grid with VRLA batteries. *Electrical Engineering - Archiv fur Elektrotechnik* [online]. 2017, **99**(4), p. 1233-1244. ISSN 0948-7921/eISSN 1432-0487. Available from: https://doi.org/10.1007/s00202-017-0618-z

[4] NOBILE, G., et al. Multi-criteria experimental comparison of batteries circuital models for automotive applications. *Communications - Scientific Letters of the University of Zilina* [online]. 2018, **20**(1), p. 97 – 104. ISSN 1335-4205/eISSN 2585-7878. Available from: http://komunikacie.uniza.sk/index.php/communications/article/view/54

[5] STEPINS, D., HUANG, J. Optimization of modulation waveforms for improved EMI attenuation in switching frequency modulated power converters. *Advances in electrical and electronic engineering* [online]. 2015, **13**(1), p. 10-21. ISSN 1804-3119/eISSN 1336-1376. Available from: https://doi.org/ 10.15598/aeee.v13i1.1142

[6] GALAD, M., SEDO, J., SPANIK, P. Developing of stand-alone power system simulation model. *International review of automatic control (IREACO)* [online]. 2014, **7**(5), p. 500-505. ISSN 1974-6059/eISSN 2533-2260. Available from: https://doi.org/10.15866/ireaco.v7i5.3867

[7] CHLEBIS, P., et al. The system of fast charging station for electric vehicles with minimal impact on the electrical grid. *Advances in electrical and electronic engineering* [online]. 2016, **14**(2), p. 89-94. ISSN 1804-3119/eISSN 1336-1376. Available from: https://doi.org/10.15598/aeee.v14i2.1318

[8] TVRDON, M., CHLEBIS, P., HROMJAK, M. Design of power converters for renewable energy sources and electric vehicles charging. *Advances in electrical and electronic engineering* [online]. 2013, **11**(3), p. 204-209. ISSN 1804-3119/eISSN 1336-1376. Available from: https://doi.org/10.15598/aeee.v11i3.795

[9] XUE, F., YU, R., HUANG, A. Q. A 98.3% efficient GaN isolated bidirectional DC-DC converter for DC microgrid energy storage system applications. *IEEE Transactions on Industrial Electronics* [online]. 2017, 64(11), p. 9094-9103. ISSN 0278-0046/eISSN 1557-9948. Available from: https://doi.org/10.1109/TIE.2017.2686307

[10] GALAD, M., SPANIK, P. Design of photovoltaic solar cell model for stand-alone renewable system. In 10th international conference ELEKTRO 2014: proceedings. Slovakia, 2014. ISBN 978-1-4799-3720-2, CD-ROM, p. 285-288.

Mykola Sysyn - Dimitri Gruen - Ulf Gerber - Olga Nabochenko - Vitalii Kovalchuk*

TURNOUT MONITORING WITH VEHICLE BASED INERTIAL MEASUREMENTS OF OPERATIONAL TRAINS: A MACHINE LEARNING APPROACH

A machine learning approach for the recent detection of crossing faults is presented in the paper. The basis for the research are the data of the axle box inertial measurements on operational trains with the system ESAH-F. Within the machine learning approach the signal processing methods, as well as data reduction classification methods, are used. The wavelet analysis is applied to detect the spectral features at measured signals. The simple filter approach and sequential feature selection is used to find the most significant features and train the classification model. The validation and error estimates are presented and its relation to the number of selected features is analysed, as well.

Keywords: *turnouts, inertial measurement systems, predictive maintenance, signal processing, data mining, machine learning, data reduction, feature selection*

1. Introduction

Common crossing of turnout is one of the weakest elements of the railway superstructure. Despite many attempts in the last years to prolong its lifecycle [1-3], it is still 5-10 times lower than the lifetime of the ordinary rail track [4]. Moreover, the maintenance costs for turnouts are comparatively high due to demand for frequent inspections with relatively low automatisation. The process of common crossing deterioration is to a great extent difficult to predict and thus to plan the maintenance works [3]. That can often cause big expenses because of unplanned traffic interruptions and train delays.

Its application on operational trains could provide almost continuous monitoring of the track state.

The inertial measurement systems ESAH-M and ESAH-F are developed with the DB AG (German railway company) for the estimation of common crossings. The systems provide acceleration measurements complemented by positioning sensors on track [5-6] with Electronic Analysis System of Crossing Portable (German ESAH-M, Figure 1, left). The vehicle axle box measurements [6-8] are provided with Electronic Analysis System of Crossing - Train (German ESAH-F, Figure 1, right).

The main problem of inertial measurements on railway track is a rather big uncertainty together with unknown criteria for the corresponding maintenance works [9]. A lot of recent researches are devoted to this problematic. A quantitative relationship between the characteristics of the axle box accelerations and the track defects for their early detection is proposed in [10-11]. The acquisition of axle box accelerations with their time-frequency analysis is shown in [12-13] for track monitoring purposes. Vibration-based condition monitoring was suggested in [14], based on in-situ measurements of the crossing vibrations of a railway turnout.

The data mining methods are widely used in transportation research. The data-driven rail-infrastructure monitoring that is based on data fusion, feature extraction, selection and other data mining methods are depicted in [15]. In [16] authors describe the general methodology of big data analytics for track maintenance planning. An example of track quality analysis for the track maintenance with application of the machine learning methods is presented in [17]. The support vector classification and regression methods are used for optimization of freight traffic planning, [18]. The application of big data analysis of surface defect measurements together with axle box acceleration is used to facilitate grinding planning of rail segments, [19]. The big-data fusion and incremental learning is applied to solve the problem of position synchronization for the track geometry inspection, [20]. In the present paper, the sequential feature selection is used to find out the meaningful spectral features that correspond to the state of turnout immediately before its fault. The statistical model is developed to identify the state with the axle box acceleration measurements.

2. Data pre-processing and feature extraction

The inertial measurements of ESAH-F system are subjected to a big number of unknown and unconsidered factors, such as the wheel profile irregularities and wear, lateral wheel position, etc.

This leads to a big deviation of measurement results that makes it very difficult to estimate the changes of a common crossing state. The usually used analysis of maximal axle box accelerations shows almost no changes of the value until the first crack of the rolling surface in common crossing occurs (Figure 2). This means that the conventional analysis suits well for condition monitoring of common crossings by detecting defects. Though the

* [1]Mykola Sysyn, [1]Dimitri Gruen, [1]Ulf Gerber, [2]Olga Nabochenko, [2]Vitalii Kovalchuk
[1]Institute of Railway Systems and Public Transport, Technical University of Dresden, Germany
[2]Department of the rolling stock and track, Lviv branch of Dnipropetrovsk National University of Railway Transport, Lviv, Ukraine
E-mail: mykola.sysyn@tu-dresden.de

Figure 1 *The inertial measurement systems (left - ESAH-M, right - ESAH-F)*

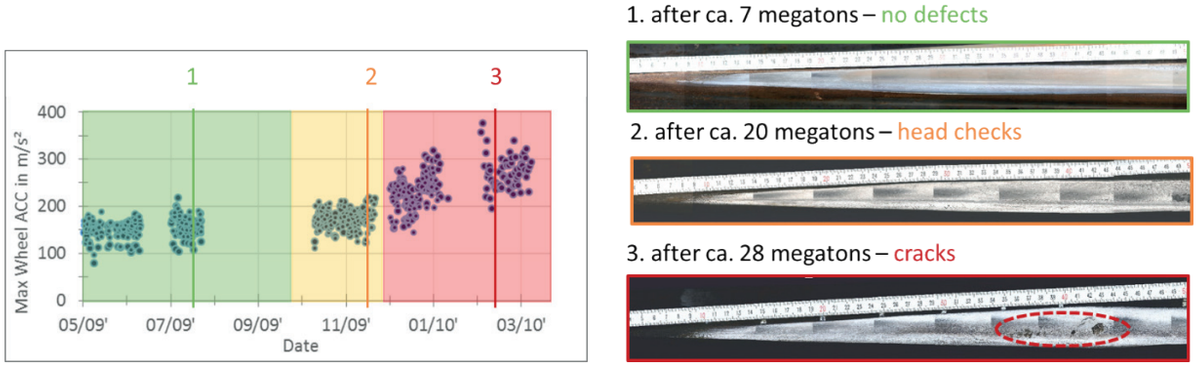

Figure 2 *Wheel ACC Amplitudes during the lifecycle (left) and surface images of a common crossing (right). Photo material: DB Systemtechnik GmbH*

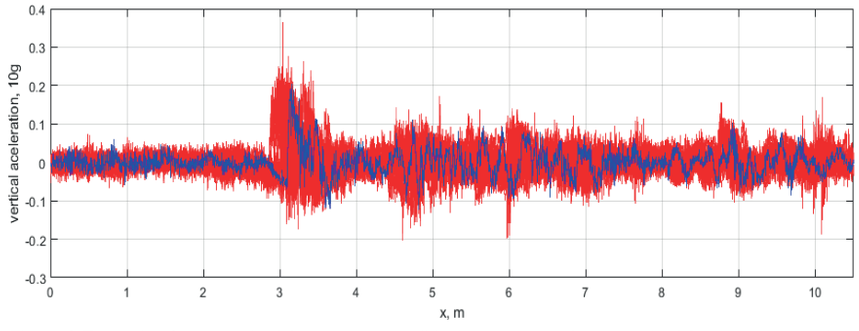

Figure 3 *Example of the wheel ACC measurement (blue) and group of the wheel ACC measurements (red)*

faults are unexpected and often unpredictable, that leads to big expenses due to unplanned maintenance works and traffic delays.

The statistical analysis is based on the acceleration measurements of the ESAH-F system of the DB Systemtechnik. The measurements were carried out at operational passenger double-decker trains on two axle boxes of one bogie.

The turnouts number as well as motion direction were detected by the GPS. The sampling rate used is 50 kHz. The analysed turnout of type 1/12 was measured along all its lifecycle ca. 32 megatons. The operating load at turnouts was 27 megatons per year with mixed traffic. The general number train passages is 229, with 2 axle box 3D acceleration measurements. The typical measurement of 1 vertical acceleration together with the cloud of other measurements is shown at Figure 3.

The measurements are divided for the statistical analysis in two groups:

- the beginning of lifecycle: 52 measurements with 104 acceleration records;
- 1.5 months before the first visible squats appearing: 73 measurements with 107 successful records.

The wavelet transform was used to extract the feature set from the random enough time series of acceleration measurements. The Signal Processing, Statistics and Machine Learning Toolboxes are used for data processing and analysis [21].

All the data are synchronised with the maximal acceleration point. Time axis is changed to wheel position coordinate to reduce the influence of different train velocities. The example of signal spectral density distribution along the 11 m track and frequency range 0-25 kHz is shown in Figure 4. The low accelerations due to ballast settlements and wing-frog rail rolling surface begin 3 m before the impact point. The maximal acceleration appear at the impact point with frequency range 90-750 Hz. The highest accelerations reach up to 20 kHz. The spectral components of signal in Figure 4 can be visually divided into 3 main groups: lower than 800 Hz, 800-4000 Hz and 4000-20000 Hz.

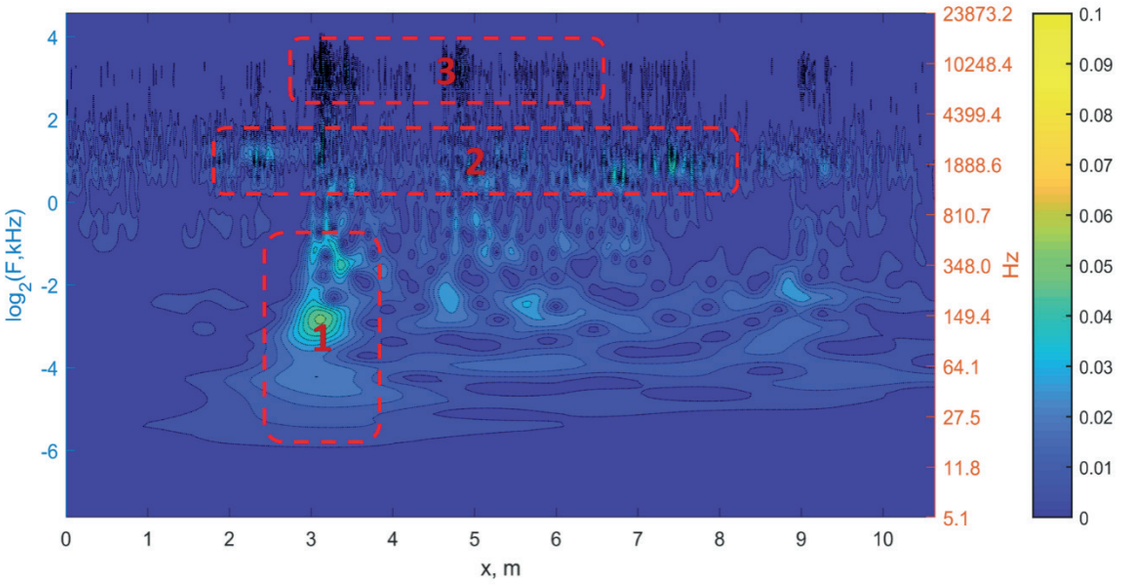

Figure 4 *Example of spectral density distribution along 11 m track (common crossing at position 2-4 m)*

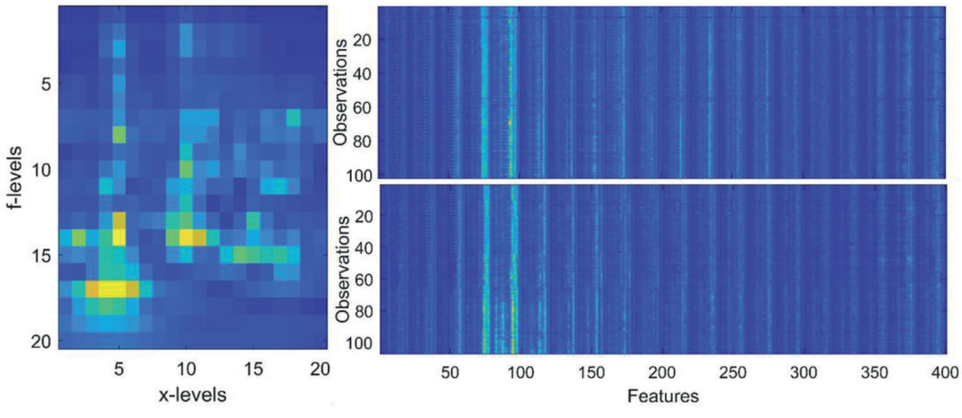

Figure 5 *Example of features reduction 20 x 20 (left) and their collection for two periods of lifetime (right: 1st group - above, 2nd group - below, see Figure 2)*

To receive the limited number of features for each observation, the wavelet coefficients are segmented in raster 20 x 20 that correspond to logarithmic frequency range 10 Hz - 20 kHz and longitudinal coordinate 1.5-8.5 m. Overall number of features are limited to 400. The segmented and collected features for two groups are shown in Figure 5.

3. Feature selection

The goal feature selection is to reduce the dimension 400 of the data by finding a small set of important features, which can give good classification performance. Feature selection algorithms are divided into 3 categories [22]: filter methods, wrapper methods and embedded methods. The simplest filter method of sequential feature selection is used for the present research. It does not consider the relationships between variables but is effective in computation time and robust to overfitting.

To estimate the performance of a classification model another data set should be chosen that was not used to build the model. All 211 observations are divided into a training set of size 155 and a test set of size 56. The model is tested in two ways: holdout validation and cross-validation. Within the holdout validation the features are selected using the training data and the performance is judge based on the test data.

To find out how well the two groups (Figure 5) are separated by each feature, the pairwise t-test statistic is applied [21]. Figure 6 shows the difference between the groups and the critical value of feature to reject the null hypothesis.

According to Figure 6, there are a lot of features with statistically significant differences between the groups. The diagram of empirical cumulative probability of null hypothesis (Figure 7) shows that there are about 50 % features with strong discrimination power.

Even though there are big statistical differences between the groups, it is not enough to estimate the classification uncertainty and decide how many features are necessary. A statistical model should be developed to classify new observations to the corresponding group. The model is developed within the quadratic discriminant analysis (QDA) [23]. The classification

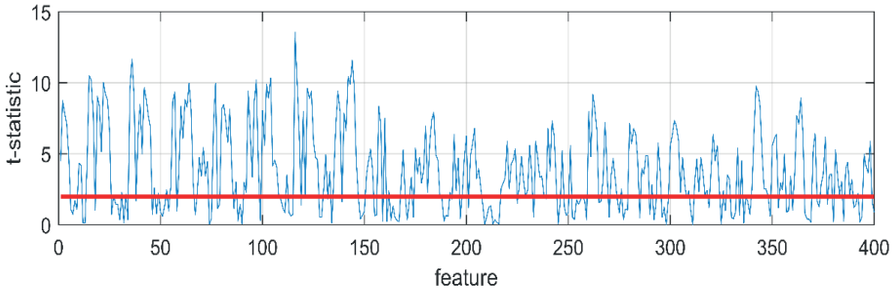

Figure 6 *T-Statistic for features values (blue) and threshold for the null hypothesis (red)*

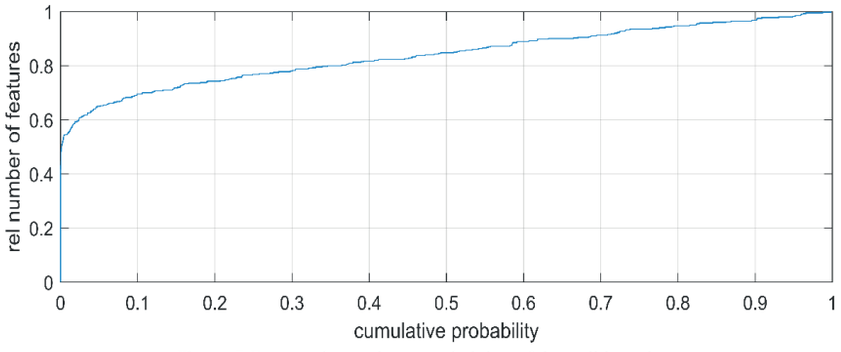

Figure 7 *Empirical cumulative probability of the null hypothesis*

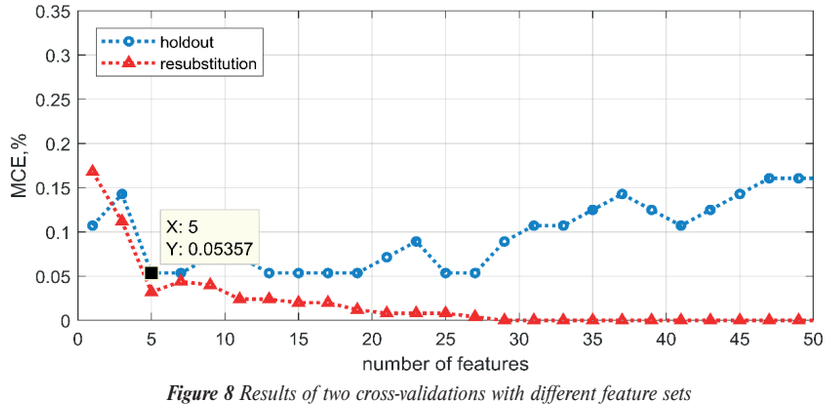

Figure 8 *Results of two cross-validations with different feature sets*

uncertainty is estimated with misclassification error (MCE), i.e. the number of misclassified observations divided by the number of observations.

The quadratic discriminant analysis as the classification algorithm can be used if the number of observations in each group is big enough to estimate a covariance matrix. In the presented case the number of features (400) is much larger than the number of observations (155) for the training set. The largest permissible number of features for QDA is about 70. To handle the restriction, the first 70 most probable features from t-test statistic are used for the cross validation. The t-test statistic is used as a criterion for simple filter selection method.

The successive cross-validations with different feature sets from 1 to 70 are done to find out the relation of misclassification error to the number of features. Figure 8 depicts the relation for two ways of validation: holdout (new test observations) and resubstitution (the test and training observations). The MCE for the holdout validation decreases to 0.536 for 5 features and increases if more than 27 features are used. The reason is the overfitting. The MCE for the resubstitution validation consistently decreases with the number of features and even reaches zero when more than 60 features are used. That means that the train data can not be used for estimation of the trained model.

The used simple feature selection method is simple, fast in calculations and enables reaching almost 5% prediction error. However, the method takes into account the interaction between one pair of features and does not consider possible interaction with all other features. Some found features can be dependent on each other so that not all the features are necessary.

The more advanced feature selection algorithms can improve the performance, such as in [24-25]: sequential algorithms, exponential algorithms, randomized algorithms. Sequential feature selection is used in this research. It is one of the most widely used techniques. It selects a subset of features by sequentially forward search or removing until certain stopping conditions are satisfied. The results of sequential feature selection

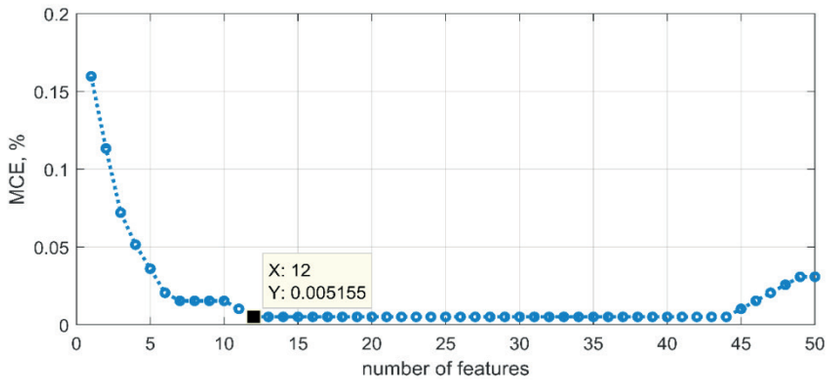

Figure 9 *Results of sequential feature selection for quadratic discriminant analysis*

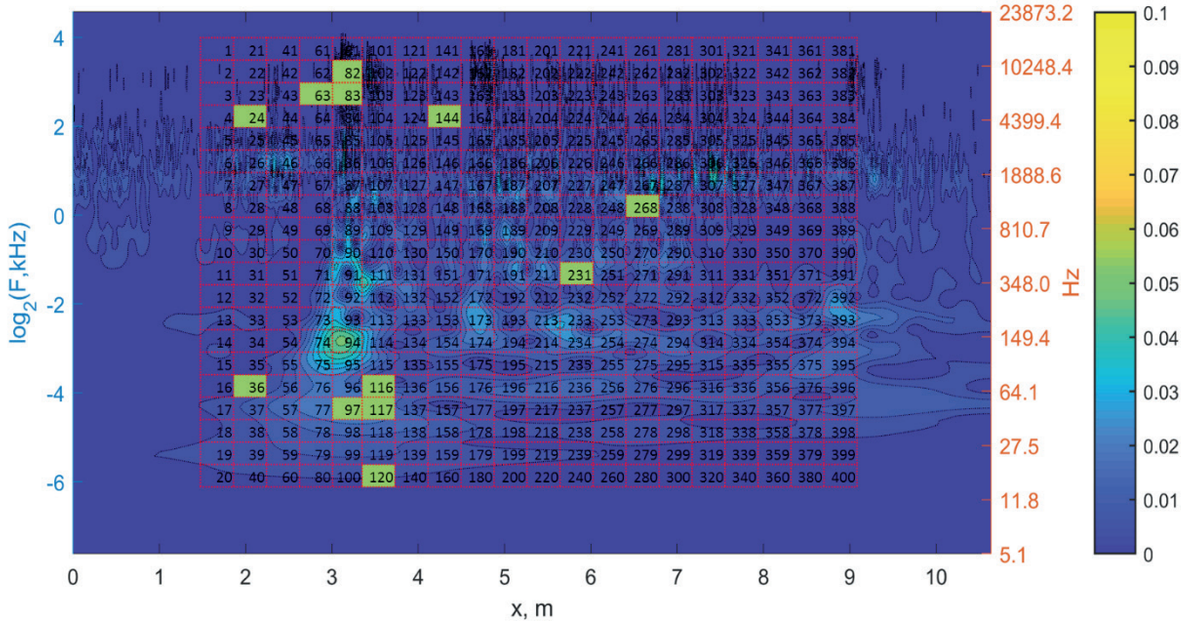

Figure 10 *Features in the raster of 20 x 20 on the wavelet diagram with highlighted selection*

for QDA are presented at Figure 9. The diagram shows that for the beginning with 12 features the minimal MCE 0.005 can be reached. The error is almost 10 times lower as for the simple filter approach due to selection of the best independent features.

The 12 selected features are depicted on the diagram of wavelet coefficients (Figure 10).

4. Conclusion and subsequent studies

The main aim of the actual research was to highlight the advantages of machine learning statistics vis-à-vis the simple statistical methods. The 12 found features within the sequential feature selection and quadratic discriminant analysis correspond to the most statistically significant frequencies and coordinates at wavelet diagram. The features have both low and high frequencies. Remarkably, there are almost no features corresponding to middle range frequencies where the amplitudes are the highest. The main statistical reason of the phenomena is big variance of the maximal values that makes them statistically insignificant. The secondary reason can be the close covariance of the features with already selected main features. A big variance in the middle range frequencies has also a technical reason: the different measurements are synchronised with acceleration maximal values that can cause some accidental transitions of the feature values between the neighbour features. The simple feature selection algorithm considers the transitions as error. There are different ways to cope with the problem. The simplest is the appropriate segmentations of the spectrogram. More advanced one is the feature transformation to a new feature set with feature extraction. The better measurement synchronization with waveform similarity, such as proposed in [20], is also a promising technique to solve the problem.

From the technical viewpoint, differences in low frequency range correspond to some changes in the ballast layer. At the same time, the high frequencies correspond to changes in dynamic response of the wheel-rail contact.

Nevertheless, the present study cannot explain the principal source of changes - they may be caused by changes in rail (common crossing) as well as the ones in the wheel. The three-factor classification analysis should be carried out to separate the influence of each factor.

Acknowledgement

We would like to express the thanks to Germany Railway Company (DB Systemtechnik GmbH) and WITT ElektronikGmbH for their experimental and financial supports.

References

[1] KOVALCHUK, V., et al. Theoretical study into efficiency of the improved longitudinal profile of frogs at railroad switches. *Eastern-European Journal of Enterprise Technologies* [online]. 2018, **94**(4), p. 27-36. ISSN 1729-3774/eISSN 1729-4061. Available from: https://doi.org/10.15587/1729-4061.2018.139502

[2] PLASEK, O., HRUZIKOVA, M. Under sleeper pads in switches & crossings. *IOP Conference Series: Materials Science and Engineering* [online]. 2017, **236**, 012045. Available from: https://doi.org/10.1088/1757-899X/236/1/012045

[3] GERBER, U., ZOLL, A., FENGLER, W. Verschleiß und Fahrflachenermudung an Weichenmit starrer Herzstuckspitze (Wear and rolling contact fatigue on common crossings of railway turnouts). *ETR - Eisenbahntechnische Rundschau*. 2015, **01**, p. 36-41. ISSN 0013-2845.

[4] FENDRICH, L., FENGLER, W. *Handbuch Eisenbahninfrastruktur (Field manual railway infrastructure)*. Berlin, Heidelberg: Springer-Verlag [online], 2013. ISBN 978-3-642-30021-9. Available from: https://doi.org/10.1007/978-3-642-30021-9

[5] ZOLL, A., GERBER, U., FENGLER, W. Das Messsystem ESAH-M (The measuringsystem ESAH-M). *EI-Eisenbahningenieur Kalender*. 2016, p. 49-62, ISSN 0934-5930

[6] SYSYN, M., KOVALCHUK, V., JIANG, D. Performance study of the inertial monitoring method for railway turnouts. *International Journal of Rail Transportation* [online]. 2018, **4**(4). ISSN 2324-8378/eISSN 2324-8386. Available from: https://doi.org/10.1080/23248378.2018.1514282

[7] GERBER, U., ZOLL, A., FENGLER, W. Fahrzeug basierte Beurteilung des Herzstuck verschleißes (Vehicle-based assessment of wear on common crossings). *EI-Eisenbahningenieur*. 2013, **05**, p. 26-30. ISSN 0013-2810.

[8] KOVALCHUK, V., et al. Development of a promising system for diagnosing the frogs of railroad switches using the transverse profile measurement method. *Eastern European Journal of Enterprise Technologies* [online]. 2018, **92**(2), p. 33-42. ISSN 1729-3774/eISSN 1729-4061. Available from: https://doi.org/10.15587/1729-4061.2018.125699

[9] MOLODOVA, M., et al. Validation of a finite element model for axle box acceleration at squats in the high frequency range [online]. *Computers and Structures* [online]. 2014, **141**, p. 84-93. ISSN 0045-7949/ISSN-L 0045-7949. Available from: https://doi.org/10.1016/j.compstruc.2014.05.005

[10] MOLODOVA, M., LI Z., DOLLEVOET, R. Axle box acceleration: Measurement and simulation for detection of short track defects. *Wear* [online]. 2011, **271**, p. 349-356. ISSN 0043-1648/eISSN 1873-2577. Available from: https://doi.org/10.1016/j.wear.2010.10.003

[11] MOLODOVA, M., et al. Health condition monitoring of insulated joints based on axle box acceleration measurements. *Engineering Structures* [online]. 2016, **123**, p. 225-235. ISSN 0141-0296/eISSN 1873-7323. Available from: https://doi.org/10.1016/j.engstruct.2016.05.018

[12] SALVADOR, P., et al. Axlebox accelerations: Their acquisition and time-frequency characterisation for railway track monitoring purposes. *Measurement* [online]. 2016, **82**, p. 301-312. ISSN 0263-2241/eISSN 1873-412X. Available from: https://doi.org/10.1016/j.measurement.2016.01.012

[13] LEDERMAN, G., et al. Track-monitoring from the dynamic response of an operational train. *Mechanical Systems and Signal Processing* [online]. 2017, **87**, p. 1-16. ISSN 0888-3270/eISSN 1096-1216. Available from: https://doi.org/10.1016/j.ymssp.2016.06.041

[14] BOOGAARD, M., Z. LI, Z., DOLLEVOET, R. In situ measurements of the crossing vibrations of a railway turnout. *Measurement* [online], 2018. **125**, p. 313-324. 1096-1216. Available from: https://doi.org/10.1016/j.measurement.2018.04.094

[15] LEDERMAN, G., et al. A data fusion approach for track monitoring from multiple in-service trains. *Mechanical Systems and Signal Processing* [online]. 2017, **95**, p. 363-379. ISSN 0888-3270/eISSN 1096-1216. Available from: https://doi.org/10.1016/j.ymssp.2017.03.023

[16] GHOFRANI, F., et al. Recent applications of big data analytics in railway transportation systems: A survey. *Transportation Research Part C: Emerging Technologies* [online]. 2018, **90**, p. 226-246. ISSN 0968-090X/eISSN 1879-2359. Available from: https://doi.org/10.1016/j.trc.2018.03.010

[17] LASISI, A., ATTOH-OKINE, N. Principal components analysis and track quality index: A machine learning approach. *Transportation Research Part C* [online]. 2018, **91**, p. 230-248. ISSN 0968-090X/eISSN 1879-2359. Available from: https://doi.org/10.1016/j.trc.2018.04.001

[18] BARBOUR, W., et al. Prediction of arrival times of freight traffic on US railroads using support vector regression. *Transportation Research Part C* [online]. 2018, **93**, p. 211-227. ISSN 0968-090X/eISSN 1879-2359. Available from: https://doi.org/10.1016/j.trc.2018.05.019

[19] JAMSHIDI, A., et al. A decision support approach for condition-based maintenance of rails based on big data analysis. *Transportation Research Part C* [online]. 2018, **95**, p. 185-206. ISSN 0968-090X/eISSN 1879-2359. Available from: https://doi.org/10.1016/j.trc.2018.07.007

[20] WANG, Y., et al. Position synchronization for track geometry inspection data via big-data fusion and incremental learning. *Transportation Research Part C* [online]. 2018, **93**, p. 544-565. ISSN 0968-090X/eISSN 1879-2359. Available from: https://doi.org/10.1016/j.trc.2018.06.018

[21] Statistics and machine learning toolbox. *The MathWorks, Inc.* [online]. Available from: https://de.mathworks.com/products/statistics/features.html

[22] RUNKLER, T. A. *Data analytics: Models and algorithms for intelligent data analysis*. 2. ed. Wiesbaden: Springer Fachmedien [online], 2016. ISBN 978-3-658-14075-5. Available from: https://doi.org/10.1007/978-3-658-14075-5

[23] LAROSE, D. T., LAROSE, C. D. *Discovering knowledge in data: an introduction to data mining*, 2. ed. John Wiley & Sons Inc., 2014. ISBN 978-0-470-90874-7

[24] GARCIA, S., et al. *Data preprocessing in data mining*. Springer, Cham [online], 2014, p. 1-17. ISBN 978-3-319-10247-4. Available from: https://doi.org/10.1007/978-3-319-10247-4_1

[25] BRAMER, M. *Principles of data mining*. 3. ed. London: Springer-Verlag [online], 2016. ISBN 978-1-4471-7307-6. Available from: https://doi.org/10.1007/978-1-4471-7307-6

Dusan Jandacka - Daniela Durcanska - Dasa Kovalova*

CONCENTRATIONS OF TRAFFIC RELATED POLLUTANTS IN THE VICINITY OF DIFFERENT TYPES OF URBAN CROSSROADS

Pollution of the air by gases and particulate matter is a problem of everyday life. Particulate matter (PM) is one of the hazardous pollutants causing deterioration of the environment and thus quality of life of the population. Long-term exposure to effects of increased concentrations of gaseous pollutants can also cause deterioration of the environment and human health. Particulate matter and gases production by the road transport is a burning issue, particularly for larger urban areas. Many factors influence the air quality what determines its development and changes. Air pollution monitoring was focused on a possible change in the concentrations of pollutants after the change of the crossroad - three-arm crossroad to the roundabout. The subject of this paper is monitoring particulate matter (PM_1, $PM_{2.5}$, PM_{10}) and gases (nitrogen oxides NO, NO_2, NO_x) in the vicinity of crossroads in the urban area and an evaluation of fraction ratios PM_{10}, $PM_{2.5}$ and PM_1 with regard to construction of crossroad, meteorological conditions and traffic volume. The roundabout has specific construction and routing traffic, what can influence on production and dispersion of traffic related emissions. The obtained results indicate a decrease in particulate matter concentrations at the roundabout over a three-arm crossroad and an increase in nitrogen oxides concentrations at the roundabout compared to the three-arm crossroad. According to the data obtained and analyzed, the PM_{10} particulate matter concentrations at the roundabout could be reduced by up to 50% over the three-arm crossroad.

Keywords: *particulate matter, nitrogen oxides, roundabout, tree-arm crossroad, traffic volume*

1. Introduction

The dispersion of pollutants in the atmosphere is a difficult process that is not subordinated only to spreading rates of different sources producing this pollution. Of course, the source of various pollutants is decisive for a number of substances that get into the ambient air. There are also other physical factors during the spreading of produced emissions, which determine the dispersion of pollutants into the surrounding environment. They are mainly meteorological parameters, the stability of the atmosphere and segmentation of the surrounding terrain [1-2]. Several studies have been devoted to the spread of pollution in the vicinity of roads, which have confirmed, to some extent, various levels of concentration of pollution considering the distance of the monitoring place from an anticipated source [3-4]. In general, it is confirmed that the greater distance from the road = lower the concentrations of pollutants. The layering of pollution in the vertical direction, has also not less important character, which shows a decrease with the higher terrain clearance [5-8]. The road traffic is one of the main sources of particulate matter, which produces particles not only in urban but in the rural environment, as well [9-11].

The concentrations of pollutants in the air may also be affected by the shape and construction of the road or crossroad (pavement, slope of the road, geometric shape of crossroad, traffic-light controlled crossroads ...) [12-16]. Crossroads are critical elements of road networks in terms of air quality impact, and their control type and geometric configuration can affect significantly vehicular emissions. At crossroads, the vehicles usually slow down and often stop, thus interrupting traffic flow in varying patterns. The main aim of one study was to compare the environmental performance of roundabouts and signal-controlled crossroads. Comparison of the crossroads was performed by a microsimulation model [17]. This paper discusses real air pollution in the vicinity of the two types of crossroads (three-arm crossroad - TAI and roundabout - ROA) and deals with the change of concentrations of pollutants (particulate matter - PM_{10}, $PM_{2.5}$, PM_1 and nitrogen oxides - NO, NO_2, NO_x).

2. Methodology of measurements

Road transport produces various pollutants whose concentrations are the highest in the vicinity of roads or crossroads. Nowadays, the particulate matter of two fractions of PM_{10} and $PM_{2.5}$ are the most mentioned. This study is focused on production of pollutants (PM_{10}, $PM_{2.5}$, PM_1, NO, NO_2, NO_x) from the road transport at the various crossroad types three-arm crossroad - TAI and roundabout - ROA.

* [1]Dusan Jandacka, [1]Daniela Durcanska, [2]Dasa Kovalova
[1]Department of Highway Engineering, Faculty of Civil Engineering, University of Zilina, Slovakia
[2]Research Centre, University of Zilina, Slovakia
E-mail: dusan.jandacka@fstav.uniza.sk

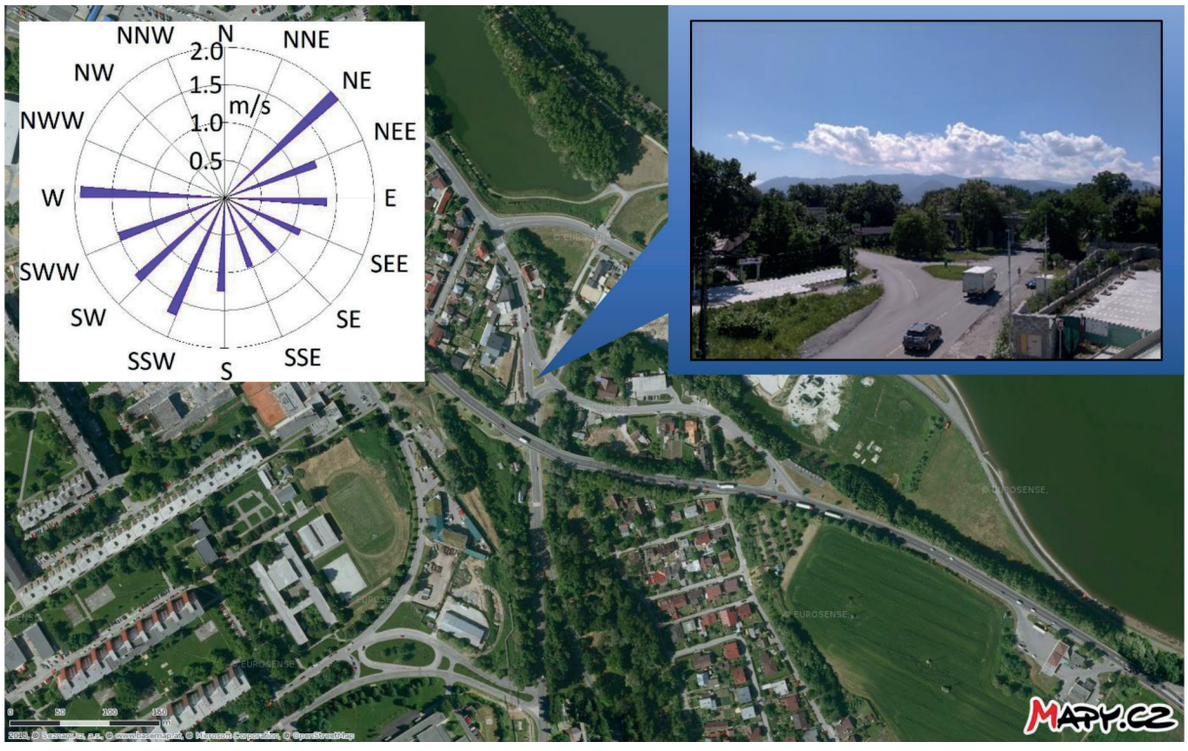

Figure 1 *Three-arm crossroad before reconstruction, predominant winds during the measurement in the year 2016*

2.1 Study area

The first measurement was realised at the TAI in the period from 25th June till 1st July 2016 (Pri celulozke Street and Rosinska Street) before the reconstruction. In that period, the reconstruction of this crossroad from tree-arm crossroad to the roundabout was planned. Existing original TAI was located at the point where industrial and recreational zone of the city of Zilina intersect with the built-up area of companies and facilities of recreation and services. It was located near the state road I/18 on the route Zilina-Martin-Kosice. It was a building of local significance that solves the reconstruction of the existing crossroad within the framework of the city development concept of the city of Zilina. In the case of an inconvenient traffic situation on the road I/18, this crossroad has become one of the strategic connections to the city of Zilina (especially from the direction of Martin). The existing crossroad was not a dangerous and accidental traffic locality in its original layout. However, the collision occurs within the encounter of pedestrians, cyclists and vehicles.

Concurrently, the construction and technical state of the intersected roads had a negative impact during the use of this traffic hub by both public and heavy vehicles transport (in the case of traffic diversion from the state road I/18 on the route Zilina-Martin) as connection of the city to the main road network. There were areas of parked cars in the solved locality of the existing original crossroad, where was an uncontrolled exit of these cars to the road traffic. The roads were being polluted from these unpaved areas and consequently the road dust was being re-suspended to air. Furthermore, the existing crossroad was the last traffic hub before the planned complete cross connection of the network of cycling and walking trails within the concept of city development, especially its relaxing and recreational areas (a dam named Vodne dielo Zilina).

The second measurement was realised at the ROA in the period from 24th June till 30th June 2016 after the reconstruction. The purpose of the reconstruction was to build a roundabout with a diameter of 36 meters in optimal location in terms of fluent and safe transport, as well as in terms of the impact of construction and operation on the population and the natural environment. The main purpose of the reconstruction of existing crossroad was to construct a high-quality and capacity convenient crossroad as a traffic hub for vehicles, but also for pedestrians and cyclists with connection to existing build-up area of companies, facilities and also with connection to residential areas and recreational zones.

Realization of this construction has increased the permeability and the capacity of the crossroad (change of the construction and technical state of the crossroad from three-arm crossroad to roundabout). By the construction of roundabout, the traffic flow has substantially increased during the occasional heavy vehicles transport, interaction between pedestrians (cyclists) and vehicles has also improved regarding to collisions, the cross connection hub of the network of cycling and walking trails has created from the Vlcince settlement (Trnova, Rosinky) in the next sequel to the dam Zilina. In addition, a coherent concept of connection of surrounding facilities, build-up area of companies and recreational zones was created. Respectively, new conditions were created for connecting to others zones.

In addition to this, there is a presumption of a change in the production of pollutants by the road transport, as the process of passing of vehicles through crossroad, vehicle speeds and pavement surfaces were changed. This is the subject of the described measurements, namely the change in the concentrations of pollutants for different types of crossroads.

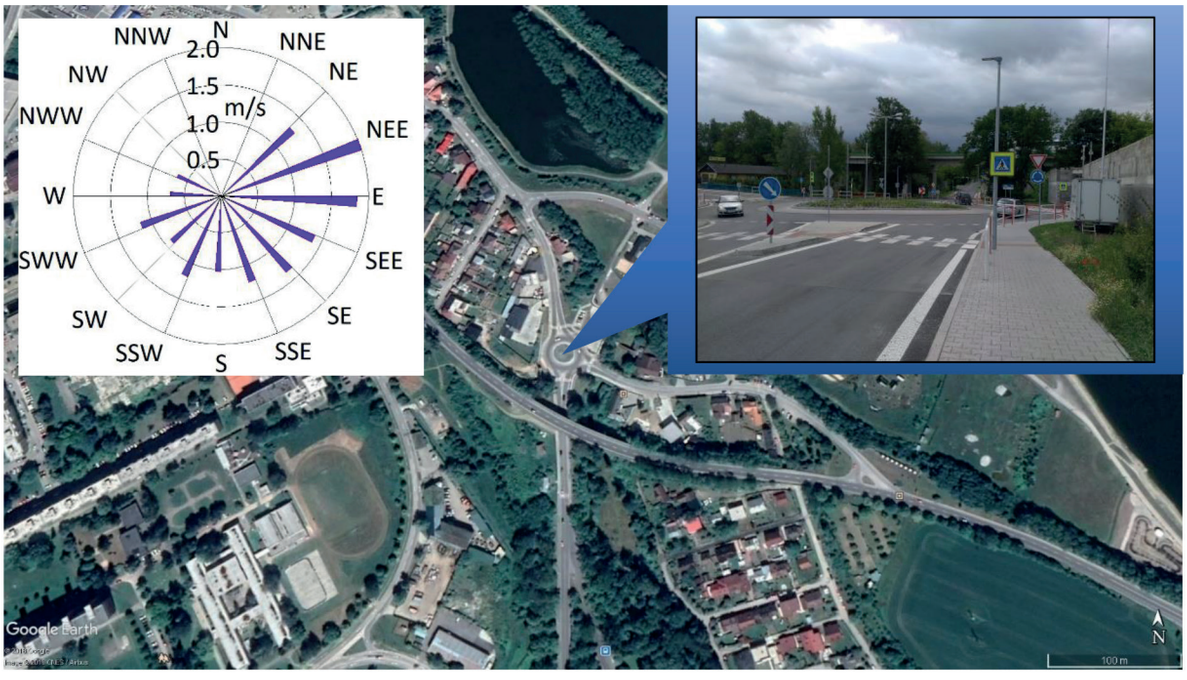

Figure 2 *Roundabout after reconstruction, predominant winds during the measurement in the year 2017*

The proposed roundabout consists of one traffic lane on a traffic circle width of 6.0 meters. The width of the center island is 3.0 meters for the passage of heavy and oversize vehicles. The widths of the entry and exit roads of the individual branches from roundabout are minimally 3.0 m alternatively minimally 5.50 meters between the rims. The curved bends at the entries to the intersection are in the range of 8 to 15 meters and at the exits are in the range of 8 to 14 meters depending on the importance of the traffic direction. For the passage of pedestrians and cyclists through the main branches of the intersection, the traffic islands with the necessary width at the point of passage were constructed.

Mobile Air Quality Monitoring Station of University of Zilina (MAQMS) was located next to the crossroads (three-arm crossroad and roundabout) at the same place in the years 2016 and 2017. The MAQMS has various measurement methods for the pollutant measuring. For the purposes of the NO_x measurements, the standard chemi-luminescence method was used. On the other hand, for the particulate matter measurements, the optical method was used.

2.2 Sample collection

At the chosen measuring station, pollutants from the road transport, namely nitrogen oxides and particulate matter, were measured. Pollutants NO, NO_2, NO_x, PM_{10}, $PM_{2.5}$ and PM_1 were measured and the following measurement methods were used at the measuring stations.

NO, NO_2, NO_x - Standard chemi-luminescence method of measuring the concentration of nitrogen dioxide and nitrogen monoxide. Environment S.A Nitrogen Oxides Analyzer AC32M was used.

The sample is led into a pre-reaction chamber to be blended with ozone. The NO molecules contained in the gas are oxidized into NO_2 before entering the reaction chamber. The signal thus measured without chemi-luminescence by the photo-multiplier, may be considered as "zero air" measurement and used as a reference signal. Next the sample is directly led into the measurement chamber where NO oxidation by ozone is carried out. The signal measured by the photo-multiplier is proportional to the number of NO molecules contained in the sample. The sample flows through the converter oven, then it is blended with ozone inside the reaction chamber. The signal measured by the photo-multiplier is proportional to the number of the NO and NO_2 (from the NO reduction) molecules contained in the sample. The ozone necessary for the chemi-luminescence reaction is generated by a discharge ozone generator.

PM_{10}, $PM_{2.5}$ and PM_1 - Optical method. Fidas® 200 fine dust aerosol spectrometer for simultaneous measurement from company Palas® was used.

The actual aerosol sensor is an optical aerosol spectrometer that determines the particle size using the Lorenz-Mie scattered light analysis of single particles. The single particles move through an optically differentiated measurement volume that is homogeneously illuminated with white light. Each particle generates a scattered light impulse that is detected at an angle of 85° to 95° degrees. The particle number is measured based on the number of scattered light impulses. The level of the scattered light impulse is a measure of the particle size diameter.

The meteorological parameters (temperature - TEMP, humidity - HUMI, wind velocity - WV and direction - WD, pressure - PRES) were measured as well as the traffic volume (Traff).

Concentrations of nitrogen oxides were measured as hourly concentrations in ppb and subsequently recalculated for standard conditions (p = 101.325 kPa and T = 293.15 K) per unit $\mu g/m^3$. Concentrations of particulate matter were measured as hourly

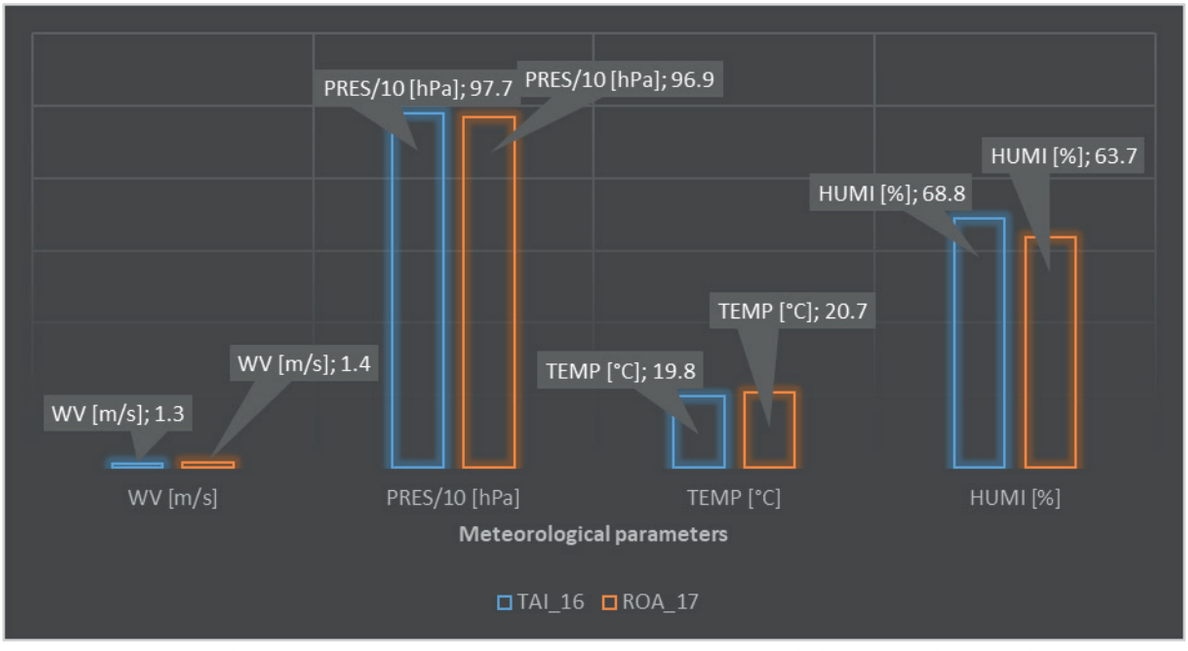

Figure 3 *Meteorological parameters during both periods of measurement at the TAI in 2016 and ROA in 2017*

concentrations in μg/m^3. Samples were captured during 7 days in 2016 (TAI) and 7 days in 2017 (ROA).

3. Results and discussion

The measurements of concentrations of pollutants were carried out near the TAI before the reconstruction and near the ROA after the reconstruction in the same place in the city of Zilina. The particulate matter concentrations of three fractions of PM_{10}, $PM_{2.5}$ and PM_1 and the nitrogen oxides NO, NO_2 and NO_X were sampled. Furthermore, the traffic volume was measured as the primary source of air pollution at the measuring place and meteorological parameters as secondary factors affecting concentrations of pollutants. All average values of pollutant concentrations were calculated from hourly values.

Both periods of measurements (TAI - 1st period from 27th June till 3rd July 2016 and ROA - 2nd period from 26th June till 2nd July 2017) were characterized by very similar meteorological conditions without rainfall. A slight change occurred in the temperature parameter (the temperature was higher by 0.9 °C on average in the year 2017) and the relative humidity parameter (the relative humidity was lower by 5.1 % on average in the year 2017) (Figure 3). The average wind speed during the measurement period (7 measuring days) was 1.3 m/s in 2016 and 1.4 m/s in 2017. The prevailing wind direction was predominantly from the road (crossroad) to the measuring station during both measurement periods (Figures 1, 2).

The traffic volume was evaluated in the unit vehicles per 24 hours in individual measuring days. The measurements were set up to measure pollutants the whole week including five working days and two weekend days. During the working days and weekend days, a higher traffic volume was observed at the ROA in 2017 in comparison to observed traffic volume at the TAI in 2016 (Figure 4). The average traffic volume for the whole measurement period increased by 8.1 % at the ROA in 2017 (15 036 vehicles/24 hours) compared to average traffic volume at the TAI in 2016 (13 910 vehicles/24 hours). Entry road "Vlcince" has been the entry to the crossroad with the highest average traffic volume at both types of crossroads. The average traffic volume at that entry at the original TAI in 2016 was 5946 vehicles per 24 hours and at the ROA in 2017 the average traffic volume was 6655 vehicles per 24 hours (Figure 5). From the perspective of the course of traffic volume, significant annual increase has been shown in 2017 compared to 2016. In terms of emission production, it is questionable how the reconstruction of the crossroad may contribute to a change of concentrations of pollutants.

The road transport produces various pollutants, especially particulate matter and nitrogen oxides. The observed mean 24-hour concentrations of nitrogen oxides were higher at the ROA in 2017 than at the TAI in 2016. The Nitrogen oxide concentrations were lower only on Wednesday and Thursday in 2017 as in 2016 (Figure 6). At the ROA in 2017, the average concentrations during the whole measurement period increased by 86 % for NO, 116 % for NO_2 and 105 % for NO_X compared to the TAI in 2016 (Figure 7). What regards the traffic volume, the increase has been observed which could contribute to higher concentrations of nitrogen oxides. The measurement periods in 2016 and 2017 were almost similar in terms of meteorological parameters because of their minimal changes. The cause of such a significant change in the concentrations of nitrogen oxides appears primarily due to the change of shape of the solved crossroad. At the original TAI before reconstruction, the vehicle speeds were higher than at the ROA on the main route Vlcince - Kosicka. Vehicles did not slowdown in this direction and crossed the TAI with maximum speed. Dispersion of gaseous emissions of nitrogen oxides was more intense and did not accumulate in the crossroad area. Also, there was no need for deceleration and acceleration during the crossing of the crossroad, which leads to the higher engine load and higher production of emissions.

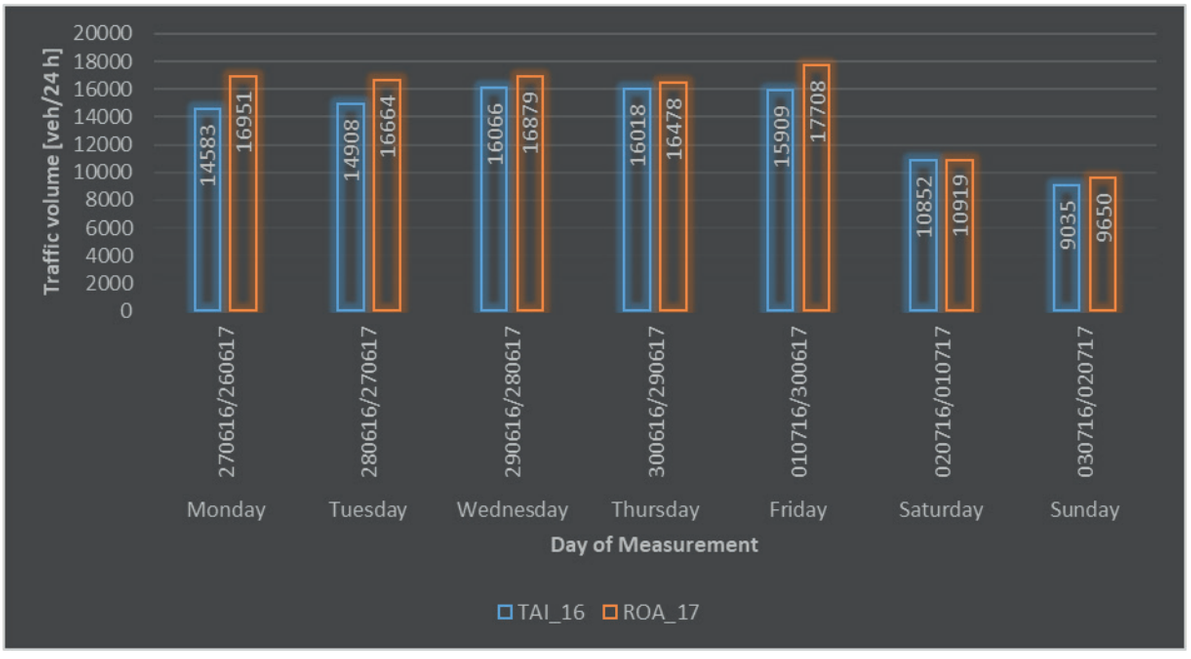

Figure 4 *Traffic volume during both periods of measurement at the TAI in 2016 and ROA in 2017*

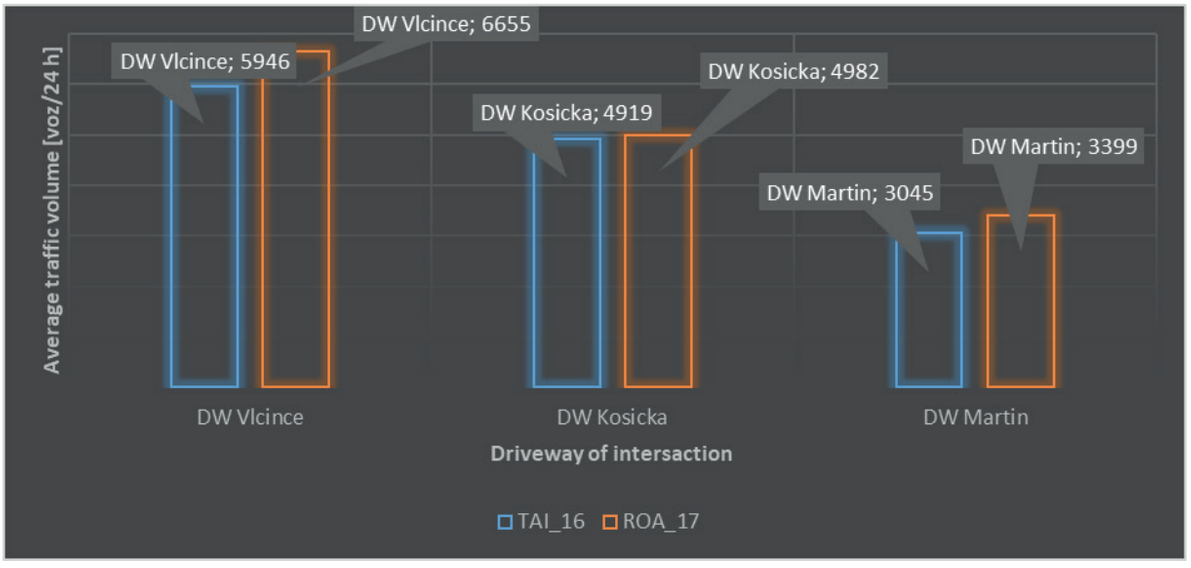

Figure 5 *Average traffic volume regarding to the direction of crossroad branch at the TAI in 2016 and ROA in 2017*

At the new ROA, vehicles have to slowdown ahead of the traffic circle and prefer the vehicles on the traffic circle. At the same time, vehicle speeds are much lower. Due to the more demanding engine operation during the deceleration and acceleration, the emissions of nitrogen oxides are produced to a greater extent. In addition, the lower speeds also cause that nitrogen oxide emissions are longer remaining in the area around the crossroad.

On the other hand, a decrease in particulate matter concentrations at the ROA in 2017 was observed compared to the TAI in 2016 (Figure 8). The average decrease in particulate matter concentrations during the whole measurement period at the ROA was 35 % for PM_{10}, 38 % for $PM_{2.5}$ and 41 % for PM_{1} (Figure 9). Due to the fact that the traffic volume in 2017 has increased compared to 2016, it is necessary to look for the causes of the reduction in particulate matter concentrations in the secondary factors affecting the PM concentrations.

The coarse fraction $PM_{2.5-10}$ comprises more than 50 % of the fraction PM_{10}. The particulate matter distribution found from measurements in 2016 and 2017 is very similar (Figure 10). The change can be seen above all in the actual concentrations of the particulate matter. In the summer when the measurements were carried out, the coarse fraction of particulate matter has a higher representation in the PM_{10} fraction. The coarse fraction $PM_{2.5-10}$ comes mainly from the resuspension of road dust and the resuspension of particulates from the surfaces around the road. These particulate matters are formed from abrasion of vehicle parts, road surfaces, but also from the earth's crust, which are subsequently deposited on the road surface. By the passing of vehicles through crossroad, the particulate matters are back

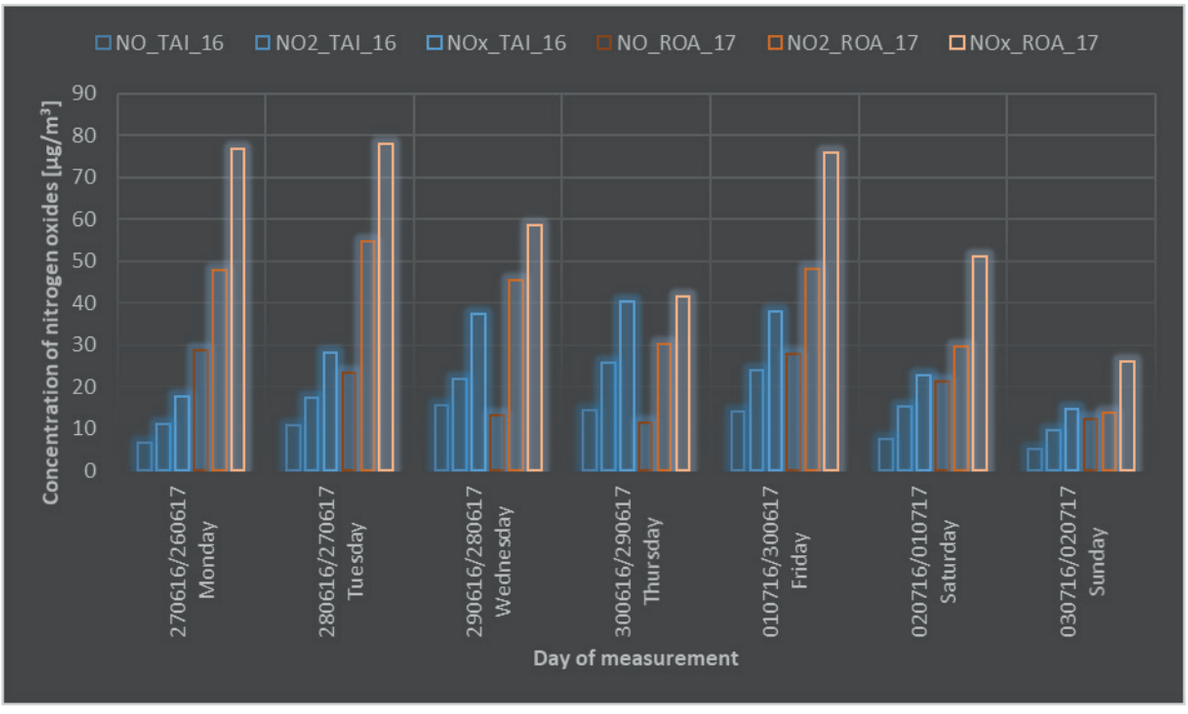

Figure 6 *Concentrations of nitrogen oxides during both periods of measurement at the TAI in 2016 and ROA in 2017*

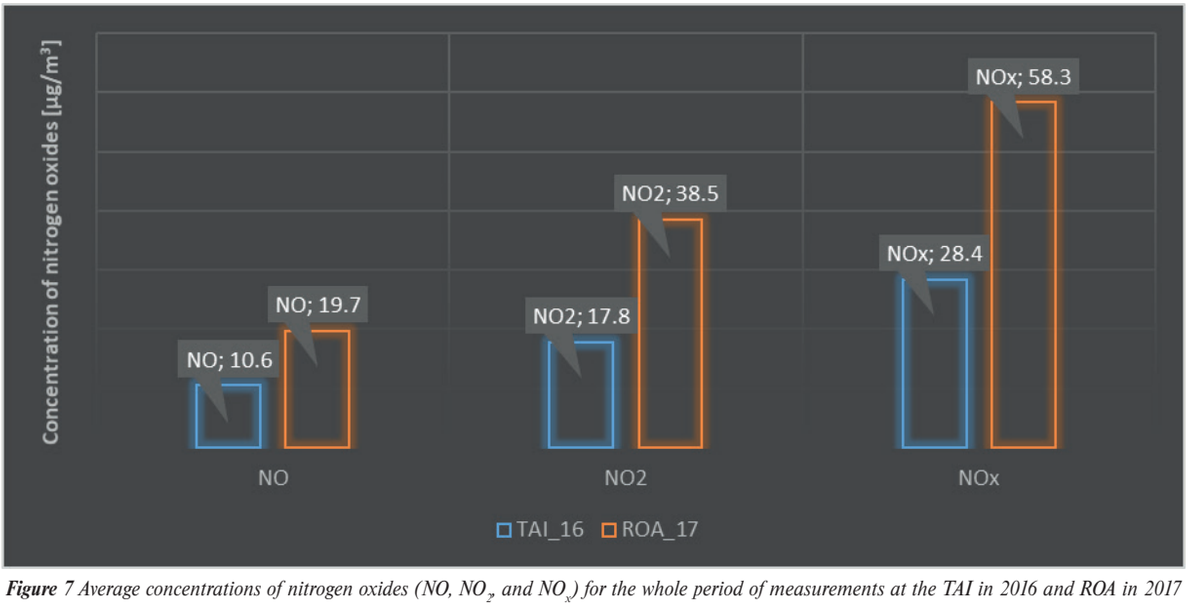

Figure 7 *Average concentrations of nitrogen oxides (NO, NO_2, and NO_x) for the whole period of measurements at the TAI in 2016 and ROA in 2017*

re-suspended into the air. At the TAI in 2016, the passing of vehicles in the main direction was faster (higher vehicle speed) so the particulates were re-suspended more intensely from the road surface into the air. Concurrently, the road surface before reconstruction was degraded and there were more unpaved areas in the vicinity of the crossroad. From these unpaved areas, the road surface was more polluted. At the ROA in 2017, the crossing vehicle speeds were lower, causing the resuspension of particulate matters from the road surface not to be so active. At the same time, the paved areas were built around the crossroad (pavements, parking areas). From meteorological parameters, the wind velocity and atmospheric precipitation have the most significant influence on particle matter concentrations. The wind speed did not change significantly in 2017 compared to 2016 and the precipitation was not observed during both measurement periods. There is probably no change of concentrations of particulate matter in terms of detected changes of meteorological parameters.

The impact of traffic volume on concentrations of pollutants can be clearly seen by comparing working days and weekend days. During the working days, the traffic volume and concentration of pollutants have always been higher. The values of decreases in concentrations of pollutants during the weekend days can be seen in Table 1.

From the point of view of the road transport impact on the environment, lower concentrations of particulate matter were recorded near the ROA than near the TAI. This fact was found despite the higher traffic volume at the ROA than on the TAI. If the minimum or no change of meteorological parameters in

Table 1 *The average concentrations of pollutants during the workdays and weekend*

Intersection type/ Year	Days	NO	NO_2	NO_x	PM_{10}	$PM_{2.5}$	PM_1	$PM_{2.5-10}$	$PM_{1-2.5}$	Traffic volume
		$\mu g/m^3$								veh/24 h
TAI/2016	Workdays	12.3	20.0	32.3	25.2	11.5	9.2	13.7	2.3	15497
	Weekend	6.4	12.4	18.8	16.7	9.4	7.8	7.3	1.7	9944
Change of value over the weekend		-5.9	-7.6	-13.5	-8.5	-2.1	-1.5	-6.4	-0.7	-5553
ROA/2017	Workdays	20.9	45.3	66.1	16.7	7.7	5.9	9.0	1.8	16936
	Weekend	16.9	21.7	38.6	10.0	4.5	3.3	5.5	1.2	10285
Change of value over the weekend		-4.0	-23.6	-27.6	-6.7	-3.2	-2.6	-3.5	-0.6	-6652

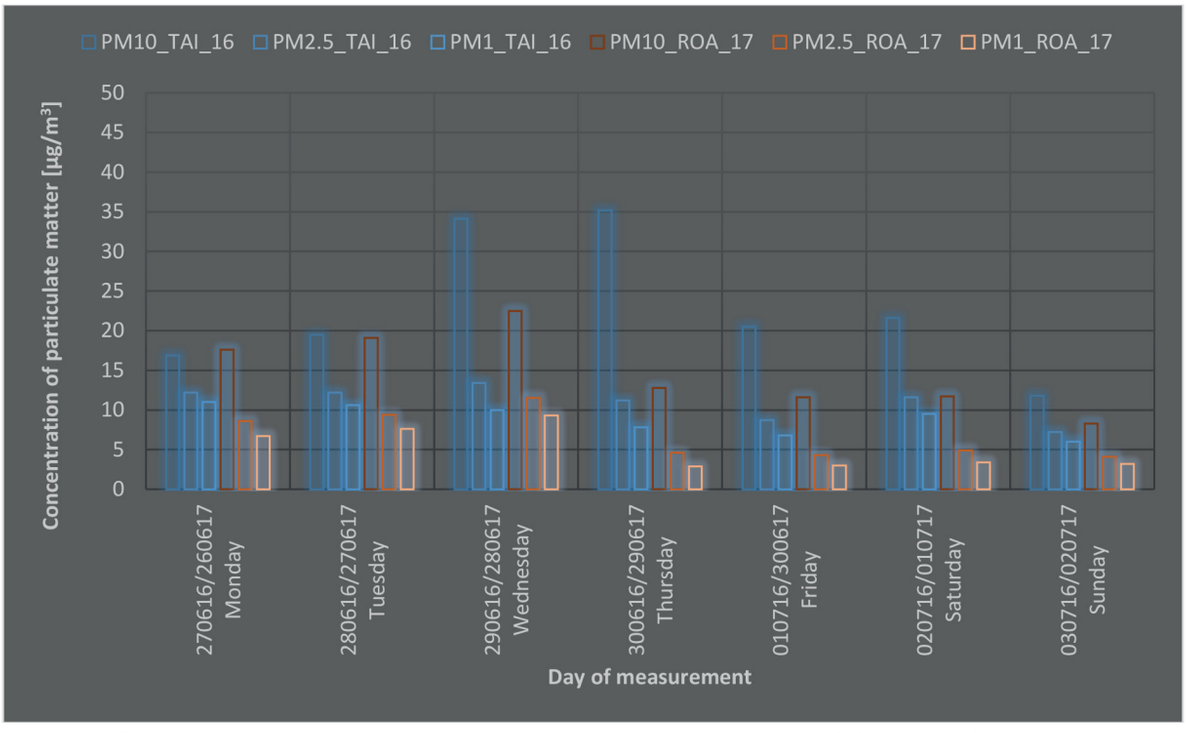

Figure 8 *Concentrations of particulate matter during both periods of measurement at the TAI in 2016 and ROA in 2017*

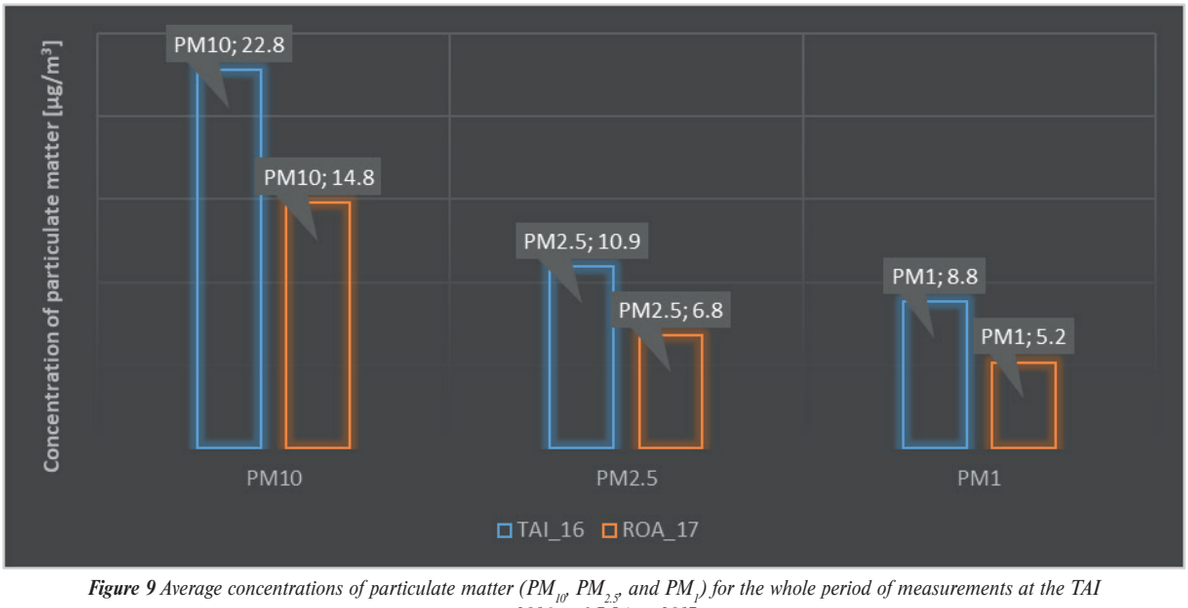

Figure 9 *Average concentrations of particulate matter (PM_{10}, $PM_{2.5}$, and PM_1) for the whole period of measurements at the TAI in 2016 and ROA in 2017*

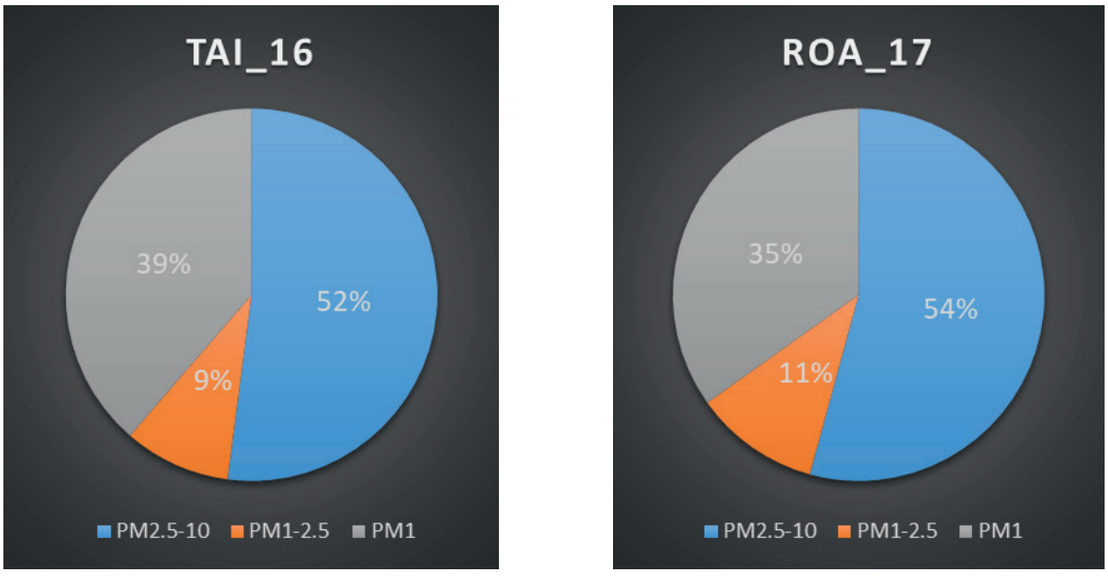

Figure 10 *Distribution of the PM fractions in the total PM_{10} fraction measurements at the TAI in 2016 and ROA in 2017*

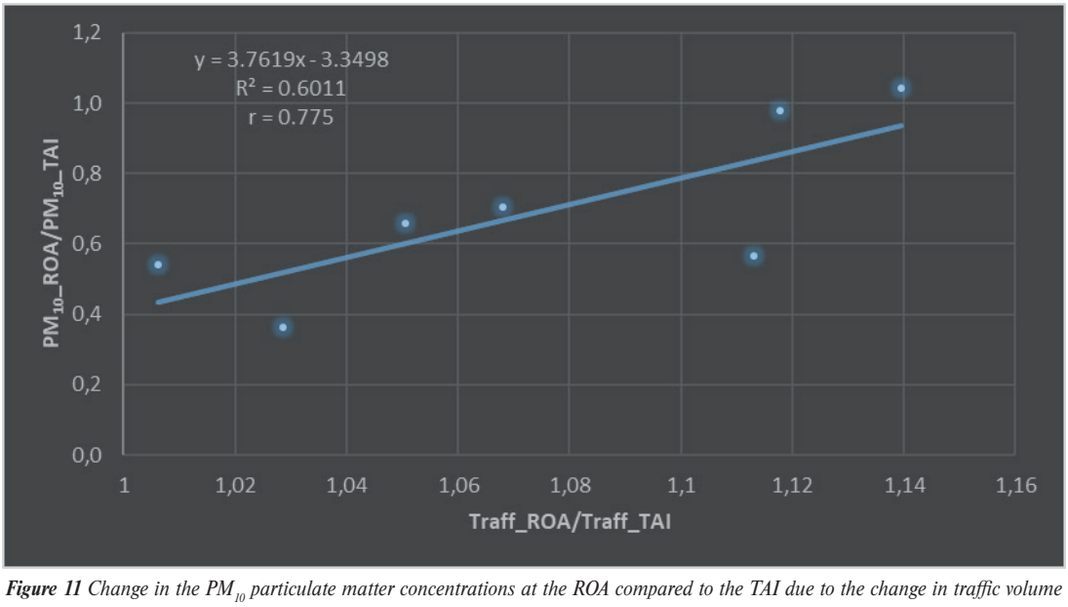

Figure 11 *Change in the PM_{10} particulate matter concentrations at the ROA compared to the TAI due to the change in traffic volume*

the atmosphere is taken into account a correlation relationship between the traffic volume change (Traff_ROA / Traff_TAI) and the particulate matter PM_{10} concentration change (PM_{10}_ROA / PM_{10}_TAI) can be created. By performing a linear regression analysis, the computational matrix consisted of an independent variable traffic volume ratio - Traff_ROA / Traff_TAI and the dependent variable particulate matter PM_{10} concentration ratio - PM_{10}_ROA / PM_{10}_TAI. The analysis showed (using the measured data) that if the traffic volume at the ROA did not increase over the TAI, a drop of the PM_{10} particulate matter concentrations could reach up to 60 %. At the same time, the largest change in the traffic volume +2034 vehicles / 24 h at the ROA compared to the TAI did not lead to a decrease in the PM_{10} particulate matter concentrations (Figure 11).

4. Conclusions

The changes in concentrations of pollutants may be influenced by different environmental factors. On one hand, there may be primary sources of pollutants, such as the road transport, industry, agriculture, local heating, etc., and on the other hand there are secondary factors such as meteorological parameters, shape and segmentation of landscape relief, various artificial barriers in the country - buildings, noise barriers, etc.

In this contribution, it was dealt with possible change in concentrations of pollutants - particulate matter of three fractions of PM_{10}, $PM_{2.5}$ and PM_1 and nitrogen oxides NO, NO_2 and NO_x from the road transport in terms of different types of crossroads. In 2016, pollutants were measured at the original three-arm crossroad - TAI, which has been then reconstructed to the new roundabout - ROA. In 2017, the measurements of pollutants were performed at the new ROA. Significant change occurred

in the shape of the crossroad, modification of its surroundings, character of the vehicle passing through the crossroad (vehicle speed, maneuvering). The traffic volume increased by 8.1 % at the ROA on average compared to the TAI during the whole measuring period (7 days). The meteorological parameters did not change significantly and can be considered very similar for both measurement periods. However, the concentrations of nitrogen oxides and particulate matter have showed substantial change. An increase of concentrations of nitrogen oxides was found, namely by 86 % for NO, by 116 % for NO_2 and by 105 % for NO_X at the ROA compared to the TAI. The increase of nitrogen oxides was mainly caused by the change in the shape of the crossroad and thus the character of the road traffic. Vehicles crossed the ROA at a lower speed, increased engine load in acceleration and deceleration, which caused a higher accumulation of nitrogen oxides and also lower dispersion near the crossroad. With regard to the particulate matter concentrations at the roundabout, the decrease was found. Concentrations of the PM_{10} decreased by 35 %, $PM_{2.5}$ by 38 %, and PM_1 by 41 %. Therefore, the change of the crossroad shape affected also the PM concentrations. In addition, the process of vehicles passing through the ROA (lower speeds, lower air swirl) caused a reduction in the re-suspended road dust, especially the coarse fraction of the $PM_{2.5-10}$ particulates. Analysis of data showed that if the traffic volume at the ROA did not increase over the TAI, a drop of PM_{10} particulate matter concentrations could reach up to 60 %.

From the conducted research it can be concluded that the modification of the crossroad can affect the concentrations of pollutants. In this case, the concentrations of nitrogen oxides increased and the concentrations of particulate matter decreased.

Acknowledgements

The paper originated as being supported by means of a grant VEGA 1/0537/17 «*The influence of pavement surface morphology on pavement serviceability and emissions production*».

References

[1] IWARI. S., et al. Variability in atmospheric particulates and meteorological effects on their mass concentrations over Delhi, India. *Atmospheric Research* [online]. 2014, **145-146**, p. 45-56 [accessed 2014-04-30]. ISSN 0169-8095. Available from: https://doi.org/10.1016/j.atmosres.2014.03.027

[2] TECER, L. H. Comparison and seasonal evaluation of the rural and urban ambient $PM_{2.5}$ and PM_{10} mass concentrations based on meteorological parameters. In 13th International Multidisciplinary Scientific GeoConference Surveying Geology and Mining Ecology Management, SGEM 2013: proceedings [online]. Section Air Pollution and Climate Change. Sofia, Bulgaria: STEF92 Technology Ltd., 2013. ISBN 978-619-7105-03-2, ISSN 1314-2704, p. 593-600. Available from: https://doi.org/10.5593/SGEM2013/BD4/S19.011

[3] JUNG, K. H., ARTIGAS, F., SHIN J. Y. Seasonal gradient patterns of polycyclic aromatic hydrocarbons and PM concentrations near a highway. *Atmosphere* [online]. 2011, **2**(3), p. 533-552. ISSN 2073-4433. Available from: https://doi.org/10.3390/atmos2030533

[4] SHARMA, A., MASSEY, D. D., TANEJA, A. Horizontal gradients of traffic related air pollutants near a major highways in Agra, India. *Indian Journal of Radio a Space Physics* [online]. 2009, **38**, p. 338-346. ISSN 0367-8393/eISSN 0367-8393. Available from: http://nopr.niscair.res.in/bitstream/123456789/6901/1/IJRSP%2038(6)%20338-346.pdf

[5] HITCHNINS, J., et al. Concentrations of submicrometre particles from vehicle near a major roads. *Atmospheric Environment* [online]. 2000, **34**(1), p. 51-59. ISSN 1352-2310. Available from: https://doi.org/10.1016/S1352-2310(99)00304-0

[6] MORAWSKA, L., et al. A study of the horizontal and vertical profile of submicrometer particles in relation to a busy road. *Atmospheric Environment* [online]. 1999, **33**(8), p. 1261-1274. ISSN 1352-2310. Available from: https://doi.org/10.1016/S1352-2310(98)00266-0

[7] ROORDA-KNAPE, M. C., et al. Air pollution from traffic in city districts near major motorways. *Atmospheric Environment* [online]. 1998, **32**(11), p. 1921-1930. ISSN 1352-2310. Available from: https://doi.org/10.1016/S1352-2310(97)00496-2

[8] WU, Y., et al. Vertical and horizontal profiles of airborne particulate matter near major roads in Macao. China. *Atmospheric Environment* [online]. 2002, **36**, p. 4907-4918. ISSN 1352-2310. Available from: https://doi.org/10.1016/S1352-2310(02)00467-3

[9] JANDACKA, D. Contributory assessment of creation of PM_{10} as impacted by vehicular traffic based on the presence of heavy metals. *Communications - Scientific Letters of the University of Zilina* [online]. 2013, **15**(3), p. 96-101. ISSN 1335-4205/eISSN 2585-7878. Available from: http://komunikacie.uniza.sk/index.php/communications/article/view/695

[10] JANDACKA, D., DURCANSKA, D., BUJDOS, M. The contribution of road traffic to particulate matter and metals in air pollution in the vicinity of an urban road. *Transportation Research Part D: Transport and Environment* [online]. 2017, **50**, p. 397-408. ISSN 1361-9209/eISSN 1879-2340. Available from: https://doi.org/10.1016/j.trd.2016.11.024

[11] PANT, P., HARRISON, R. M. Estimation of the contribution of road traffic emissions to particulate matter concentrations from field measurements: A review. *Atmospheric Environment* [online]. 2013, **77**, p. 78-97. ISSN 1352-2310. Available from: https://doi.org/ 10.1016/j.atmosenv.2013.04.028

[12] FULLOVA, D., et al. Mass distribution of particulate matter produced during abrasion of asphalt mixtures in laboratory. *Communications - Scientific Letters of the University of Zilina* [online]. 2016, **18**(4), p. 37-43. ISSN 1335-4205/eISSN 2585-7878. Available from: http://komunikacie.uniza.sk/index.php/communications/article/view/286

[13] DURCANSKA, D. Analysis of particulate matter composition. *Communications - Scientific Letters of the University of Zilina* [online]. 2010, **12**(3A), p. 17-22. ISSN 1335-4205/eISSN 2585-7878. Available from: http://komunikacie.uniza.sk/index.php/communications/article/view/939

[14] REMISOVA, E., DECKY, M., KOVAC, M. The influence of the asphalt mixture composition on the pavement surface texture and noise emissions production. In: 14th International multidisciplinary scientific conference SGEM 2014, Geoconference on Energy and clean Technologies: proceedings [online]. Section Air pollution and Climate change. Albena, Bulgaria, 2014, Vol. 2, Book 4, ISBN 978-619-7105-16-2/ISSN 1314-2704, p. 583-590. Available from: https://doi.org/10.5593/SGEM2014/B42/S19.077

[15] TROJANOVA, M., DECKY, M., REMISOVA, E. The implication of climatic changes to asphalt pavement design. In: 24th Russian-Polish-Slovak Seminar on Theoretical Foundation of Civil Engineering, TFoCE 2015: proceedings [online]. Samara, Russian Federation, 2015. Vol. 111. ISSN 1877-7058, p. 770-776. Available from: https://doi.org/10.1016/j.proeng.2015.07.144

[16] KOCIANOVA, A., DRLICIAK, M., PITLOVA, E. Influence of roundabout capacity enhancement on emission production. *IOP Conference Series: Materials Science and Engineering* [online]. 2017, **236**, 012035. ISSN 17578981. Available from: https://doi.org/10.1088/1757-899X/236/1/012035

[17] GASTALDI, M., et al. Evaluation of air pollution impacts of a signal control to roundabout conversion using microsimulation. *Trans. Res. Procedia* [online]. 2014, **3**, p. 1031-1040. ISSN 2352-1465. Available from: https://doi.org/10.1016/j.trpro.2014.10.083

Milan Moravcik*

ACCELERATION RESPONSE OF THE RAILWAY BRIDGES -VERIFICATION OF THE LIMIT STATE OF ACCELERATION

The dynamic response of a girder bridge under trains is studied with an emphasis on the vertical track acceleration. The vehicles are modelled as a series of moving loads. The efficiency of the method is demonstrated on the simply supported railway bridge of the length L_b = 38 m subjected to the series of the bogie forces of the conventional IC train. The closed-form solution of the bridge response with the intention to resonance and cancellation effects is applied. The acceleration response is investigated for the resonance train speed c = 65 m/s = 234 km/h, considering the modes of vibration j = 1 and j = 1+3, because higher modes can have significant influence on the acceleration amplitude. The limits of acceleration due to the ballast stability and the traffic safety are evaluated.

Keywords: *dynamic response of the railway bridges, acceleration, resonant speed, modal superposition method*

1. Introduction

Dynamic response of railway bridges subjected to the real trains moving at the speed c most often via the dynamic displacement ${}^{(c)}w(x,t)$ and the vertical acceleration ${}^{(c)}\ddot{w}(x,t)$. In this direction, the most analyses are formed for the load considered as a single point load (the axle loads P_{ax} or the bogie loads P_{bg}) [1-4], but the practical case of the response corresponds to the passage of whole train. At present time, the actual question becomes vibrations of railway bridges due to the train moving at speeds above 200 km/h. It poses dynamic problems of higher order, due to the possibility of resonance effects and their possible limitation. The presented numeric study is focused to the loads by conventional IC passenger trains running on the Slovak railways lines, Figure 1.

In this study, the acceleration response of the small and medium weakly damped bridges ($\xi_d < 0.05$), modelled as a simply supported 2D beam, subjected to a row of bogie forces $P_{bg,n}$, n = 1, 2,.... N of IC-cars is presented. The acceleration response is focussed on the mid-point response for the train speed c and will be marked in the form ${}^{(c)}\ddot{w}_{(j)(P_{bgn})}(L_b/2,t)$, considering modes of vibrations j = 1 and j = 1+3 because higher modes can impose significant influence on the acceleration amplitude. The response will be analysed with the purpose to evaluate the effect of individual components of the acceleration on the total vertical acceleration. Typical cross sections of the railway bridge are shown in Figure 2. The vertical plane of symmetry of the cross-section coincides with the track axes, which is the plane of the bridge vibrations.

The solution of the problem is presented for the real railway steel bridge of the length L_b = 38 m subjected by the whole passenger train with eight IC cars for one resonance speed c = 65 m/s = 234 km/h.

The spacing length between concentrated bogie loads $P_{bg,n}$ corresponds to full length $d_{ch} = d_v$ = 24.5 m of the IC-carriage (the conventional passenger IC-car of Slovak IC-trains) as is shown in Figure 1.

2. Resonance and cancellation conditions of the bridge

The resonance conditions belongs to the periodic excitation of concentrated loads moving over a bridge, can be obtained from the theoretical solution of the vertical vibrations of the beam subjected to a moving load series [5-7]. The resonant condition is calculated from the time necessary for crossing the characteristic length d_{ch} at speed c, which is equal to the k-multiple of the period of natural vibrations $T_j = \frac{1}{f_j} = \frac{2\pi}{\omega_j}$, for j = 1, 2, 3,.... and gives

$$f_{ex} = f_{(j)}k = \frac{\omega_{(j)}}{2\pi}k, k = 1,2,3,\ldots, \tag{1}$$

where: $f_{ex} = \frac{c}{d_v}$ is the excitation frequency.

A) Resonant speed

For simply supported bridges it is significant that the fundamental mode $\omega_{(1)} = 2\pi f_{(1)}$ provides the largest contribution to the response and from the resonant condition (2) results the resonant train speeds $c_{(k)res}$:

$$c_{(k)res} = \frac{\omega_{(1)}d_v}{k2\pi} = \frac{f_{(1)}d_v}{k}[\mathrm{m/s}], k = 1,2,3,\ldots. \tag{2}$$

Each load force $P_{bg,n}$, n = 1, 2, 3, ... N in a moving load series may induce the transient response of the bridge and the successive forces $P_{bg,n+1}$ form a periodical excitation. The response will be successively amplified with increase of the number of forces

* **Milan Moravcik**
Faculty of Civil Engineering, University of Zilina, Slovakia
E-mail: mimo@fstav.uniza.sk

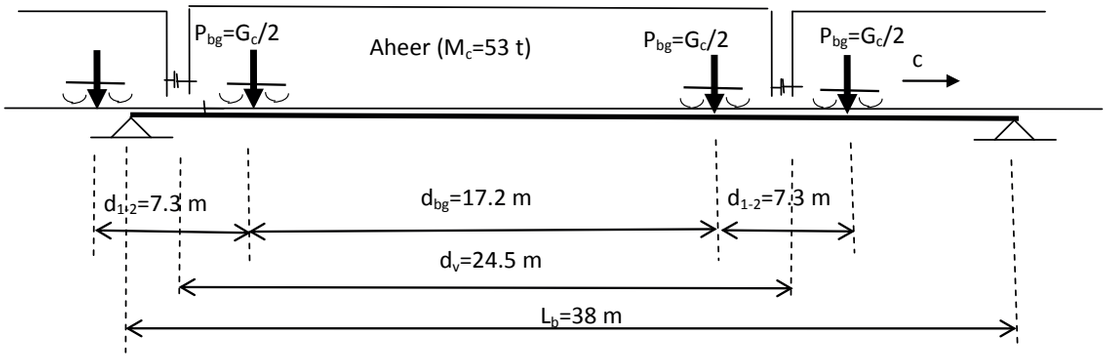

Figure 1 *Simply supported bridge subjected to series moving loads - the bogie loads of IC-cars*

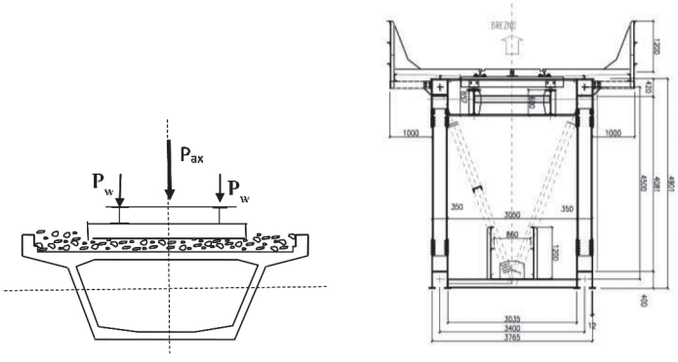

Figure 2 *Typical cross sections of the railway bridges*

travelling through the beam. The real resonant speed (2) is also affected by the span velocity ratio [6]

$$\cos(\omega_{(1)} L_b / c_{(k)res}) . \quad (3)$$

If the condition (3) approaches the value -1.0, the resonant amplitude may be suppressed.

For example, the resonant train speed $c_{(k=2)res}$ for the bridges of the length L_b = 38 m, and d = 24.5 m, and for $\omega_{(1)} = \frac{\pi^2}{L_b^2}\sqrt{\frac{EI}{m_1}} = 33.34 s^{-1}$ is $c_{(k=2)} = \frac{\omega_{(1)} d_v}{k \cdot 2\pi} =$ 65 m/s = 234 km/h and the span velocity ratio and $\cos(\omega_{(1)} L_b / c_2) = 0.8072.$

B) Cancellation of the resonance

Unlike the resonance effect that enlarges the bridge response, the cancellation effect may suppress the vibrations of the bridge. The cancellation phenomenon implies that the waves associated with the free vibrations response of the bridge cancel out each other. For a load series, the condition of cancellation of the resonance vibrations results from the general solution of the dynamic response and gives the condition which is defined in [6] as the first type of the vibrations cancellation:

$$\cos\left(\frac{\omega_{(1)} d}{2c}\right) = 0, \frac{\omega_{(1)} d}{2c} = \frac{\pi(2k-1)}{2}, k = 1, 2, 3, \ldots . \quad (4)$$

where: $d = (d_v, d_{c1}, d_{c2})$ is the characteristic interval of the load series (Figure 1). This type of cancellation is induced by each individual load and is independent on the composition of the load series.

For example: For the considered case L_b = 38 m, $\omega_{(1)} = 33.34 s^{-1}$, $d_{ch} = d_v = 24.5 m$ and for k = 3 the cancellation speed is $c_{(3)can} = \frac{33.34 \cdot 24.5}{(2 \cdot 3 - 1)\pi}$ = 52 m/s² = 187.3 km/h.

2.1 Serviceability limit state - traffic safety

The limits of vibrations and deformation in railway bridges should be reviewed and evaluated just over acceleration of the bridge. Excessive deformations and vibrations can endanger the track geometry, the ballast stability and functionality of the train-bridge. In EN1991-2 [7-8], the criteria for the traffic safety are defined taking into account the following dynamic effects: the vertical acceleration, the vertical deformations and vibrations, the deck twist, and longitudinal displacements.

The maximum peak values for the bridge deck acceleration should not exceed the following values:

1) ${}^{(c)}\ddot{w}(x,t)_{\max} = 3.5$ - m/s² for ballasted tracks,
2) ${}^{(c)}\ddot{w}(x,t)_{\max} = 5.0$ = 5.0 - m/s² for direct fastened tracks.

3. Formulation of the acceleration response of the beam

The elementary theoretical model for bridges used in the bridge dynamics is considered as a simple beam of span L_b subjected to a row of moving forces P_n, n = 1, 2, ... N, which are moving at a constant speed c (Figure 3). The governing Bernoulli-Euler partial differential equation describes the behaviour of the beam (without the damping term) - the transverse beam deflection $w(x,t)$ due to a series of moving forces:

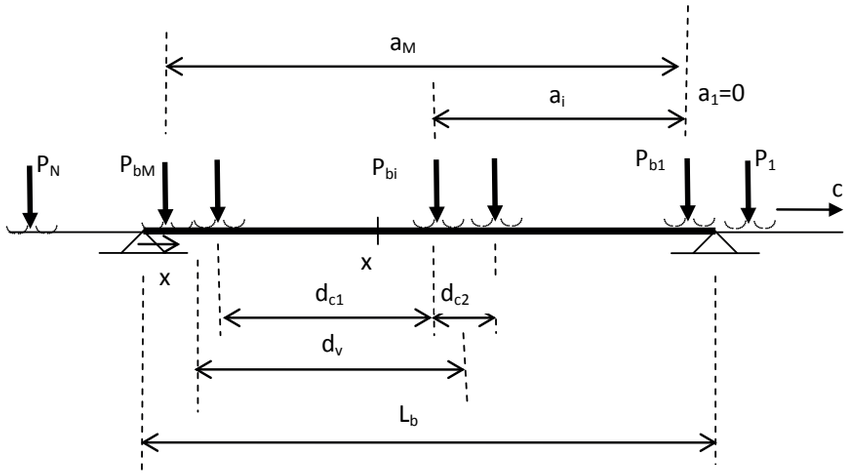

Figure 3 *Simple beam of the span L_b subjected to a row of forces P_n, n = 1, 2, ... N, which are moving at a constant speed c*

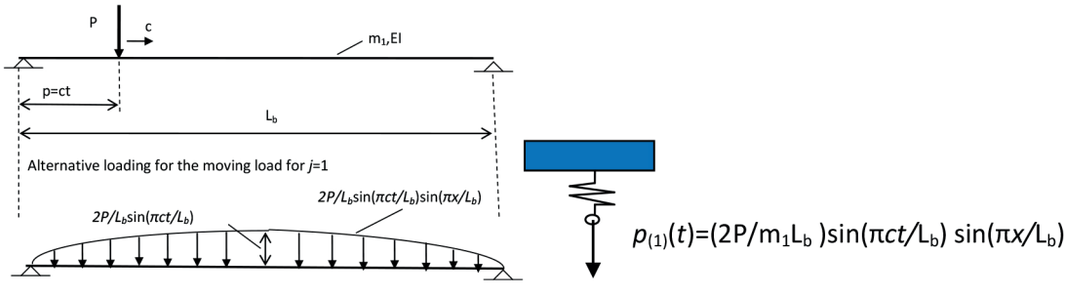

Figure 4 *Replacing of the single moving load $P\delta(x-ct)$ by the fixed load $p_{(1)}(t)$*

$$EI\frac{\partial^4 w(x,t)}{\partial x^4}+m_1\frac{\partial^2 w(x,t)}{\partial t^2}=\sum_{n=0}^{M-1}P\delta\left(x-c\left(t-\frac{d_{v,n}}{c}\right)\right)H_{(n)},$$

n = 1, 2, ... M (5)

where: $H_{(n)}(t)=\left(\theta\left(t-\frac{d_{bg,n}}{c}\right)-\theta\left(t-\frac{d_{bg,n}}{c}-\frac{L_b}{c}\right)\right)$ is the Heaviside function, $\delta(x-ct)$ is the Dirac function.

The solution to Equation (5) can be expressed in terms of the modal shapes $\phi_{(j)}(x)$ and associated modal coordinates $q_{(j)}(t)$ as in [1-2]:

$$w(x,t)=\sum_j q_{(j)}(t)\cdot\phi_j(x)=\sum_j q_{(j)}(t)\sin\left(\frac{j\pi x}{L_b}\right),$$

j = 1, 2, 3, ... (6)

where: $q_{(j)}(t)$ are the generalized coordinates that define the amplitude of vibrations, $\phi_j(x)=\sin\left(\frac{j\pi x}{Lb}\right)$ are the fundamental mode shapes known and for the simply supported beam of a sinusoidal type.

The modal equation corresponding to a general concentrated moving load $P\delta(x-ct)$ corresponds to the solution an one degree of freedom (1DOF) system for the jth mode of vibrations and can be expressed as

$$\ddot{q}_{(j)}(t)+\omega_{(j)}^2 q_{(j)}(t)=\frac{2P}{m_1 L_b}\sin\frac{j\pi p}{L_b},\ p=ct \quad (7)$$

The constant moving load $P\delta(x-ct)$ (considering only the fundamental shape j = 1) can be replaced by the fixed load $p_{(1)}(t)$ variables over time, Figure 4.

The j-th generalized equation of motion of the beam (without damping) corresponding (5) can be written in the form [1, 7]

$$\frac{d^2 q_{(j)}(t)}{dt^2}+\omega_{(j)}^2 q_{(j)}(t)=\frac{2P}{m_1 L_b}\sum_{n=0}^{M-1}\sin\frac{j\pi p}{L_b}\cdot\left(t-\frac{d_{v,n}}{c}\right)H_{(n)} \quad (8)$$

for n = 1, 2, ... M, $0\le t\le L_b/c$

Since the maximum acceleration was expected at the mid-point of the beam, the acceleration response was focused on the mid-point response $x=L_b/2$ and it was obtained by superposition of components of the acceleration dependence on number of modes of vibrations (j) acceleration. While for the displacement response modes of vibrations higher than j = 1 may be neglected without serious loss of accuracy, for the acceleration response of the beam higher modes can have significant influence on the acceleration amplitude.

3.1 Vertical mid-span acceleration for modes of vibrations j = 1 and j = 1+3

Solution of the problem begins with displacement ${}^{(c)}w(x,t)$ of the bridge that is expressed in term of the vibrations mode shapes j as follows [1, 7]. Corresponding acceleration response

${}^{(c)}\ddot{w}(x,t)$ can be obtained by differentiating the displacement ${}^{(c)}w(x,t)$ twice with respect to the time:

$$ {}^{(c)}\ddot{w}(x,t)=\frac{d^2}{dt^2}[{}^{(c)}w(x,t)] \tag{9}$$

The acceleration response is marked as ${}^{(c)}\ddot{w}_{(j),(P_{bgn})}(L_b/2,t)$ and was analysed for the purpose to evaluate the impact of individual components on the total response with the following labelling:

A*) *The midpoint acceleration - ${}^{(c)}\ddot{w}^{(A)}_{(j),(Pbg,n)}(L_b/2,t)$, for modes j due to the bogie loads $P_{bg,n}$, n = 1, 2, 3, ... M , moving direct over the beam, ignoring the difference between the damped and un-damped vibrations, which includes the two components:

- *Forced vibrations part (the quasi-static component)* ${}^{(c)}\ddot{w}_{(j)st,(Pbg,n)}(L_b/2,t)$
- *Free vibrations part (the dynamic component)* ${}^{(c)}\ddot{w}_{(j)dyn,(Pbg,n)}(L_b/2,t)$.

B*) *The midpoint acceleration - the free vibrations of the beam ${}^{(c)}\ddot{w}^{(B)}_{(j),(Pbg,n)}(L_b/2,t)$ due to loads $P_{bg,n}$, n = 1, 2, 3, ... K moving out the beam after they have left the span.

C*) *The complex midpoint acceleration ${}^{(c)}\ddot{w}^{(C)}_{(j),(Pbg,n)}(L_b/2,t)$ due to the loads n = *1, 2, ... M* moving direct over the beam and the loads n = *1, 2, ... K* moving out the beam after they have left the beam and it can be expressed by the superposition:

$$\begin{aligned}&{}^{(c)}\ddot{w}^{(C)}_{(j),(Pbg,n)}(L_b/2,t)={}^{(c)}\ddot{w}^{(A)}_{(j),(Pbg,n)}(L_b/2,t)+\\&+{}^{(c)}\ddot{w}^{(B)}_{(j)dyn,(Pbg,n)}(L_b/2,t)={}^{(c)}\ddot{w}_{(j)st,(Pbg,n)}(L_b/2,t)+\\&+{}^{(c)}\ddot{w}_{(j)dy,(Pbg,n)}(L_b/2,t)+\ddot{w}^{(B)}_{(j)dyn,(Pbg,n)}(L_b/2,t)\end{aligned} \tag{10}$$

3.2 Vertical mid-span acceleration due to the loads moving direct over the beam

Components of the vertical mid-span acceleration can be written in the form:

A*) *Component of the acceleration ${}^{(c)}\ddot{w}^{(A)}_{(j),(Pbg,n)}(L_b/2,t)$, for j = 1+3...., n = 1, 2, ... M bogie forces moving direct over the beam at speed c and can be expressed as [7] (the damping of the beam is not considered):

$$\begin{aligned}&{}^{(c)}\ddot{w}^{(A)}_{(j),(Pbg,n)}(L_b/2,t)=\frac{d^2}{dt^2}\left[{}^{(c)}w^{(2)*}_{(j),(P_{bg,n})}(L_b/2,t)\right]=\\&=\frac{d^2}{dt^2}\left[\sum_{n=0}^{M-1}\sum_{j=1}^{m=3}\frac{\hat{w}_{(j),(P_{bg})}(L_b/2,t)}{1-{}^{(c)}\alpha^2_{(j)}}\left(\sin{}^{(c)}\Omega_{(j)dr}\left(t-\frac{d_{bg,n}}{c}\right)-\right.\right.\\&\left.\left.-{}^{(c)}\alpha_{(j)}\sin\omega_{(j)}\left(t-\frac{d_{bg,n}}{c}\right)\right)\sin\frac{j\pi x}{2}H_{(n)}\right]=\\&=\sum_{n=0}^{M-1}\sum_{j=1}^{m=3}\frac{\hat{w}_{(j),(P_{bg})}(L_b/2,t)}{1-{}^{(c)}\alpha^2_{(j)}}\left(-{}^{(c)}\Omega^2_{(j)dr}\sin{}^{(c)}\Omega_{(j)dr}\cdot\right.\\&\left.\cdot\left(t-\frac{d_{bg,n}}{c}\right)+{}^{(c)}\Omega_{(j)dr}\omega_{(j)}\left(t-\frac{d_{bg,n}}{c}\right)\right)\sin\frac{j\pi x}{2}H_{(n)}\end{aligned} \tag{11}$$

For: $\frac{d_{bg,n}}{c}\le t\le\frac{d_{bg,n}}{c}+\frac{L_b}{c}$,

$$H_{(n)}=H\left(t-\frac{d_{bg,n}}{c}\right)-H\left(t-\frac{d_{bg,n}}{c}-\frac{L_b}{c}\right),$$

where:

$$\hat{w}_{(j),(P_{bg})}(L_b/2)\equiv\hat{q}_{(j),(P_{bg})}(L_b/2)=\frac{2P_{bg}L_b^3}{EI\pi^4}\approx\frac{P_{bg}L_b^3}{48EI}$$

is the static deflection at mid-span caused by the load P_{bg} with respect to the jth mode of vibrations, ${}^{(c)}\Omega_{(j)dr}=\frac{j\pi c}{L_b}$ is the jth circular driving frequency of the force P_{bg}, $\omega_{(j)}=\frac{j^2\pi^2}{L_b^2}\sqrt{\frac{EI}{\bar{m}_1}}$ [s^{-1}] is the jth natural frequency of the beam, ${}^{(c)}\alpha_{(j)}=\frac{{}^{(c)}\Omega_{(j)dr}}{\omega_{(j)}}=\frac{j\pi c}{L_b\omega_{(1)}}\equiv\frac{c}{c_{cr}}$ is the dimensionless speed parameter corresponding to the jth mode of vibrations.

B*) *Component of the acceleration ${}^{(c)}\ddot{w}^{B}_{(j),(P_{bg,n})}(L_b/2,t)$ corresponding to the free vibrations response of the beam for the j-th mode and for n = 1, 2, 3, ... K loads moving out the beam after they have left the beam (the damping of the beam is considered) can be expressed as:

$$\begin{aligned}&{}^{(c)}\ddot{w}^{(B)}_{(j),(Pbg,n)}(L_b/2,t)=\frac{d^2}{dt^2}\left[{}^{(c)}w^{(B)}_{(j),(P_{bg,n})}(L_b/2,t)\right]=\\&=\frac{d^2}{dt^2}\left[\frac{\hat{w}_{(j)st,(P_{bg})}(L_b/2)}{1-{}^{(c)}\alpha^2_{(j)}}\sum_{n=0}^{K-1}\sum_{j=1}^{m=3}-e^{-\omega_d\left(t-\frac{d_{bg,n}}{c}-\frac{L_b}{c}\right)^{(c)}}\right.\\&\left.\alpha_{(j)}\sin\omega_{(j)}\left(t-\frac{d_{bg,n}}{c}-\frac{L_b}{c}\right)\sin\frac{j\pi}{2}H_{(n^*)}(t)\right]=\\&=\frac{\hat{w}_{(j)st,(P_{bg})}(L_b/2,t)}{1-{}^{(c)}\alpha^2_{(j)}}\sum_{n=0}^{K-1}\sum_{j=1}^{m=3}-e^{-\omega_d\left(t-\frac{d_{bg,n}}{c}-\frac{L_b}{c}\right)^{(c)}}\Omega^2_{(j)dr}\omega_{(j)}\\&\sin\omega_{(j)}\left(t-\frac{d_{bg,n}}{c}-\frac{L_b}{c}\right)\sin\frac{j\pi}{2}H_{(n^*)}(t)\end{aligned} \tag{12}$$

For: $\frac{d_{bg,n}}{c}+\frac{L_b}{c}\le t\le\frac{d_{bg,n}}{c}+\frac{L_b}{c}+\Delta t$,

$$H_{(n^*)}(t)=\left(\theta\left(t-\frac{d_{bg,n}}{c}-\frac{L_b}{c}\right)-\theta\left(t-\frac{d_{bg,n}}{c}-\frac{L_b}{c}-\Delta t\right)\right),$$

Δt is a selected time of the beam free vibrations of the beam.

4. Numerical studies for the mid-point vertical acceleration of the railway steel bridge L_b = 38 m for the speed c = 65 m/s = 234 km/h

To verify the theoretical expressions, the numerical study has been performed. The mid-point acceleration response of the bridge L_b = 38 m during the passage of the passenger train with the eight IC-cars (16xP_{bg} = 16x256 KN), the length of car d_v = 24.5 m, and for the resonance speed $c_{res(2)}$ = 65.03 m/s = 234.16 km/h have been analysed.

Input parameters of the solution:

The bending stiffness of the beam: EI = 7.58·10^7 kNm^2, the mass $m_1=m_{1(Bc)}+m_{1(Sup)}=3.18$ t/m , the circular frequencies of the bridge: $\omega_{(1)}$ = 33.34 s^{-1}, $\omega_{(3)}$ = 300.06 s^{-1}, the driving frequencies ${}^{(c=65)}\Omega_{(1)dr}=\frac{\pi c}{L_b}=5.3711\,\mathrm{s}^{-1}$,

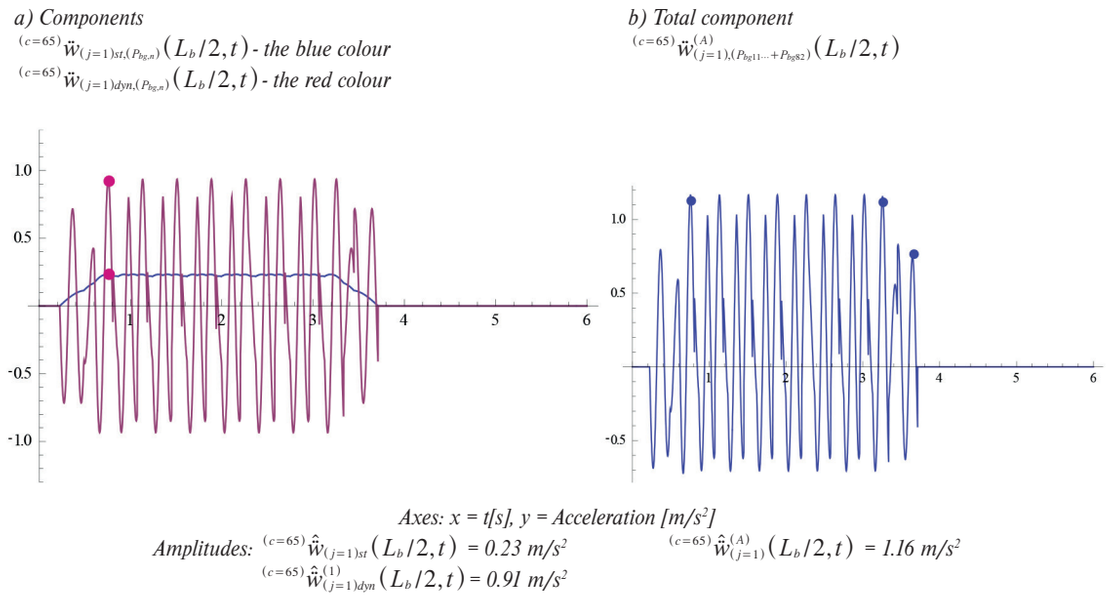

Axes: x = t[s], y = Acceleration [m/s²]

Amplitudes: $^{(c=65)}\hat{\ddot{w}}_{(j=1)st}(L_b/2,t)$ = 0.23 m/s² $^{(c=65)}\hat{\ddot{w}}^{(A)}_{(j=1)}(L_b/2,t)$ = 1.16 m/s²

$^{(c=65)}\hat{\ddot{w}}^{(1)}_{(j=1)dyn}(L_b/2,t)$ = 0.91 m/s²

Figure 5 *Acceleration response* $^{(c=65)}\ddot{w}^{(A)}_{(j=1)st,(P_{bg,n})}(L_b/2,t)$ *and its components.*

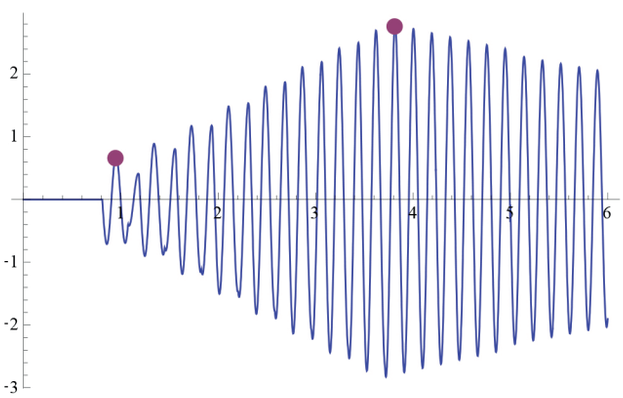

Axes: x = t[s], y = $^{(c=65)}\ddot{w}^{(B)}_{(j=1)dyn,(P_{bg,n})}(L_b/2,t)$ *[m/s²]*

Amplitudes: $^{(c=65)}\hat{\ddot{w}}^{(2)*}_{(j=1)dyn,(P_{bg,n})}(L_b/2,t)$ = 0.7.... 2.7 m/s²

Figure 6 *Acceleration response* $^{(c=65)}\ddot{w}^{(B)}_{(j=1)dyn,(P_{bg,n})}(L_b/2,t)$ *for t = 0 ÷ 6.0 s.*

$^{(c=65)}\Omega_{(3)dr} = \frac{3\pi c}{L_b} = 16.1133\ \mathrm{s}^{-1}$, the non-dimensional speed parameters $^{(c=65)}\alpha_{(1)} = \frac{\Omega_{(1)dr}}{\omega_{(1)}} = 0.1611$, $^{(c=65)}\alpha_{(3)} = \frac{\Omega_{(3)dr}}{\omega_{(3)}} = 0.1611$, the damping coefficient $\omega_d = f_{(damp)}\vartheta = \frac{\omega_{(1)}}{2\pi}\vartheta = \frac{33.34}{6.26}0.025 = 0.1327\ \mathrm{s}^{-1}$.

Results of the analysis are presented in the time domain [9]. Vertical midpoint acceleration of the beam $^{(c)}\ddot{w}^{(A)}_{(j),(P_{bg,n})}(L_b/2,t)$ due to the loads moving over the beam for j = 1, Equation (11), are presented in Figures 5 to 7 and result $^{(c)}\ddot{w}^{(B)}_{(j),(P_{bg,n})}(L_b/2,t)$ for j = 1+3, Equation (12), are presented in Figures 8 to 9. Comparison is presented in Figures 10 to 11.

4.1 Vertical midpoint acceleration of the beam due to the loads moving over the beam for *j* = 1

This response includes the two components:

1) *The forced vibrations part* (the quasi-static component of acceleration) $^{(c=65)}\ddot{w}_{(j=1)st,(P_{bg,n})}(L_b/2,t)$.
2) *The free vibrations part* (the dynamic component) $^{(c=65)}\ddot{w}_{(j=1)dyn,(P_{bg,n})}(L_b/2,t)$, for j = 1, Equation (11), for the time section t = 0 ÷ 6.0 s, Figure 5.

4.2 Free vibrations response of the beam due to the loads moving out the beam for *j* = 1

The time history of the vertical acceleration of the beam $^{(c=65)}\ddot{w}^{(B)}_{(j=1),(P_{bg,n})}(L_b/2,t)$, for the mode shape j = 1, corresponds to loads $P_{bg,n}$, n = 1, 2, 3, ... K moving out the beam after they have left the span (Equation 12), for the time section t = 0 ÷ 6.0 s, is in Figure 6.

a) Components
$^{(c)}\ddot{w}^{(A)}_{(j),(P_{bg,n})}(L_b/2,t)$ *- the blue colour*
$^{(c)}\ddot{w}^{(B)}_{(j)dyn,(P_{bg,n})}(L_b/2,t)$ *- the red colour*

b) Total component
$^{(c=65)}\ddot{w}^{(C)}_{(j=1),(P_{bg,n})}(L_b/2,t)$

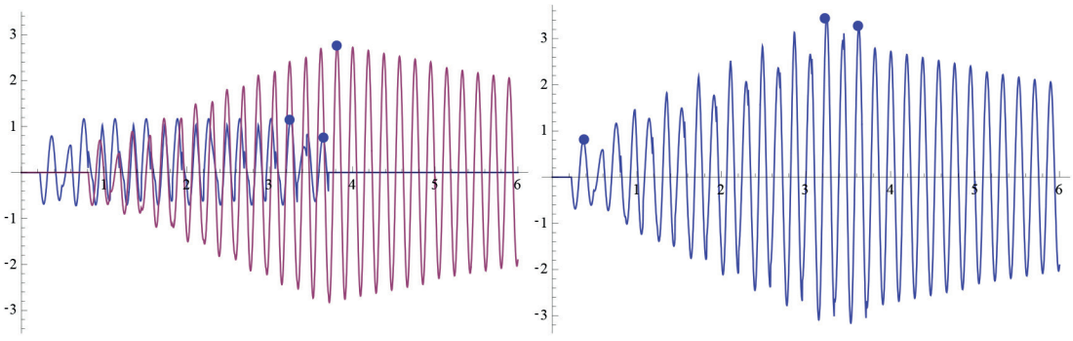

Amplitude of the total acceleration:

$^{(c=65)}\hat{\ddot{w}}^{(A)}_{(j=1),(P_{bg,n})}(L_b/2,t)$ = 1.26 m/s²
$^{(c)}\hat{\ddot{w}}^{(B)}_{(j=1)dyn}(L_b/2,t)$ = 0.7.... 2.7 m/s²

$^{(c=65)}\hat{\ddot{w}}^{(C)}_{(j=1)}(L_b/2,t)$ = 0.7.... 3.5 m/s²

Axes: x = t[s], y = Components and the complex response $^{(c)}\ddot{w}^{(C)}_{(j),(P_{bg,n})}(L_b/2,t)$ *[m/s²] Amplitudes of components:*

c) Detail of the response for t = 3.0 ÷ 4.5 s

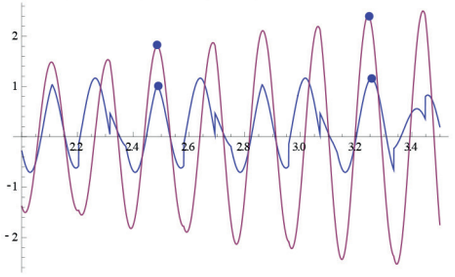

***Figure** 7 Complex acceleration* $^{(c=65)}\ddot{w}^{(C)}_{(j=1),(P_{bg,n})}(L_b/2,t)$ *and its components, for j = 1*

4.3 Complex acceleration response due to the loads moving over the beam and the loads moving out the beam for *j* = 1

The complex response $^{(c)}\ddot{w}^{(C)}_{(j),(P_{bg,n})}(L_b/2,t)$ obtains by superposition (Equation 10):

$$^{(c)}\ddot{w}^{(C)}_{(j),(P_{bg,n})}(L_b/2,t) = {}^{(c)}\ddot{w}^{(A)}_{(j),(P_{bg,n})}(L_b/2,t) + {}^{(c)}\ddot{w}^{(B)}_{(j)dyn,(P_{bg,n})}(L_b/2,t)$$

Results of the solution for the time section $t = 0 \div 6.0$ s, are shown in Figure 7.

4.4 Vertical midpoint acceleration of the beam due to the loads moving over the beam, for *j* = 1+3

The midpoint acceleration $^{(c=65)}\ddot{w}^{(A)}_{(j=1+3),(P_{bg,n})}(L_b/2,t)$ for the modes j = 1+3 obtains by superposition and includes the two components:

1) The forced vibrations part (the quasi-static component) $^{(c=65)}\ddot{w}_{(j=1+3)st,(P_{bg,n})}(L_b/2,t)$.
2) The free vibrations part (the dynamic component) $^{(c=65)}\ddot{w}_{(j=1+3)dyn,(P_{bg,n})}(L_b/2,t)$, for j = 1+3. The solution for the time section $t = 0 \div 6.0$ s, is shown in Figure 8.

4.5 Acceleration due to loads moving out the beam - the residual acceleration for *j* = 1+3

Comparison of the residual free vibrations acceleration components for j = 1 and j = 3 $^{(c=65)}\ddot{w}^{(B)}_{(j=1)dyn,(P_{bg,n})}(L_b/2,t)$ for j = 1 and $^{(c=65)}\ddot{w}^{(B)}_{(j=1+3)dyn,(P_{bg,n})}(L_b/2,t)$ for j = 1+3, Figure 9.

$$^{(c=65)}\ddot{w}^{(B)}_{(j=1+3)dyn,(P_{bg,n})}(L_b/2,t) = {}^{(c=65)}\ddot{w}^{(B)}_{(j=1)dyn,(P_{bg,n})}(L_b/2,t) + {}^{(c=65)}\ddot{w}^{(B)}_{(j=3)dyn,(P_{bg,n})}(L_b/2,t) \quad (13)$$

4.6 Comparison of accelerations for modes of vibrations *j* = 1and *j* = 1+3

A) Comparison* of *the residual total free vibrations
$^{(c=65)}\ddot{w}^{(B)}_{(j=1)dyn,(P_{bg,n})}(L_b/2,t)$ for j = 1 and
$^{(c=65)}\ddot{w}^{(B)}_{(j=1+3)dyn,(P_{bg,n})}(L_b/2,t)$ for j = 1+3, Figure 10.

B) Complex acceleration due to the loads moving over the beam and the loads moving out the beam, for j = 1+3

The complex acceleration response $^{(c=65)}\ddot{w}^{(C)}_{(j=1+3)dyn,(P_{bg,n})}(L_b/2,t)$ for the modes j = 1+3, is obtained by superposition:

1) For the loads moving over the beam.

a) Components

$^{(c=65)}\ddot{w}_{(j=1+3)st,(P_{bg,n})}(L_b/2,t)$ - *the blue colour*

$^{(c=65)}\ddot{w}_{(j=1+3)dyn,(P_{bg,n})}(L_b/2,t)$ - *the red colour*

b) Total component

$^{(c=65)}\ddot{w}^{(A)}_{(j=1+3),(P_{bg,n})}(L_b/2,t)$

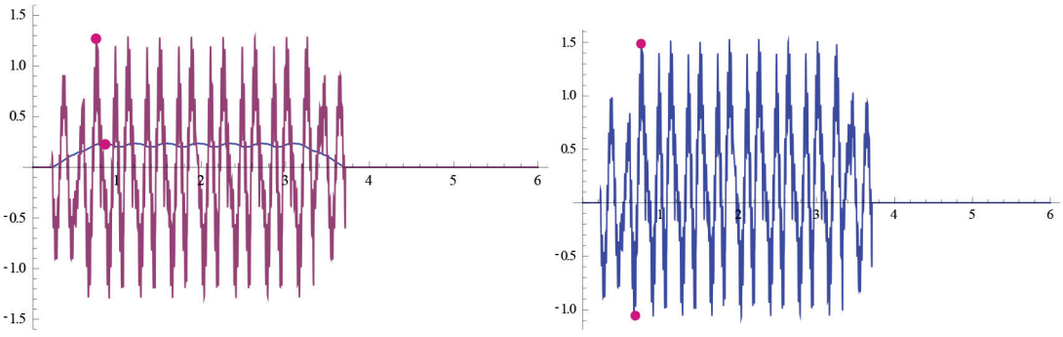

Axes: x = t[s], y = Components and the total acceleration $^{(c=65)}\ddot{w}^{(A)}_{(j=1+3),(P_{bg,n})}(L_b/2,t)$ *[m/s²]*

Amplitudes: $^{(c=65)}\hat{\ddot{w}}^{(A)}_{(j=1+3),(P_{bg,n})}(L_b/2,t)$ *= 1.50 m/s²*

Figure 8 *Components and total acceleration* $^{(c=65)}\ddot{w}^{(A)}_{(j=1+3),(P_{bg,n})}(L_b/2,t)$ *for j = 1+3*

a) Components

$^{(c=65)}\ddot{w}^{(B)}_{(j=1)dyn,(P_{bg,n})}(L_b/2,t)$ - *the red colour*

$^{(c=65)}\ddot{w}^{(B)}_{(j=1+3)dyn,(P_{bg,n})}(L_b/2,t)$ - *the blue colour*

b) Total component

$^{(c=65)}\ddot{w}^{(B)}_{(j=3)dyn,(P_{bg,n})}(L_b/2,t)$

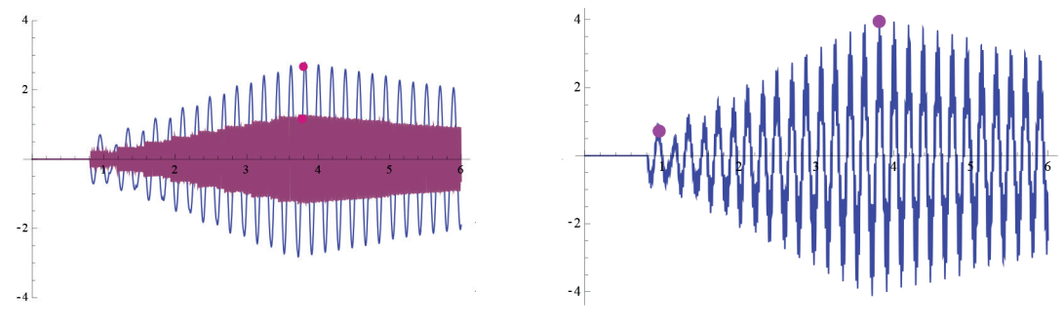

Axes: x = t[s], y = Parts and the total acceleration $^{(c=65)}\ddot{w}^{(B)}_{(j=1+3)dyn,(P_{bg,n})}(L_b/2,t)$ *for j = 1+3.*

Amplitudes of parts:

$^{(c=65)}\hat{\ddot{w}}^{(B)}_{(j=1),(P_{bg,n})}(L_b/2,t)$ - *the blue colour*

$^{(c=65)}\hat{\ddot{w}}^{(B)}_{(j=3)dyn,(P_{bg,n})}(L_b/2,t)$ - *the dark red colour*

Total amplitudes:

$^{(c=65)}\ddot{w}^{(2)*}_{(j=1+3)dyn,(P_{bg,n})}(L_b/2,t)$ *= 0.86 ÷ 4.02 m/s²*

Figure 9 *Acceleration* $^{(c=65)}\ddot{w}^{(B)}_{(j=1+3)dyn,(P_{bg,n})}(L_b/2,t)$ *corresponding to the free vibrations and its parts*

a) Residual accelerations for the mode j = 1

b) Residual accelerations for j = 1+3

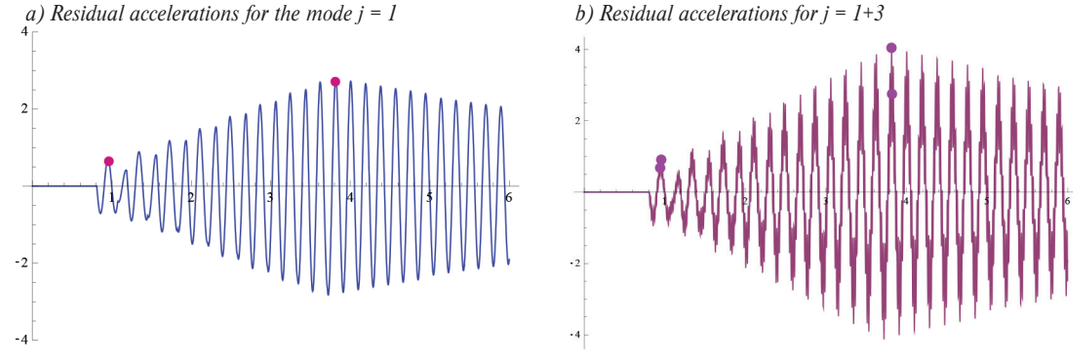

Amplitudes:

$^{(c=65)}\hat{\ddot{w}}^{(B)}_{(j=1)dyn,(P_{bg,n})}(L_b/2,t)$ *= 0.7 ÷ 2.7 m/s²,*

$^{(c=65)}\hat{\ddot{w}}^{(B)}_{(j=1+3)dyn,(P_{bg,n})}(L_b/2,t)$ *= 0.86 ÷ 4.2 m/s²*

Figure 10 *Comparison of the free acceleration components* $^{(c=65)}\ddot{w}^{(B)}_{(j=1)dyn,(P_{bg,n})}(L_b/2,t)$ *for j = 1 and* $^{(c=65)}\ddot{w}^{(B)}_{(j=1+3)dyn,(P_{bg,n})}(L_b/2,t)$ *for j = 1+3*

a) Components
$^{(c=65)}\ddot{w}^{(A)}_{(j=1+3),(P_{bg,n})}(L_b/2,t)$ *- the red colour*
$^{(c)}\ddot{w}^{(B)}_{(j=1+3),(P_{bg,n})}(L_b/2,t)$ *- the blue colour*

b) Total component
$^{(c=65)}\ddot{w}^{(C)}_{(j=1+3),(P_{bg,n})}(L_b/2,t)$

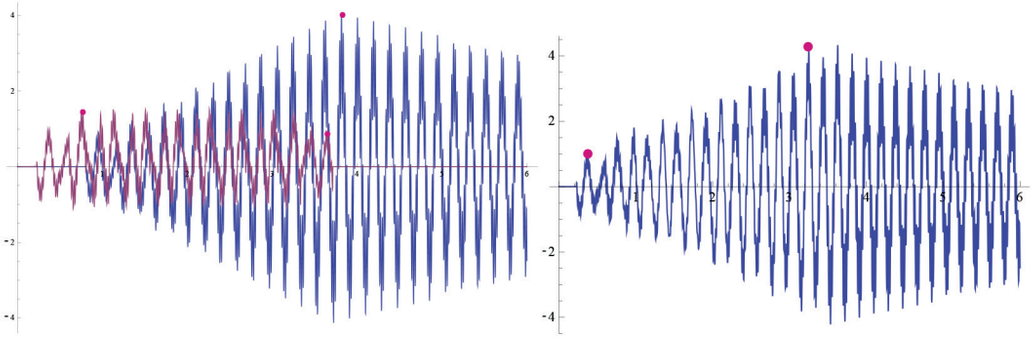

c) Detail superposition for t = 3.0 ÷ 4.5 s

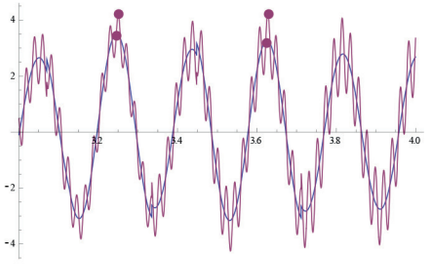

Axes: x = t[s], y = Parts and the total component $^{(c)}\ddot{w}^{(C)}_{(j),(P_{bg,n})}(L_b/2,t)$ *[m/s²]*

Amplitudes: $^{(c=65)}\hat{\ddot{w}}^{(A)}_{(j=1+3)}(L_b/2,t) = 1.27$ *m/s²* $^{(c=65)}\hat{\ddot{w}}^{(C)}_{(j=1+3)}(L_b/2,t) = 1.0 \div 4.3$ *m/s²*

Figure 11 *The complex response* $^{(c=65)}\ddot{w}^{(C)}_{(j=1+3),(P_{bg,n})}(L_b/2,t)$ *for t = 0 ÷ 6.0 s and for t = 3.0 ÷ 4.5 s*

2) For the loads moving out the beam, for the time section t = 0 ÷ 6.0 s**,** Figures 11 a), b), and for the time segment t = 3.0 ÷ 4.5 s, Figure 11c.

$$^{(c=65)}\ddot{w}^{(C)}_{(j=1+3),(P_{bg11}\cdots+P_{bg82})}(L_b/2,t) = \\ = {}^{(c=65)}\ddot{w}^{(A)}_{(j=1+3),(P_{bg11}\cdots+P_{bg82})}(L_b/2,t) + \\ + {}^{(c=65)}\ddot{w}^{(2)*}_{(j=1+3)(P_{bg11}\cdots+P_{bg82})}(L_b/2,t)$$

5. Conclusions

The vertical mid-point acceleration for the resonant speed c = 65 m/s = 234 km/h for the simply supported railway bridge of the length L_b = 38 m subjected to the loads by conventional IC passenger trains with eight cars, running on the Slovak railways lines (Figure 1) has been investigated through numerical simulation. Since the maximum acceleration is expected at the mid-point of the beam, the acceleration response-was focused on the mid-point response $x = L_b/2$. The closed form of solution has been applied.

The numerical study was focused to:

1) Evaluating the influence of the free and forced vibrations components on the total acceleration.
2) The influence of mode vibrations j = 1 and j = 1+3 on the total acceleration.
3) The serviceability limit state for the bridge deck acceleration [8] was controlled.

The following conclusions can be drawn:

1) Dynamic response components, due to forced vibrations, increase with speed. When the running speed of moving loads c coincides with any of the resonant speeds $c_{(k)\text{res}}$ the sum of the free vibrations response components generated by each moving force $P_{bg,n}$ is determining part of the acceleration response. The total response due to a series of moving loads is the sum of response to each moving load. If the number of vehicles is sufficiently large, the acceleration response may occur. If the number of vehicles is small, the acceleration response may not occur. The most unfavourable effect in the response causes the moving loads when the last force P_n passes through the bridge and the other forces ($P_1 \div P_{(n-1)}$) have already left the bridge.
2) The fundamental mode j = 1 provides the largest contribution to the midpoint acceleration, but at least the third mode must also be taken into account. The third mode of vibrations j = *3* have also significant influence on the acceleration amplitude, especially for bridges with light damping. The analysis showed that the impact of the mode of vibrations j = 3 reaches up to 31 %, therefore the mode j = 3 cannot be neglected.
3) The maximally acceptable value of the acceleration of the bridge in terms of EN1991-2, for direct fastened tracks must fulfil the condition $^{(c)}\ddot{w}(x,t)_{\max} < 5$ m/s. The aforementioned simulation, for the resonant speed c = 65 m/s = 234 km/h, gives the acceleration amplitude $^{(c=65)}\hat{\ddot{w}}^{(C)}_{(j=1)dyn}(L_b/2,t) =$ 4.2 m/s². For the cancellation

speed c = 57 m/s = 205 km/h gives the acceleration amplitude ${}^{(c=57)}\hat{\ddot{w}}^{(C)}_{(j=1)}(L_b/2,t)$ = 1.2 m/s^2.

Acknowledgments

This study was supported by the Grant VEGA No. 1/0336/15 and No. 2/0033/15 of the Grant Agency of the Slovak Republic.

References

[1] KOLOUSEK, V. Dynamics of structures I. (in Czech). Monograph. Praha: SNTL, 1954, p. 263.
[2] BIGGS, J. M. Structural mechanics. Monograph. New York, NY: McGraw-Hill, 1964. ISBN 07005255-7.
[3] YEONG-BIN, Y., et al. Vibrations of simple beams due to trains moving at high speeds. *Engineering Structures* [online]. 1997, **19**(11), p. 936-944. ISSN 0141-0296/eISSN 1873-7323. Available from: https://doi.org/10.1016/S0141-0296(97)00001-1
[4] XIA., H., et al. Vibrations resonance and cancellation of simply supported bridges under moving train loads. *Journal of Engineering Mechanics* [online]. 2014, **140**, p. 1-11. ISSN 0733-9399/eISSN 1943-7889. Available from: https://doi.org/10.1061/(ASCE)EM.1943-7889.0000714
[5] NAPRSTEK, J. Resonance speeds of axle forces row moving along a beam (in Czech). Colloquium "Dynamics of machines 2000". ASCR Prague, 2000, p.145-152
[6] LI J., SU M. The resonant vibrations for a simply supported girder bridge under high-speed trains. *Journal of Sound and Vibration* [online]. 1999, **224**(5), p. 897-915. ISSN 0022-460X. Available from: https://doi.org/doi.org/10.1006/jsvi.1999.2226
[7] MORAVCIK, M., MORAVCIK, M. Resonance vibrations of railway bridges subjected to passing vehicles. *Communications - Scientific Letters of the University of Zilina* [online]. 2017, 19(3), p. 96-101. ISSN 1335-4205/eISSN 2585-7878. Available from: http://komunikacie.uniza.sk/index.php/communications/article/view/241
[8] *STN 1991-2. Slovak standard* (in Slovak). The European Standard 1991-2, Actions on structures - part 2, 2006.
[9] Wolfram Mathematica10.0. Program system for technical computing. *Wolfram Computation Meets Knowledge* [online]. Available from: https://www.wolfram.com/mathematica

Katarina Makka - Darina Stachova - Katarina Kampova*

ASSESSMENT OF THE MOBILE RISK SOURCE IN ROAD TRANSPORT

Assessment of the mobile risk sources is not yet established in the European Union by law and therefore there is not enough pressure to manage and reduce risks. However, the transport of dangerous goods poses a special risk in terms of the nature of the transported material, especially for densely populated urban areas. The release of toxic or flammable substances into the air may endanger the health and life of many inhabitants. The assessment of consequences of the mobile accident hazards has been dealt with only seldom and not in details. The aim of this paper is to assess the risks associated with the transport of dangerous flammable substance. Authors would like to point out that the mobile resources represent a significant source of risk through the transport of dangerous goods in the event of an emergency occurrence associated with their leakage.

Keywords: *risk assessment, dangerous goods, emergency accident, mobile risk source, road transport*

1. Introduction

The road transport is becoming increasingly important in the transport system of developed countries. One of the trends of the last decade is a marked increase in road traffic intensity. Approximately 1.8 million tons of gasoline use the petrol-powered cars in the Slovak Republic; passenger cars with diesel engines and trucks consume an additional 2.3 million tons of diesel per year [1].

The growth trend of product transfers between sites of production, further processing and consumption, also affects the transport of products, which are called dangerous goods or dangerous substances. Transit routes are run by industrial agglomerations and storage and spending facilities are located in areas densely populated by the population. Traffic accidents associated with leakage of dangerous substances occur more and more frequently and can pose a serious threat to the population or cause environmental pollution. Every day we are through various media informed about road traffic accidents and their various consequences - the number of injured and killed people, escaped amounts of hazardous substances, damage of property and the environment.

2. The legal framework for the transport of dangerous goods

Dangerous Goods or Dangerous Substance are substances or articles, which by their properties such as flammability, toxicity, etc. may endanger human health, even cause death or seriously endanger the environment [2]. For this reason, their carriage is a subject to special conditions governed by international agreements and conventions for the road, rail, inland waterway, maritime and air transport.

Those agreements and conventions are valid not only for international transport but are implemented into the national legal environment through the laws that refer to these agreements and conventions and apply also to national transport [3].

2.1 The legal framework for the transport of dangerous goods in European Union

The EU's basic legal instrument governing the carriage of dangerous substances in the road transport The European Agreement on the International Carriage of Dangerous Goods by Road (ADR Agreement) [4]. The ADR Agreement prescribes the conditions for the transport of dangerous goods. It breaks down freight by hazard classes; identifies and classifies hazardous substances and articles according to their hazardous properties; determines the conditions for their transport, packaging and marking and prescribes the use and completion of specified accompanying documents. It lays down the requirements for entries in transport documents, means of transport, including technical requirements for the vehicle by class and further provides for additional rules, such as restrictions on the number of items carried, supervision, mode of parking, etc. [5].

In addition to international agreements and conventions, there are directives and regulations of the European Parliament and the EC Council, as well. The basic legal norms of this nature are:

- Directive 2008/68/EC of the European Parliament and of the Council on the inland transport of dangerous goods.
- Council Directive 95/50/EC on uniform procedures for checks on the transport of dangerous goods by road.
- Regulation (EC) 1907/2006 REACH - Regulation on the Registration, Evaluation, Authorization and Restriction of Chemicals, sets out procedures for the collection and

* **Katarina Makka, Darina Stachova, Katarina Kampova**
Faculty of Security Engineering, University of Zilina, Slovakia.
E-mail: Katarina.Makka@fbi.uniza.sk

evaluation of information on the properties and risks of substances.

- Regulation (EC) No 1907/2006 on the Registration, Evaluation, Authorisation and Restriction of Chemicals (REACH). The REACH abbreviation includes the registration, evaluation, authorization and restriction of the chemical.
- Regulation (EC) No 1272/2008 on classification, labelling and packaging of substances and mixtures has sought to classify, label and package substances and mixtures. The CLP Regulation links past EU legislation to the GHS (Global Harmonized System of Classification and Labeling of Chemicals), the United Nations System for the Identification of Hazardous Chemicals and to inform users of these hazards. It also contains links to the REACH legislation.

2.2 The legal framework for the transport of dangerous goods in Slovak Republic

The legal framework for the transport of dangerous goods has been given by the European Agreement on the International Carriage of Dangerous Goods by Road. In the legislation of the Slovak Republic it was promulgated by the Decree of the Minister of Foreign Affairs no. 64/1987 Coll. on the European Agreement on the International Carriage of Dangerous Goods by Road [6].

The transport of dangerous goods by the road transport in the Slovak Republic, in addition to the provisions of the international agreement ADR, is also a subject to the following legal standards:

- Act no. 56/2012 Coll. on the road transport, as amended, lays down the requirements of the ADR, regulates the conditions for the transport of dangerous goods and puts specific requirements on the consignor, the transporter or the consignee of the dangerous consignment.
- Decree no. 43/2016 Coll. on the road transport deals with the scope of controls on the transport of dangerous goods on the road. Specifies individual violations of ADR-related regulations.
- Act no. 106/2018 Coll. on the conditions for the operation of vehicles in traffic on roads introduces so-technical inspection of vehicles intended for the transport of dangerous goods.
- Implementing Decree No. 134/2018 Coll. of the Ministry of Transport and Construction of the Slovak Republic laying down details on the operation of vehicles in the road traffic.
- The Decree No. 533/2006 on details of the population protection against the effects of dangerous substances, which describes the procedure in the event of an emergency, provides details to ensure the protection of the population against the effects of hazardous substances in an emergency related to their escape during the production, with dangerous pollutants.
- Act no. 67/2010 Coll. on the conditions for placing on the market of chemical substances unifies the requirements for labeling of dangerous substances. It specifies packaging requirements as a basic assumption of the transport safety and use of the hazardous substances.
- Government Decree No. 176/2003 Coll. laying down the details of technical requirements and conformity assessment procedures for the transport pressure equipment.
- Road Traffic Act no. 8/2009 of 3 December 2008 Act no. Act No. 8/2009 Coll. on the Road Traffic Act and on the amendment of some laws.
- Government Regulation no. No 349/2009 on the maximum authorized dimensions and weights and special marking of vehicles and combinations of vehicles.

2.3 Authorities responsible for assessment of mobile risk sources in transport in Slovak Republic

The main authority responsible for risk assessment of mobile risk sources in the Slovak Republic is Transport Authority, it was established by the Act No. 402/2013 Coll. on Regulatory Authority for Electronic Communications and Postal Services and on Transport Authority and on amendments of several acts, coming into force on 1 January 2014 as a state administrative body with nationwide operation in the area of railways and other guided transport, civil aviation and inland waterway transport. The Transport Authority is a legal successor of the Railway Regulatory Authority, Civil Aviation Authority of the Slovak Republic and State Navigation Administration.

The assessment of the road transport risks at a district level falls within the competence of district authorities, namely the Road Transport and Road Transport Department.

3. Emergency accident by dangerous goods transport

In Slovakia, 17,439 road haulers are registered to 12.5.2015 under SK-NACE 6024. Of this quantity approximately 5,200 carriers are involved in transport of dangerous goods. Although there are no precise statistical data on volumes or transport performance associated with the transport of dangerous goods in the Slovak Republic, it is estimated that dangerous goods account for up to 30 % of the total freight transport over the long distances and over the shorter distances (up to 100 km) 60 % of the total freight transport volume. Road transport accounts for approximately 70 %, rail for about 10 % and the remainder for other modes of transport. Up to 80 % of the dangerous goods transported are flammable liquids that are transported by the tank transport [7]. Transport of dangerous goods by road differs from ordinary freight transport, in particular by the fact that a number of technical, operational, transport and safety conditions and requirements must be met.

Carriage of dangerous substances by tanks brings many risks, compared to freight transport. In addition to the possibility of explosion and fire products in the event of a tanker accident, there is a great deal of damage to the environment, human life or health [8].

The long-term statistics from different countries agree that the most common cause of traffic accidents is a human factor in approximately 85 % of cases, traffic is the primary cause in 10 % of cases, and the means of transport is the source of accidents for about 5 % of cases. There are many factors involved in the occurrence of accidents at the same time [7].

The largest share in the occurrence of accidents in transport have traffic accidents with leakage of liquid hazardous substances

Table 1 *Number of Emergencies with Occurrence of Dangerous Substances (2013-2018) [10]*

Extraordinary events	2013	2014	2015	2016	2017
Chemical liquid	446	631	604	529	615
Gaseous chemical	128	143	198	134	125
Chemical substance solid	7	13	7	8	11
Powder	43	22	25	25	19
Biological material	10	3	8	4	6
Radioactive material	0	1	1	0	0
Other	148	123	77	67	78
Total	782	936	920	767	854

Figure 1 *Tank accident on D1 [12]*

[9]. Overview of numbers of incidents during the transport of dangerous goods by road in Slovakia in 2013-2015 is shown in Table 1.

4. Assessing the negative consequences of an emergency event related to transport of dangerous goods

Broadly speaking, a risk assessment is a combined effort of: 1) identifying and analyzing potential (future) events that may negatively impact individuals, assets, and/or the environment (i.e. risk analysis); and 2) making judgements "on the tolerability of the risk based on the risk analysis" while considering influential factors (i.e. risk evaluation) [7, 11].

To put in simpler terms, a risk assessment analyzes what can go wrong, how likely it is to happen, what the potential consequences are and how tolerable the identified risk is. As a part of this process, the resulting determination of risk may be expressed in a quantitative or qualitative fashion. The risk assessment plays an inherent part of an overall risk management strategy, which attempts to, after the risk assessment, "introduce control measures to eliminate or reduce" any potential risk-related consequences [7, 11].

Given the fact that 80 % of dangerous substances, transported on the roads, are flammable liquids, the case study was focused on assessing the risks associated with leakage of fuels during their transport in tankers.

Despite the fact that safety issues and compliance with the standards, rules and regulations for the transport of dangerous substances in road transport are handled by the authorities, carriers and drivers, we are occasionally informed of accidents involving the escape of dangerous substances [12]. Luckily, none of those accidents have passed into a disaster of catastrophic proportions, which would endanger the lives and health of population, infect large areas of land or water with toxic substances that act on the environment for a long period of time.

An example may be a recent tragic accident on the D1 motorway in the Slovak Republic (see Figure 1), where a 33-year-old driver died. The driver, for not identified reasons, went out of the way to the field, where he overturned the fully loaded tanker (30 000 liters of fuels). Transport on the D1 motorway, at the place where a tragic accident occurred, was diverted for safety reasons because there was a risk of explosion [12].

Table 2 *Risk source*

Equipment	Volume [m^3]	Dangerous good	Amount of substance [kg]
Tank	30	petrol	24 000

Table 3 *Outflow frequencies for different road types [13]*

Road Type	Outflow frequency [/veh.km]	
	Pressurized	Atmospheric
Motorway	$4.32 * 10^{-9}$	$8.38 * 10^{-9}$
Outside built-up area	$1.22 * 10^{-8}$	$2.77 * 10^{-8}$
Inside built-up area	$3.54 * 10^{-9}$	$1.24 * 10^{-8}$

Table 4 *Probability of direct ignition for transport units in an establishment [13]*

Source	Probability of direct ignition
Road tanker continuous	0.1
Road tanker instantaneous	0.4

The next part of the paper will deal with modeling the consequences of the above mentioned traffic accident in Slovakia on D1. The focus was set on the impact of consequences to population, in the case if this accident happened in a densely populated area.

The CPR 18E methodology for modeling the consequences was used [13]. The CPR 18E methodology, known as the "Purple Book, is a recognized approach for a comprehensive risk assessment and includes two parts - the assessment of the risks of stationary equipment and the assessment of the transport of dangerous substances. It is used to determine the risks in the operation, handling, transport and storage of dangerous substances.

The first step in determining the negative consequences is to identify the risk sources, Table 2.

Determining the most unfavorable situation, where the effects of explosion, toxicity or fire of leaked fuel threaten the people and the environment, is based on estimate and determination of emergency scenarios. The selection of possible emergency scenarios is based on: the projected escape of the maximum amount of individual hazardous substances, the largest area of the fire, the potential threat to the environment by explosion and the radiated heat and the number of persons at risk in the affected areas [14].

4.1 Quantification of total frequency of emergency scenario

Determination of total frequency of an emergency scenario in the fuel transportation process estimates of representative events for leakage of dangerous goods from the Purple Book is shown in Tables 3 and 4 [15].

Total frequencies of the emergency scenario were determined to be the product of the outflow frequency and the probability of direct ignition.

$F_t = F * P$

$F_t = 1.24 * 10^{-8}$ vehicle. km*170 km *0.4 (1)

$F_t = 8.42* 10^{-7}$ vehicle

with:
F_t - total frequency of emergency scenario
F - outflow frequency
P - probability of direct ignition.

4.2 Determination of severity of the accident and the societal risk

The modeling of the emergency scenario consequences showed that, in the case of air stability class F, the impact of the fatal consequences on the population in the event of a fire is in the vicinity of 66 m from the point of escape, which represents an area of 1.4 ha [13]. At an estimated population density of 80 people / ha (according to the Decree of the Ministry of the Environment No. 489/2002 as amended), the number of people on the affected area is about 112 people (1.4 ha x 80 people / ha).

The acceptability of risk is currently set only for the stationary risk sources, yet thus recommended risk acceptance limit was also used for the resulting fuel transport risk. According to the Purple Book, the acceptable risk limit is given by the following equation:

$$F = \frac{10^{-3}}{N^2} \quad \text{for N} \geq 10 \qquad (2)$$

with: N = number of fatalities.

Societal risk is defined as the relationship between the number of fatalities in the case of accidents and the probability that this number will not be exceeded [13, 16].

The societal risk for the selected emergency scenario was determined from the probability and consequence matrix (Figure 2). For the activity analyzed, a pair of numbers was determined - the total frequency of the emergency scenario and the number of fatalities. The societal risk for the population was estimated by combining both values (Figure 2).

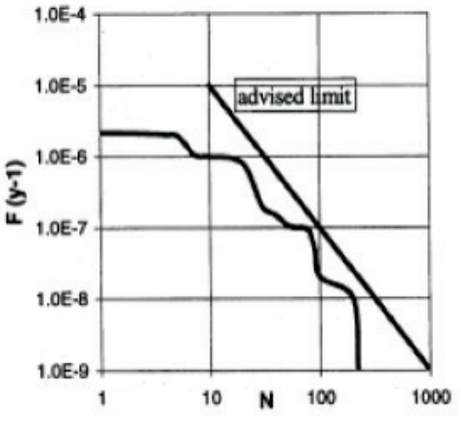

Figure 2 *Societal risk curve. Abscissa axis represents the number of fatal cases of persons, the ordinate shows the frequency of events per year [13]*

5. Conclusion

The objective of this contribution was to provide practical guidance in the assessment of risks related to the transport of dangerous goods in terms of the likely outcome of an accident. The presented study presents a detailed assessment of the risks of transporting dangerous substances on the roads, which is a prerequisite for reducing the risks. The results could be useful for various societal and environmental risk studies related to the accidental release of dangerous goods into the air when measures for prevention or mitigation of consequences are to be proposed.

In view of the increasing number of hazardous substances transported and the preparation of legislation on the prevention of accidents involving the transport of dangerous substances in the European Union, this issue will need to be dealt with in more detail.

Acknowledgment

This paper is an output of the science project Vega 1/0628/18 1/0628/18 Minimizing the level of experts' estimations subjectivity in safety practice using quantitative and qualitative methods and project Vega grant No. 1/0240/15 named „Process model of critical infrastructure safety and protection in the transport sector.

References

[1] Yearbook of transport, posts and telecommunications in 2015. *Statistical Office of the Slovak Republic* [online]. ISBN 978-80-8121-391-5. Available from: http://193.87.31.84/0213168/Rocenka_dopravy_post_a_telekomunikacii_2015.pdf

[2] HOLLA, K., RISTVEJ, J., SIMAK, L. *Systematic method of risk assessment in industrial processes.* In: Risk analysis VII: Simulation and Hayard Mitigation & Brownfields V: Prevention, Assessment, Rehabilitation and Development of Brownfield Sites: proceedings. Wessex Inst Technol, Wit, Transact Ecol & Environm., 2010. ISBN 978-1-84564-472-7/eISBN 978-1-84564-473-4, p. PI-115-PI-126.

[3] MAKKA, K., SVENTEKOVA, E. The assessment of population safety in the vicinity of unclassified risk sources. *Advanced Materials Research* [online]. 2014, **1001**, p. 498-503. ISSN 1022-6680/eISSN 1662-8985. Available from: https://doi.org/10.4028/www.scientific.net/AMR.1001.498

[4] SVENTEKOVA, E., SVETLIK, J. Permeable performance testing of limiting road section. In Transport Means 2015, PTS I and II. Klaipeda Univ, JSC Lietuvos Gelezinkeliai, Lithuanian Railways, IFToMM Natl Comm Lithuania, Lithuanian Soc Automot Engineers, Lithuanian Acad Sci, Div Tech Sci, Vilnius Gediminas Tech Univ, Best Practice Factory Freight Transport. 2015. p. 543-546.

[5] KAMPOVA, K., LOVECEK, T. Uncertainty in quantitative analysis of risks impacting human security in relation to environmental threats. In: Meško G., Dimitrijević D., Fields C. (eds) Understanding and Managing Threats to the Environment in South Eastern Europe. NATO Science for Peace and Security Series C: Environmental Security, vol 2. Springer, Dordrecht [online]. 2010. ISBN 978-94-007-0610-1/eISBN 978-94-007-0611-8, p. 349-363. Available from: https://doi.org/10.1007/978-94-007-0611-8_19

[6] HOLLA, K., MITASOVA, V., PAVLENKO, T. Risk assessment model verification in hazardous industrial processes. *Procedia Engineering* [online]. 2017, **192**, p. 324-329. ISSN: 1877-7058. Available from: https://doi.org/10.1016/j.proeng.2017.06.056

[7] RAUSAND, M. *Chapter 1: Introduction.* In: Risk Assessment: Theory, Methods, and Applications. John Wiley & Sons, 2013, p. 1-28. ISBN: 978-0-470-63764-7.

[8] ZAGORECKI, A., et al. Executive dashboard systems for emergency management. *Communications - Scientific letters of the University of Zilina* [online]. 2012, **14**(2), p. 82-89. ISSN 1335-4205, ISSN 2585-7878. Available from: http://komunikacie.uniza.sk/index.php/communications/article/view/751

[9] SVETLIK, J., VELAS, A. Design of equipment to improve safety on roads. In: 20th international scientific conference Transport Means 2016: proceedings. Juodkrante, Lithuania. Kaunas: Kaunas University of Technology, 2016. p. 614-617.

[10] PULCOVA, S. *Number of emergencies with the occurrence of dangerous substances.* Analytical and expertise department, Institute of Fire Engineering and Expertise of the Ministry of the Interior of the Slovak Republic. 2018.

[11] MANUELE, F. A. *Chapter 1: Risk assessments: Their significance and the role of the safety professional.* In: Popov, G., Lyon, B. K., Hollcraft, B. Risk Assessment: A Practical Guide to Assessing Operational Risks. John Wiley & Sons. *2016*, p. 1-22. ISBN: 978-1-118-91104-4

[12] SIVY, P. Tank accident on D1 [online]. [accessed 2018-10-05]. Available from: https://www.noviny.sk/galeria/13573-nehoda-cisterny-na-d1/6d5fdc2dbd17c13b4378436386e461ca?back_url=https%3A%2F%2Fwww.noviny.sk%2Fkrimi%2F330784-tragicka-nehoda-na-d1-cisterna-prevazajuca-benzin-sa-prevratila-mimo-cestu

[13] Guidelines for quantitative risk assessment, "Purple Book". CPR 18E, TNO. *Gevaarlijke Stoffen* [online]. 2005. p. 237. Available from: http://content.publicatiereeksgevaarlijkestoffen.nl/documents/PGS3/PGS3-1999-v0.1-quantitative-risk-assessment.pdf

[14] KAMPOVA, K. The concept of social risks perception. In Risk Analysis VII: Simulation and Hazard Mitigation & Brownfields V: Prevention, Assessment, Rehabilitation and Development of Brownfield Sites: proceedings. Wessex Inst Technol; Wit, Transact Ecol & Environm. 2010. p. PI-127-PI-135.

[15] MAKKA, K., SVENTEKOVA, E. *Risk evaluation by transport of dangerous substances.* In 18th International Conference on Transport Means, Transport Means 2014. Juodkrante, Lithuania. Kaunas: Kaunas University of Technology, *2014, p. 308-311.*

[16] HOLLA, K., et al. Results and conclusions of the project "complex model for risk assessment and treatment in industrial processes" (MOPORI). *Communications - Scientific letters of the University of Zilina* [online]. 2015, **17**(1), p. 46-51. ISSN 1335-4205, ISSN 2585-7878. Available from: http://komunikacie.uniza.sk/index.php/communications/article/view/392

COMMUNICATIONS – Scientific Letters of the University of Zilina
Author guidelines

- All papers have to deal with the topic of transport and be submitted strictly within one of the listed subtopics. Please, refer to list of topics and subtopics on our webpage and indicate it clearly when submitting your paper.
- Submitted papers must be unpublished and must not be currently under review for any other publication.
- Manuscripts written in good English must include abstract and keywords also written in English. The abstract should not exceed 10 lines.
- Submitted manuscripts should not exceed 20 pages including figures and graphs
- Submission should be sent by e-mail – as an attachment – to the following address: komunikacie@uniza.sk.
- The author's exact mailing address, full names, E-mail address, telephone or fax number, the name and address of the organization and workplace (also written in English) must be enclosed.
- For all manuscripts a double-blind peer review by at least two independent reviewers and language correction is mandatory.
- After reviewing and incorporating the editor's comments, the final draft (before printing) will be sent to authors for final review and minor adjustments.

The full author quidelines are available at:
http://komunikacie.uniza.sk/index.php/communications/guidelines

Errata: Communications – Scientific Letters of the University of Zilina, Vol. 20, No. 3, 2018, „Electrochemical Characterization of Az31 Magnesium Alloy Treated by Ultrasonic Impact Peening (Uip)", pp. 24-29. The proper Acknowledgement should be as follows:
The research was supported by project ITMS 26220220048 and by Slovak Research and Development Agency by the project No. APVV-14-0772.

komunikácie
COMMUNICATIONS

VEDECKÉ LISTY ŽILINSKEJ UNIVERZITY
SCIENTIFIC LETTERS OF THE UNIVERSITY OF ZILINA
VOLUME 21 Issue 1

https://doi.org/10.26552/com.J.2019.1

Address of the editorial office:
University of Zilina
EDIS – Publishing House
Univerzitna 8215/1
010 26 Zilina
Slovakia

E-mail: komunikacie@uniza.sk

Individual issues of the journal can be found on:
http://komunikacie.uniza.sk

Each paper was reviewed by two reviewers.

Journal is excerpted in **SCOPUS, EBSCO** and **COMPENDEX**.

Published quarterly by University of Zilina in EDIS – Publishing House of University of Zilina

Registered No: EV 3672/09

ISSN (print version) 1335-4205
ISSN (online version) 2585-7878

ICO 00397 563

February 2019